PERFORMANCE OF CODE DIVISION MULTIPLE ACCESS ON MULTIPATH CHANNELS - AN EXACT ANALYSIS

David J. Cowl

A thesis presented for the degree of
Doctor of Philosophy in Electrical and Electronic Engineering
at the University of Canterbury, Christchurch, New Zealand.

February 1994

ABSTRACT

This thesis presents an exact analysis approach to the investigation of the average probability of error performance for a code division multiple access (CDMA) system operating over multipath fading channels. The system in question has K users transmitting direct sequence spread spectrum signals over the same bandwidth. The receiver employs a selection diversity algorithm to select the path with the strongest desired signal at any given time. Performance results are presented for three classes of channel model, those being the single path non-fading channel, the single path fading channel and the multiple path fading channel. The performance is also presented for a system where ideal power control is applied.

The channel model for the single path fading channel is a single path whose gain has a Rayleigh distribution. The channel model for the multiple path fading channel is a tapped delay line model, where each tap is equally spaced in time, and has a gain with a Rayleigh distribution. The average gain for each tap is specified by an average delay profile.

The exact analysis approach involves finding the probability density functions (pdf's) for the per-user multi-user interference and the inter-symbol interference from the desired user. These probability density functions are derived from the pdf's of each contributing factor to the interference, including the empirical cross-correlation function pdf.

The characteristic functions of the per-user multi-user interference and the inter-symbol interference are found from the pdf's, and the characteristic function of the total interference is given by the product of the inter-symbol interference characteristic function and the $K - 1$ multi-user interference characteristic functions. The average probability of error is calculated using the characteristic function of the total interference.

Conclusions on the performance of the selection diversity algorithm and the power control algorithm are drawn, based on the results.

CONTENTS

PREFACE

This thesis presents a study of a code division multiple access (CDMA) system in a multipath environment, such as the indoor wireless channel. This research was motivated by the lack of an exact analysis approach to spread spectrum communications where the channel is modelled by an average delay profile.

The aim is to present the reader with a work which stands well in isolation. To ensure the system in question is well understood, background material covering spread spectrum communications and multipath channel concepts is included. For the reader who may not be familiar with the random variable manipulation and statistical techniques employed, explanations are grouped in an appendix. Further insight into the indoor wireless channel is included in an appendix covering indoor multipath channel measurement techniques and results. References to technical literature are also extensively used.

Chapter 1 presents an introduction to the research, including the potential arrival of personal communications services and the potential use of CDMA in such systems. A brief review of the literature leading to this research is presented, followed by the main aims of the research.

Chapter 2 introduces spread spectrum techniques, including frequency hopped and direct sequence spread spectrum. Direct sequence spread spectrum with binary phase shift keying is presented, along with techniques available to form families of spreading codes for direct sequence CDMA.

Chapter 3 describes the nature of multipath channels and briefly summarises measurements made for the indoor wireless channel and multipath channel models based on these measurements. The effects of multipath on spread spectrum communications is also outlined.

Much of the original contribution is contained in the exact analysis techniques and results presented in chapters 4, 5, and 6.

Chapter 4 introduces the system model and outlines the exact analysis method for the analyses. After presenting the means for finding the empirical probability density function of the cross-correlation function, the analyses for the single non-fading path model and the single Rayleigh fading path model are addressed. For each case, the analysis includes the derivation of the probability density functions and characteristic functions of the interference, numerical calculation considerations and the average probability of error performance results.

Chapter 5 presents the multiple fading paths case. Firstly the signal from the

desired user is considered, which takes into account the selection diversity algorithm, the received signal from the desired user and the inter-symbol interference (ISI) from the desired user. Next the multi-user interference (MUI) is considered. The analysis presented here includes finding the probability density functions and characteristic functions of the ISI and MUI, considerations for the numerical calculations and performance results for a selection of multiple fading path profiles.

Chapter 6 investigates the effects of power control, with the inclusion of a power control algorithm along with the selection diversity algorithm. The case for a single fading path is briefly considered, followed by an analysis of a multiple fading paths case, where there are three paths, each with equal average gain. One begins by determining the effect of the power control algorithm on the effective path gain. The analysis then includes the effect of the other factors contributing to the interference, finding the probability density functions and characteristic functions of the MUI and ISI. The received signal from the desired user and the numerical calculation considerations are presented, followed by the performance results for the system with power control.

Chapter 7 summarises the system model, including the assumptions made and the exact analysis method employed. Conclusions are drawn based on the results and suggestions for continuing research in this area based on the exact analysis method are presented.

Appendix A contains a summary of random variable manipulation and statistical techniques gathered from several sources, to provide some understanding of the statistical methods employed for those inexperienced in this area. Appendix B presents techniques for indoor wireless channel measurement which, along with measurement results, provide more insight into the multipath channel environment.

List of Papers

The following papers have been written, presenting some of the research of this thesis. The ISSSTA '92 paper was presented by myself in Yokohama, Japan in December 1992.

Cowl, D.J., Squires, P.L. and Shafi, M. (1992) "An analytical approach to multipath and inter-user interference in multiple access direct sequence spread spectrum systems," In *ISSSTA '92 Conf. Proc.*. Yokohama, Japan, December. pp. 279–282.

Cowl, D.J., Squires, P.L. and Shafi, M. (1993) "Performance of CDMA systems with selection diversity on multipath channels — an exact analysis," Submitted for publication in *IEEE Trans. Vehicular Tech.*

Acknowledgements

Many thanks to my supervisor Peter Squires for his support and encouragement through the course of my postgraduate studies. Many thanks also to Prof. Des Taylor for his technical input and interest in my research. I also wish to acknowledge my co-supervisors Bill Kennedy and Mansoor Shafi for the inspiration to continue in the face of adversity.

Thanks to Telecom New Zealand Ltd. for providing funding both personally and for the wireless indoor channel / spread spectrum project.

I would also like to thank all other members of the university community who have contributed to my work or enjoyment throughout my postgraduate studies. In particular I would like to acknowledge John, Chris, Matt and Robert for their support and companionship, and Mike and Dave for keeping the system going.

Thanks also to my flatmates Nonie and Katrina, and my many friends for sharing the good times and tolerating the not so good times.

GLOSSARY

Mathematical Notation

		Typical Usage
$\forall$	for all	(5.2)
$\equiv$	equivalent to	p. 21
$\rightleftharpoons$	Fourier transforms to	(4.55)
$\Rightarrow$	implies that	(5.23)
$\odot$	convolution	(5.14)
j	imaginary unit, $\sqrt{-1}$	(3.3)
$\lfloor x \rfloor$	largest integer less than or equal to x	p. 36
$\lvert x \rvert$	absolute value of x	(5.24)
$\Re[x]$	real part of x	(3.1)
x^*	complex conjugate of x	(3.6)
$U(x)$	unit step function	(5.5)
$P_T(x)$	rectangular waveform of T seconds duration	(4.1)
$J_0(x)$	zero order Bessel function	(4.56)
$\delta(x)$	Dirac delta function	(3.4)
$\chi_{1k}(\tau)$	cross-correlation function	(4.7)
$\triangle t$	difference in time	(3.6)
$\{x_k\}$	set or sequence of elements indexed by k	p. 25
gcd	greatest common denominator	p. 14
min	minimum of a set	p. 36
max	maximum of a set	p. 36
$P\{X\}$	probability of event X	(4.57)
$\mathbf{x}$	random variable $\mathbf{x}$	(4.57)
$\overline{x}$	mean value of x	p. 25
$E[x]$	expected value of x	(3.6)
$F_{\mathbf{x}}(x)$	distribution function of $\mathbf{x}$	p. 55
$f_{\mathbf{x}}(x)$	probability density function of $\mathbf{x}$	(4.24)

$h_y(y)$	probability density function of y	(4.41)
$\varphi_x(x)$	characteristic function of x	p. 35
$G_x(x)$	complementary distribution function of x	(4.58)
$[a, b]$	real interval $a \leq x \leq b$	p. 32
$E_1(x)$	exponential integral, $= \int_x^\infty \frac{e^{-u}}{u} du$	(4.72)
$\text{erf}(x)$	error function, $\frac{2}{\sqrt{\pi}} \int_0^x e^{-u^2} du$	(4.83)
$Q(x)$	Q function, $\frac{1}{2\pi} \int_x^\infty e^{u^2/2} du$	(4.59)

Abbreviations

		Typical Usage
BPSK	binary phase-shift keying	p. 10
CDMA	Code Division Multiple Access	p. 2
DS	Direct Sequence	p. 10
DSSS	Direct Sequence Spread Spectrum	p. 29
FH	Frequency Hop	p. 8
FM	Frequency Modulation	p. 7
FDMA	Frequency Division Multiple Access	p. 2
GHz	gigahertz	p. 23
ISI	inter-symbol interference	p. 26
LFSR	linear feedback shift register	p. 13
Mb/s	megabits per second	p. 22
MFSK	M-ary frequency shift keying	p. 8
MHz	megahertz	p. 22
MSK	minimum shift keying	p. 10
MUI	multi-user interference	p. 30
PCM	Pulse Code Modulation	p. 1
PCS	Personal Communications Services	p. 1
pdf	probability density function	p. 30
PN	pseudonoise	p. 12
QPSK	quadrature phase-shift keying	p. 10
s	seconds	p. 31
rms	root-mean-squared	p. 21
TDMA	Time Division Multiple Access	p. 2
W/Hz	watts per hertz	p. 32

Chapter 1

INTRODUCTION

Human beings have a natural social desire to communicate. This desire to inform and to be informed has been the impetus for the development of increasingly effective communications systems.

There are many milestones on the path to modern communication systems. Single characters were transmitted by Morse in the 1830's, using Morse code and an electric telegraph circuit. Voiced words were transmitted over a wire by Bell. Wireless communication was introduced around 1900 by Marconi, with his wireless telegraph. This was soon followed by wireless speech, demonstrated by Reginald Fessenden in 1906. In 1937 Reeve presented Pulse Code Modulation (PCM), a system on which much of today's digital communications systems are based. Factors which favour digital communications include:

- Computer communication requirements.
- Efficient regeneration of digital signals.
- Ability to integrate digital signals from various sources.
- The availability of wideband channels, such as satellite and optical fibre channels.
- Digital communications are robust in the presence of noise.

Other recent advances have addressed the quality, flexibility and spectral efficiency of communications systems. Interest in the flexibility of communications systems has been evident in the popularity of mobile telephone services. The need for spectrally efficient communications has become clear as current mobile service capacity is reached.

Further improvement in the flexibility of communications systems is expected with the inevitable [Cox, 1989] introduction of widespread tetherless portable radio communications in the form of Personal Communications Services (PCS). These personal communications systems are likely to employ wideband channels, and some form of multiple access scheme is needed to ensure efficient use of the bandwidth.

1.1 Multiple Access Schemes

For many wideband channels, the total bandwidth available is in excess of that required by one user on average. For efficient spectrum usage in this case, it is desirable to use some form of multiple access scheme where the channel and the available bandwidth is divided between a number of users in some fashion. The three major multiple access schemes used in digital communications systems are Frequency Division Multiple Access (FDMA), Time Division Multiple Access (TDMA) and Code Division Multiple Access (CDMA).

In FDMA the available bandwidth is simply divided into smaller bands, where each band is assigned to a different user. Each user may transmit continuously over the assigned frequency band. There is typically a guard band between the assigned channels to ensure that neighbouring channels do not interfere with each other.

For TDMA each user has access to the entire bandwidth, but transmissions are restricted to non-overlapping time slots. In a typical TDMA system, transmissions are organised into frames. A frame consists of K data bursts, typically 1 reference burst and one burst from each of the $K-1$ users. There may be a guard band time between bursts to ensure that bursts from different users do not overlap due to timing errors. Each burst from each user usually contains a preamble for synchronisation and a message part which contains the user's transmitted data.

With CDMA users are allowed to transit simultaneously over the same bandwidth, and thus some means of separating the signals at the receiver is required. Typically each user is given a unique code, which is approximately orthogonal (i.e. has a low cross-correlation) with all the other users' codes. This code is used to spread the spectrum of the data. In CDMA systems all the users transmit asynchronously, with no knowledge of any other users' timing.

1.2 Personal Communications Services

The personal communications label is taken to encompass a wider range of capabilities than those of the current analogue and digital mobile radio technology. For the implementation of personal communications, the radio systems should be optimised to provide voice and moderate-rate data services. There are many issues to be resolved for the implementation of personal communications, including the system architecture and multiple access schemes.

There have been many publications on the choice of multiple access schemes and system architectures, including the possibility of spectrum sharing [I *et al.*, 1993], where small microcells use TDMA and larger macrocells use CDMA, or vice-versa, thus sharing the same bandwidth. TDMA supporters present anti-multipath techniques such as adaptive equalisation [Quereshi, 1985] and spectrally efficient coding techniques such as Trellis coded modulation [Ungerboeck, 1987] to improve performance on mobile channels.

Proponents of CDMA continue to present new studies on CDMA capacity [Viterbi

et al., 1992; Viterbi and Viterbi, 1993; Jung *et al.*, 1993] and novel techniques to improve CDMA performance [Yoon *et al.*, 1993]. Some attractive features of CDMA are:

- CDMA does not require an external synchronisation network, which is required for TDMA systems.
- CDMA offers gradual degradation in performance as the number of users in the system is increased. It is therefore easy to add or remove users from the system.
- CDMA offers an external interference rejection capability (e.g., multipath rejection or resistance to deliberate jamming).

Complementing the supporters of CDMA, this thesis presents a novel exact analysis technique for the investigation of direct sequence CDMA in a typical PCS environment, the indoor wireless channel.

1.3 Review of Spread Spectrum in Fading Channels

In order to understand the impetus for the original work presented in this thesis, it is useful to be aware of the previous research in spread spectrum communications over multipath channels. The summary to follow briefly describes the research of Turin [Turin, 1984] and Kavehrad [Kavehrad, 1985; Kavehrad and Ramamurthi, 1987].

Turin was one of the first researchers to investigate the anti-multipath properties of spread spectrum techniques [Turin, 1980]. In the mid-eighties, Turin presented research on the effects of multipath and fading on the performance of direct sequence CDMA systems [Turin, 1984]. Turin presented capacity analysis for single path non-fading links, multiple path fading links and single path fading links. For his analysis, Turin assumed that the interference from other users in the system could be modelled as a Gaussian random variable.

Kavehrad's research into spread spectrum performance avoided the Gaussian assumption for the interference, extending work by Laforgia [Laforgia *et al.*, 1984] to cover channels with multipath fading. In preference to using a Gaussian assumption, the inter-user interference is tackled using moment generating techniques and numerical Gauss quadrature integration [Golub and Welsh, 1969; Meyers, 1982].

The system analysed in [Kavehrad, 1985] is very similar to the one analysed here (see chapter 4 for details), with the exception of the multipath channel model. Kavehrad presents a propagation channel for user 1 modelled by L paths with Rayleigh fading path gains, uniform random phase and a time delay. The time delays are assumed to be independent and uniformly distributed over the interval of the bit period. Kavehrad also assumed that the kth interferer is linked by a single path with a delay uniformly ranging over the bit period, a Rayleigh distributed gain and uniform phase.

In a sequel paper [Kavehrad and McLane, 1985] all users have L paths, though the paths still have independent delays which are uniformly distributed over the bit period. It is not possible to analyse an arbitrary multipath delay profile as the time delays of each of the paths are independent. For an average delay profile to be adequately modelled, the relative delay for the paths for any given user have to bear some relation to each other, an example being path delays which are equally spaced in time. When the relative time delay of each path is known, an average gain can be assigned to each path to conform to a given average delay profile.

In later research [Kavehrad and Ramamurthi, 1987], a study of arbitrary multipath models is presented. In this paper a Monte Carlo integration technique is used to perform the required numerical integration.

It is desirable to be able to study the arbitrary multipath model case using an exact analysis technique.

1.4 Aim of the Thesis

This thesis presents an analysis of a spread spectrum CDMA system with a multipath channel described by an average delay profile.

The aim is to formulate an exact analysis of the CDMA system, along with suitable numerical procedures to calculate the system performance based on the analysis. The technique presented here involves finding the actual empirical probability density functions and characteristic functions of the interference, and using these to calculate the average probability of error of the system. The analytical procedure is described and the procedure applied to three classes of channel model, those being the single path non-fading channel, the single flat fading path channel model and the multiple path fading channel. The original contribution to the body of knowledge in this area is as follows:

- The formulation of a suitable exact analysis technique for the study of the average probability of error for a spread spectrum CDMA system. This analysis involves finding the probability density functions of the factors contributing to interference, including the empirical probability density function of the spreading sequence cross-correlation terms.

- The application of the exact analysis technique to the non-fading channel case and the presentation of the system performance, making comparisons with approximate methods.

- The application of the exact analysis technique to the flat fading and multipath fading model cases, the comparison of the results for several different multipath delay profiles and the evaluation of the performance of the selection diversity algorithm.

- The extension of the analysis to include an ideal power control algorithm and the presentation of the power control system performance in comparison to the

selection diversity performance and the non-fading channel case.

The presentation of exact analysis results allows comparisons with approximate and other simplified methods, giving some measure of the accuracy for these less computationally expensive techniques.

Chapter 2

AN INTRODUCTION TO SPREAD SPECTRUM

Spread spectrum techniques have been used for many years and have been employed in applications which make direct use of its properties. These include antijamming communications, secure transmissions, antimultipath systems and multiple access communications. Spread spectrum techniques are primarily used in radio systems, though the application of such techniques has been considered for optical fibre systems [Foschini and Vannucci, 1988]. The aim of this chapter is to introduce spread spectrum communications, to present the reasons for using spread spectrum and explain the architecture of a spread spectrum system.

A definition which reflects the characteristics of spread spectrum is as follows:

> Spread spectrum is a means of transmission in which the signal occupies a bandwidth in excess of the minimum necessary to send the information, thereby distributing a relatively low dimensional data signal in a high dimensional environment; the band spread is accomplished by means of a code which is independent of the data, and a synchronised reception with the code at the receiver is used for despreading and subsequent data recovery. [Pickholtz *et al.*, 1982]

Under this definition, other standard modulations such as FM and PCM which also expand the spectrum of an information signal do not qualify as spread spectrum.

Some of the benefits of spreading the spectrum are:

- Antijamming
- Low probability of intercept
- Multiple user random access communications with selective addressing capability
- Low interference

The means by which the spectrum is spread are varied, with the main types investigated being direct sequence and frequency hopping. In direct sequence the spectrum is spread by modulating the data directly using a high rate pseudorandom sequence. Frequency hopping techniques involve the data being represented by a

series of frequency chirps specific to the user. Both systems are demodulated using correlation techniques.

The amount of performance improvement achieved through the use of spread spectrum is defined as the processing gain of the spread spectrum system. A common definition of the processing gain is the ratio of the spread bandwidth B_{ss} to the information bandwidth B_D, giving

$$G_P = \frac{B_{ss}}{B_D} \tag{2.1}$$

2.1 Frequency Hop Spread Spectrum

A method for widening the spectrum of a data-modulated carrier is to change the frequency of the carrier periodically [Ziemer and Peterson, 1985]. Typically, each carrier frequency is chosen from a set of 2^k frequencies which are spaced approximately the width of the data modulation apart, although neither condition is necessary. The spreading code in this case is used to control the sequence of carrier frequencies. This type of spread spectrum is called frequency hop (FH), due to the data-modulated carrier 'hopping' from one frequency to another. In the receiver, the frequency hopping is removed by synchronous mixing with a local oscillator signal which follows the same hopping sequence.

2.1.1 Slow-Frequency-Hop Spread Spectrum

A fully coherent frequency-hop system is theoretically possible, but due to the difficulty of building truly coherent frequency synthesisers and code tracking requirements, in most cases non-coherent or differentially coherent data modulating schemes are used. No effort is made to precisely recover the phase of the data-modulated carrier in the receiver, since it is not required by the demodulator.

A common data modulation system for FH systems is M-ary frequency shift keying (MFSK). For example, the data modulator may output one of $M = 2^L$ tones with a symbol duration $T_s = LT$ seconds, where T is the duration of an information bit. Usually these tones are spaced far enough apart to be orthogonal. Thus the frequency spacing is at least $1/LT$ and the data modulator output spectral width is approximately $2^L/LT$. In order to spread the spectrum of the modulated data, each T_c seconds the data modulator output is translated to a new frequency by the frequency-hop modulator. If $T_c \geq LT$ then the FH system is called a slow-frequency-hop system. Figure 2.1a shows the transmitted signal for a slow-frequency-hop system where $L = 2$, resulting in a $M = 4$ level FSK data modulation. The frequency is hopped over 2^k frequencies, where $k = 3$. Thus, symbol time $T_s = 2T$, and in this case $T_c = 2T_s$.

In the receiver, the transmitted signal is down-converted using a local oscillator which follows the hop frequency sequence, shifting the modulated data into the same band, where it may be demodulated using a conventional MFSK demodulator.

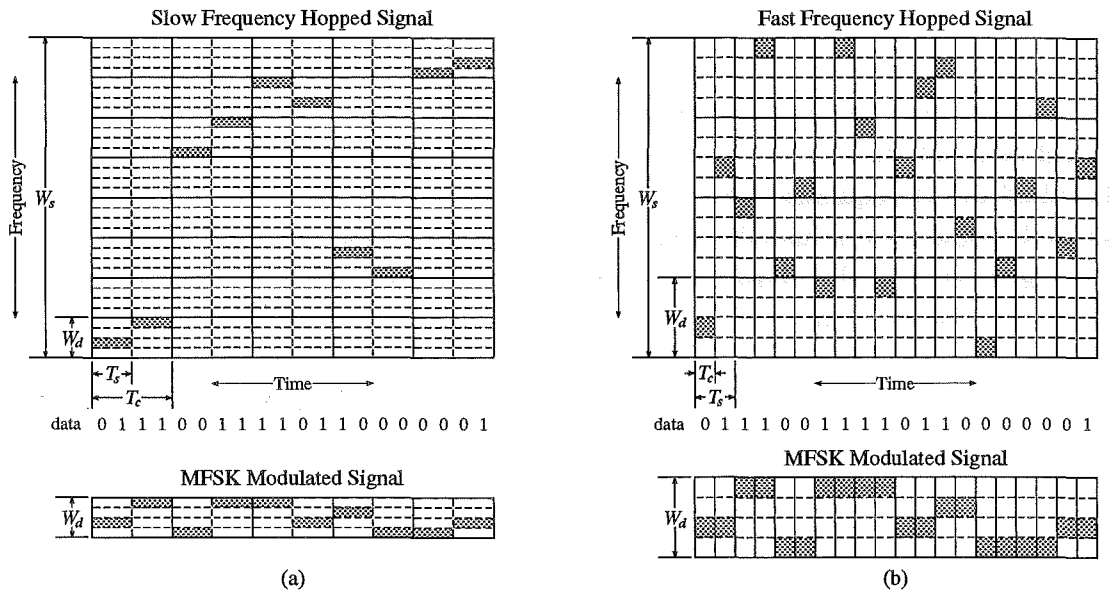

Figure 2.1 Slow and fast frequency hop. In these diagrams, W_d is the bandwidth of the 4-level FSK modulated data and W_s is the bandwidth of the frequency hopped transmitted signal.

2.1.2 Fast-Frequency-Hop Spread Spectrum

In contrast to the slow-FH system, where the hop-frequency band changes more slowly than the symbols come out of the data modulator, the hop-frequency can change many times per symbol in a fast-frequency-hop system. An advantage achieved when fast frequency hop is used is that the frequency diversity gain is seen on each transmitted symbol.

Once again MFSK is used, where the modulator output is one of $M = 2^L$ tones, but now this tone is divided into K equal time periods called chips. After each chip, the MFSK modulator is hopped to a different carrier frequency. Since the chip duration T_c is less than the symbol duration T_s (see figure 2.1b), the minimum tone spacing for orthogonal signals becomes $1/T_c = K/LT$. The receiver frequency-dehopping functions in the same way as for slow-FH.

The demodulator can make detection decisions in a variety of ways. One method is to make a decision on each frequency-hop chip as it is received and to make an estimate of the data modulated output using a majority rules vote from all K chip decisions. Another method is to calculate the likelihood of each data modulator output symbol as a function of the total output over all K chips and choose the symbol which has the highest probability of being sent. This method would be optimum in the sense that minimum probability of error is achieved for a given signal to noise ratio. These possible modes have different performance and complexity, making the choice of method the one that best solves a given problem.

2.2 Direct Sequence Spread Spectrum Techniques

It is possible to spread the spectrum of a data-modulated signal by modulating the signal a second time using a wide bandwidth spreading signal. Bandwidth spreading by direct modulation of a data-modulated carrier by a wideband spreading signal or code is called direct-sequence (DS) spread spectrum [Ziemer and Peterson, 1985]. This second modulation is usually some form of digital phase modulation. The spreading signal is typically chosen to have properties which allow demodulation by the intended receiver, while making demodulation from an unintended receiver difficult. If the bandwidth of the spreading signal is large relative to the data bandwidth, the transmitted spectrum is dominated by the spectral shape of the spreading signal and nearly independent of the spectral shape of the data signal.

2.2.1 BPSK Direct-Sequence Spread Spectrum

The simplest form of DS spread spectrum uses binary phase-shift keying (BPSK) as the spreading modulation (see figure 2.2). Other forms of modulation, such as quadrature phase-shift keying (QPSK) or minimum shift keying (MSK), could also be used, but are not considered in this thesis.

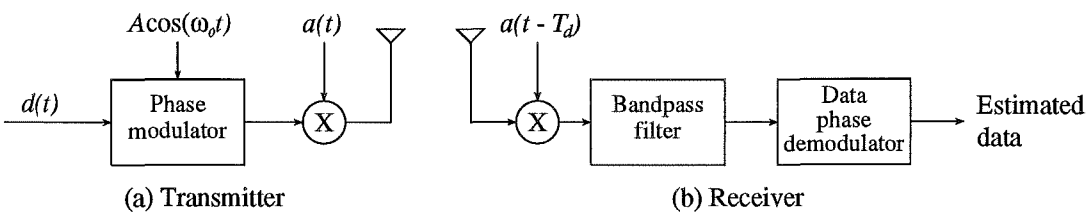

Figure 2.2 (a) Transmitter model for BPSK direct sequence spread spectrum. (b) Receiver model for BPSK direct sequence spread spectrum. The time delay T_d is chosen to equal the time delay in the channel between the transmitter and receiver.

Consider a phase-modulated carrier having power P, angular frequency ω_0, and data phase modulation $\theta_d(t)$ given by

$$s_d(t) = \sqrt{2P}\cos[\omega_0 t + \theta_d(t)] \tag{2.2}$$

BPSK spreading is achieved by multiplying $s_d(t)$ by a function $a(t)$ representing the spreading waveform, where $a(t)$ has values ± 1. The transmitted signal is

$$s_t(t) = \sqrt{2P}a(t)\cos[\omega_0 t + \theta_d(t)] \tag{2.3}$$

The spectrum of the transmitted signal is spread by a factor equal to the number of chips in one period of the spreading code $a(t)$. Thus, if the spreading code has a period of p, the processing gain

$$G_P = \frac{B_{ss}}{B_D} = p \tag{2.4}$$

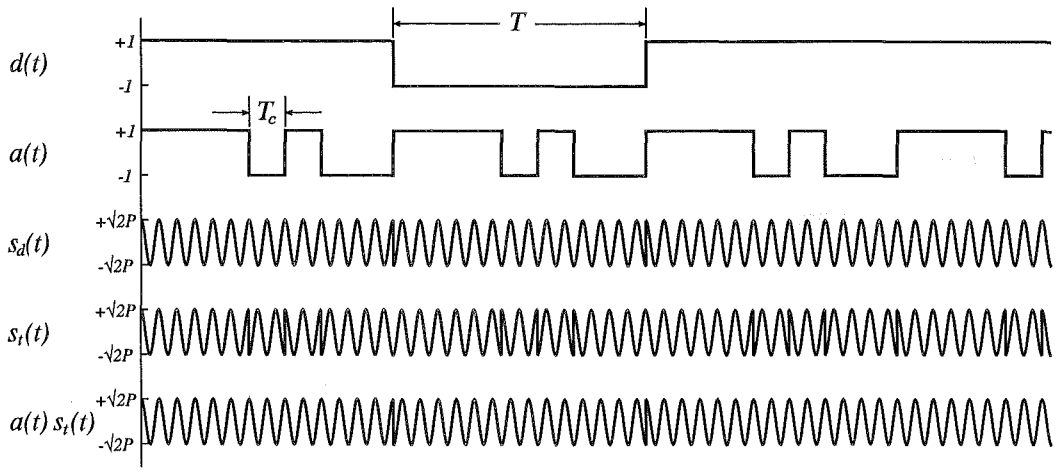

Figure 2.3 Direct sequence spread spectrum signal diagram for BPSK spreading of BPSK modulated data. In this diagram, $d(t)$ is the data signal, $a(t)$ is the spreading code, $s_d(t)$ is the BPSK modulated data and $s_t(t)$ is the transmitted spread spectrum signal. Taking the product of $a(t)$ and $s_t(t)$ despreads the transmitted signal, leaving the original phase-modulated data signal.

Demodulation is accomplished in part by remodulating with an appropriately delayed spreading code, which despreads the transmitted signal. When the spreading codes in the transmitter and receiver are perfectly synchronous, the second modulation (despreading) effectively cancels the spreading modulation, as the spreading code multiplied by itself is always unity. The despread signal can then be demodulated using a conventional coherent phase demodulator.

Note that the data modulation in equation 2.2 does not have to be BPSK. However, it is common to use the same modulation type for the data modulation and the spreading modulation. When BPSK is used in both modulators (as in figure 2.3), one phase modulator can be eliminated, and replaced by a single modulation by the modulo-2 sum of the data and the spreading code.

2.2.2 Direct Sequence Spreading Codes

For the spread spectrum system to operate efficiently, the spreading waveform $a(t)$ is chosen to have certain desirable properties. For example, the phase of the received spreading code must be determined and tracked by the receiver. Thus a good spreading code would have a high in-phase autocorrelation peak, and low out of phase autocorrelaion. For wide bandwidth spreading, fast and electronically simple code generators are desirable. When the spread-spectrum system is used for multiple access, the chipping sequence utilised by each user must be selected from a set of near orthogonal codes, where any given code pair has low cross-correlation properties so as to achieve a low level of interference between users. For secure communications, and anti-jamming systems, long waveforms are desired, to ensure low probability of intercept. The codes discussed in this section have one or more of these properties,

and are typical of those used in spread spectrum systems.

A periodic pseudonoise (PN) sequence has many of the properties required in a spread spectrum system. The following properties of a given set of K PN sequences of length p should be considered when choosing a set of codes for a given spread spectrum application.

1. The discrete periodic autocorrelation function $C(\tau)$

$$C(\tau) = \frac{1}{p}\sum_{l=1}^{p} a_l a_{l+\tau}$$

2. The discrete aperiodic autocorrelation function, given by

$$\frac{1}{p}\left[\sum_{l=1}^{p-\tau} a_l a_{l+\tau} - \sum_{l=p-\tau+1}^{p} a_l a_{l+\tau}\right], \qquad 1 \le \tau \le p-1$$

3. The discrete cross-correlation function of two different spreading codes from a given code set, given by

$$\theta_{a,b}(\tau) = \frac{1}{p}\sum_{l=1}^{p} a_l b_{l+\tau}$$

4. A lower bound on the maximum value of the out of phase autocorrelation and cross-correlation functions of a set of K codes of length p is given by Welch [Welch, 1974; Sarwate and Pursley, 1980] as

$$\theta_{max} \ge \left[\frac{K-1}{pK-1}\right]^{1/2}$$

Maximal Length Sequences

A maximal length pseudonoise sequence, also known as an m-sequence, is defined by Golomb [Golomb, 1967] as follows.

1. In every period p, of a binary sequence $\{a_k\}$, the difference between the number of +1's and -1's does not exceed one.

2. In every period p half the runs have length one, one-fourth have length two, one-eighth have length three, etc., as long as the number of runs exceeds one. Moreover, for each of these lengths there are equally as many runs of +1's and -1's (see figure 2.4).

3. The periodic autocorrelation function $C(\tau)$ is two valued. Explicitly

$$pC(\tau) = \sum_{k=1}^{p} a_k a_{k+\tau} = \begin{cases} p & \text{if } \tau = 0 \bmod p \\ K & \text{if } \tau \neq 0 \bmod p \end{cases}$$

This implies that the auto-correlation function has the value p when correlated with itself with zero shift, and a constant value K when correlated with any non-zero shift (within a full period p).

Figure 2.4 Maximal Length Pseudorandom Sequence, length 127

Mersenne Prime Maximal Length Sequences

Mersenne prime codes are defined as those maximal length codes of length $p = 2^r - 1$ for which both p and r are prime numbers [Dixon, 1976]. Judge [Judge, 1962] shows that Mersenne prime sequences have cross-correlation values superior to others, in some cases superior to nonprime sequences longer than the prime sequences.

Generating Maximal Length Shift Register Sequences

Linear feedback shift registers (LFSR) provide a simple method of generating binary sequences. A block diagram of a LFSR sequence generator with r stages may be seen in figure 2.5. The shift register contents are added modulo two after being multiplied by taps C_i (with values 0 or 1) to give a feedback value, which is loaded into stage one of the shift register when the contents are shifted through. The output from the shift register is a periodic sequence of zeros and ones $\{b_k\}$. As 0's and 1's do not satisfy the correlation equation, one usually uses the sequence $\{a_k\} = \{1 - 2b_k\}$ which has values -1 and $+1$ instead of 0 and $+1$ respectively.

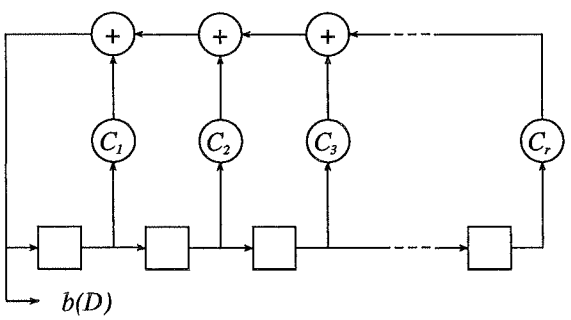

Figure 2.5 Linear Feedback Shift Register Sequence Generator

The tap values C_i determine the output sequence, which decide whether the ith stage is or is not involved in the feedback. The sequence generated by an r-stage register is periodic with $p \leq 2^r - 1$. If p equals $2^r - 1$, then the sequence is called a maximal length shift register sequence or m-sequence.

To generate an m-sequence of length $p = 2^r - 1$, the first step is to find a primitive polynomial of degree r for use as the characteristic polynomial of the sequence $\{b_k\}$,

$$f(x) = 1 + C_1x + C_2x^2 + \ldots + C_rx^r = 1 + \sum_{i=1}^{r} C_ix^i \qquad (2.5)$$

This can be found in a table of irreducible polynomials [Peterson and E. J. Weldon, 1972]. Properties of the polynomials including whether or not the polynomial is primitive are listed. The binary equivalent of the listed numbers (in this case the listed numbers are octal) are the coefficients of irreducible polynomials of the specified degree. The C_i coefficients of the characteristic equation are used for the tap values in the shift register generator. Once a characteristic polynomial is chosen, the C_i can be determined. Thus the binary equivalent of the number listed (excluding the last '1') also represents the tap values for the shift register generator.

Gold Codes

The Gold sequences are large families of linear binary sequences with low cross-correlation values. Gold [Gold, 1967] described a class of pairs of m-sequences, where the modulo 2 sum of the m-sequences forms a set of sequences whose cross-correlation functions have three low values which can be determined precisely. The large difference between the in-phase autocorrelation function value and the cross-correlation function of any two Gold sequences makes these sequences useful in Code Division Multiple Access (CDMA) systems, where each user is assigned a different code from the family of Gold codes. The out of phase auto-correlation of the Gold codes is also limited to the same three low values.

Generating Gold Code Sets

The procedure to generate a set of Gold codes relies on the theorems set out by Gold [Gold, 1967]. The theorems allow the selection of two m-sequences which perform better with respect to cross-correlation properties than do purely random sequences.

Consider an m-sequence that is represented by the binary vector $\mathbf{b}$ of length p, and a second sequence $\mathbf{b}'$ obtained by sampling every qth symbol of $\mathbf{b}$. The second sequence is said to be a decimation of the first, and the notation $\mathbf{b}' = \mathbf{b}[q]$ is used to indicate that $\mathbf{b}'$ is found by sampling every qth symbol of $\mathbf{b}$. The decimation of an m-sequence may or may not be another m-sequence, and when $\mathbf{b}'$ is an m-sequence, the decimation is said to be a proper decimation. A table of irreducible polynomials [Peterson and E. J. Weldon, 1972] may be used to determine whether a particular decimation of a given m-sequence is proper, as each polynomial entry has associated with it an integer q which indicates that the sequence generated by that polynomial is the qth decimation of the sequence generated by the first polynomial listed in that table. It has been proven [Sarwate and Pursley, 1980] that $\mathbf{b}' = \mathbf{b}[q]$ has period p also, if and only if $\gcd(p, q) = 1$, where "gcd" denotes the greatest common denominator. They [Sarwate and Pursley, 1980] have also shown that proper decimation by odd integers q will give all of the m-sequences of period p. Thus any pair of m-sequences having the same period p can be related by $\mathbf{b}' = \mathbf{b}[q]$ for some q.

The cross-correlation function of pairs of m-sequences can be three valued, four valued or possibly many valued. Certain special pairs of m-sequences whose cross correlation spectrum is three valued are called preferred pairs of m-sequences, where

the three values are

$$-\frac{t(r)}{p}, \qquad -\frac{1}{p}, \qquad \frac{t(r)-2}{p}$$

where

$$t(r) = \begin{cases} 2^{(r+1)/2} + 1 & \text{(n odd)} \\ 2^{(r+2)/2} + 1 & \text{(n even)} \end{cases}$$

and the code period $p = 2^r - 1$. Finding preferred pairs of m-sequences is necessary to generate Gold codes.

The following conditions are necessary and sufficient to define a preferred pair $\mathbf{b}$ and $\mathbf{b}'$ of m-sequences.

1. $r \neq 0 \bmod 4$; that is r is odd or $r = 2 \bmod 4$
2. $\mathbf{b}' = \mathbf{b}[q]$ where q is odd and either

$$q = 2^k + 1$$

or

$$q = 2^{2k} - 2^k + 1$$

3.

$$\gcd(r, k) = \begin{cases} 1 & (r \text{ odd}) \\ 2 & (r = 2 \bmod 4) \end{cases}$$

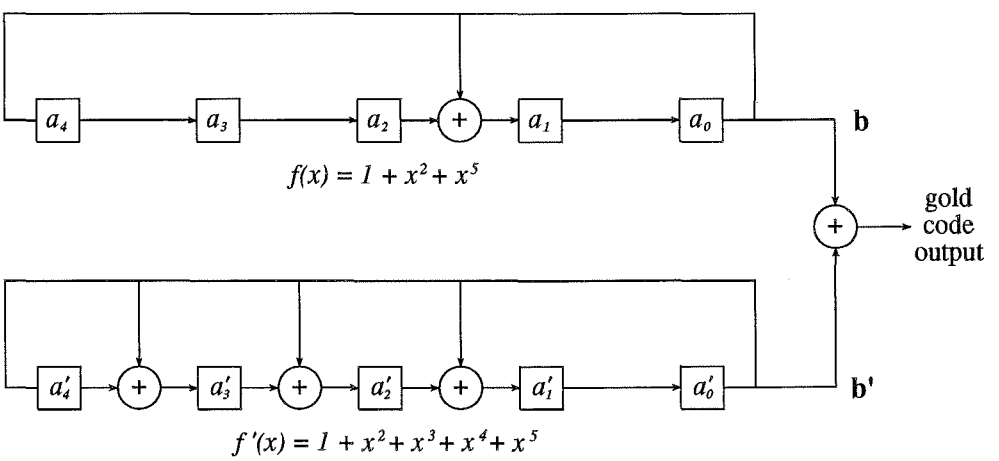

Figure 2.6 Typical Gold Code Sequence Generator

Once a preferred pair $\mathbf{b}$ and $\mathbf{b}'$ of m-sequences is found, the family of Gold codes is found by modulo 2 addition of $\mathbf{b}$ and $\mathbf{b}'$, through the p possible relative phases of $\mathbf{b}$ and $\mathbf{b}'$. These p sequences and the original pair of m-sequences comprise the $p + 2$ sequences in the Gold code family. A typical shift register configuration to generate 31 chip gold codes is shown in figure 2.6. The complete family of Gold codes may be obtained by using different initial loads of the shift register. One may generate either of the preferred pair of m-sequences by loading the opposite shift register with all zeros.

Kasami Sequences

Kasami discovered a set of sequences [Kasami, 1966; Sarwate and Pursley, 1980] which, like the Gold codes, have bounded cross-correlation values. The values of the cross-correlation functions of the *small set of Kasami sequences* with length $2^r - 1$ take on the values in the set $\{-1/p, -s(r)/p, (s(r)-2)/p\}$ where $s(r) = 2^{r/2}$. There are $2^{r/2}$ sequences in the set, and the small set of Kasami sequences is optimal with respect to the Welch bound [Welch, 1974].

The *large set of Kasami sequences* contains both the small set of Kasami sequences and a set of Gold sequences (or Gold-like sequences) as subsets [Sarwate and Pursley, 1980]. Interestingly, the cross-correlation bound is the same as that for the latter subset.

Hadamard Sequences

Hadamard codes are based on Hadamard matrices [Ryser, 1963]. A matrix H of order n with entries $+1$ and -1 is called a *Hadamard matrix* provided

$$HH^T = nI, \tag{2.6}$$

where H^T denotes the transpose of H and I denotes the identity matrix of order n. It is conjectured that Hadamard matrices exist for all orders $n \equiv 0 (\text{mod } 4)$.

From the definition of the Hadamard matrix, one can see that if the rows of the matrix were selected as spreading codes, the in-phase cross correlation between any given pair of sequences would be zero, and thus Hadamard codes are truly orthogonal if used synchronously.

2.3 Code Division Multiple Access

The two most common multiple access techniques are frequency division multiple access (FDMA) and time division multiple access (TDMA). In FDMA, all the users transmit simultaneously, but use disjoint frequency bands. In TDMA, all the users occupy the same bandwidth, but use different slots in time. When all users are allowed to transmit simultaneously in time and occupy the same bandwidth, some other means of separating the signals at the receiver is required. Code division multiple access (CDMA) provides the capability.

In direct sequence CDMA, each user is given a unique spreading code, which is approximately orthogonal (i.e. has a low cross-correlation) with all the other users' codes. This code is used to spread the spectrum of the data. Typically, in CDMA systems all the users transmit asynchronously, with no knowledge of any other users' timing.

A potentially large problem for CDMA systems is the "near-far problem". Since the users are typically in separate physical locations, a receiver trying to receive the signal for the kth user may be closer to the ith user, resulting in a greater received

power from the ith user. This problem causes severe performance degradation, and some form of received power control is usually required to maintain good performance.

It is naturally of interest to compare the capacity of CDMA to that of FDMA and TDMA. In a perfectly linear, perfectly synchronous system, the number of orthogonal users for all three systems is the same, assuming equal overall system bandwidth and power. If a given time-bandwidth product is divided into p disjoint time slots for TDMA, it can also support p binary orthogonal codes (assuming $p = 2^m$, m is a positive integer).

The differences in the three multiple access schemes become more apparent when real world constraints are placed on the channel. One attractive feature of CDMA is that, unlike TDMA, there is no requirement for synchronisation among the various users. Note that there is a performance penalty when CDMA is asynchronous, due to the spreading codes no longer being truly orthogonal. It is also relatively simple to add users to a CDMA system, and for voice channels to take advantage of voice inactivity. Often the main reason for considering CDMA is the need for some form of interference rejection, such as multipath rejection or resistance to intentional jamming.

For an asynchronous CDMA system, even ignoring the near-far problem effects, the number of users the system can support is markedly less than G_P. From [Pursley, 1977], a rough rule of thumb appears to be that a system with processing gain G_P can support around $G_P/10$ users. This thesis presents an investigation of the performance and capacity of CDMA systems.

Chapter 3

THE NATURE OF THE INDOOR RADIO CHANNEL

The use of radio transmission for indoor data or voice communications is an attractive proposition. It would conveniently allow mobility for users within the given building, drastically reduce the wiring requirements and provide flexibility in the configuration of communications systems without the need for rewiring. In order to investigate the performance of a radio system in an indoor environment, one requires knowledge of the statistics of the signal attenuation, and the nature of the impulse response of the channel. Knowledge of the channel characteristics is important when considering a communications system's design, as it typically influences system parameters such as the inclusion of equalisation and the choice of error correction codes. This thesis analyses a direct sequence spread spectrum code division multiple access communications system operating in a multipath environment like the indoor channel. Thus, it is important for the reader to have some understanding of the characteristics of the indoor radio channel.

The aim of this chapter is to discuss the nature of the indoor radio channel. This discussion includes a description of multipath channels in general and a look at some of the indoor channel measurement systems. Possible statistical models of the indoor channel based on the channel measurements are presented.

3.1 Multipath Fading Channels

Multipath fading channels occur in communication channels such as mobile radio and indoor radio due to radio wave scatterers in the physical environment. If a single pulse was transmitted in such an environment, reflections of the signal from the scatterers would result in a train of pulses at the receiver. Thus, one characteristic of the multipath channel is a time spread introduced on the transmitted signal.

The scatterers in a multipath channel are often physically moving, which results in a time variation in the multipath characteristics. So, if a pulse channel sounding experiment was repeated many times, the observed pulse train would change with time. Variations in the pulse train would include changes in the pulse amplitude and delay, and the number of observed pulses. The variations over time appear to be unpredictable; therefore a statistical model is often used to take the variations in the multipath into account.

Consider the effects of a multipath channel on a transmitted signal represented by

$$s(t) = \Re[u(t)e^{j2\pi f_c t}] \tag{3.1}$$

Assuming a multiple path propagation with time varying attenuation $\alpha_n(t)$ and time varying delay time $\tau_n(t)$, the received bandpass signal may be expressed as

$$x(t) = \sum_n \alpha_n(t)s[t - \tau_n(t)] \tag{3.2}$$

From this the low-pass equivalent of the received signal may be derived [Proakis, 1983] and expressed as

$$r(t) = \sum_n \alpha_n(t)e^{-j2\pi f_c \tau_n(t)}u[\tau - \tau_n(t)] \tag{3.3}$$

Since $r(t)$ is the response of an equivalent low-pass channel to an equivalent low-pass signal $u(t)$, it follows that the equivalent low-pass channel may be described by the time variant impulse response as

$$c(\tau; t) = \sum_n \alpha_n(t)e^{-j2\pi f_c \tau_n(t)}\delta[\tau - \tau_n(t)] \tag{3.4}$$

where t is the time instant and τ is the delay time. $c(\tau; t)$ represents the impulse response of the channel at time t, due to an impulse applied at time $t - \tau$.

Now consider the transmission of an unmodulated carrier at frequency f_c. The received signal for a discrete multipath channel becomes [Proakis, 1983]

$$\begin{aligned} r(t) &= \sum_n \alpha_n(t)e^{-j2\pi f_c \tau_n(t)} \\ &= \sum_n \alpha_n(t)e^{-j\theta_n(t)} \end{aligned} \tag{3.5}$$

where $\theta_n(t) = 2\pi f_c \tau_n(t)$. The received signal becomes the sum of a number of time variant phasors having amplitude $\alpha_n(t)$ and phase $\theta_n(t)$. It is noted that large changes in the physical environment of the channel are needed for the change in $\alpha_n(t)$ to be large enough to cause a significant change in the received signal. However, a small variation in $\tau_n(t)$ can cause a large change in $\theta_n(t)$. The delays $\tau_n(t)$ associated with the different signal paths also change in an unpredictable random fashion, and therefore the received signal $r(t)$ may be modeled as a random process. When the number of paths becomes large, the central limit theorem may be applied to the sum of the phasors and $r(t)$ may be modeled as a complex gaussian random process. This means that the time-variant impulse response $c(\tau; t)$ is a complex-valued gaussian random process in time t.

Another characteristic of multipath channels is carrier fading, which is due to the varying phases of the channel paths. If the phase vectors of all the paths at some given time add destructively, $r(t)$ becomes very small. At some other time, the phase vectors may add constructively, giving a large received signal. Thus the amplitude variations in the received signal, termed signal fading, are a result of the time-variant multipath characteristics of the channel.

When the impulse response $c(\tau;t)$ is modeled as a zero-mean complex valued gaussian process, the envelope $|c(\tau;t)|$ has a Rayleigh distribution. In this case the channel is called a Rayleigh fading channel. When there are fixed scatterers or signal reflectors in the environment, the channel complex gaussian may have a non-zero mean and the envelope $|c(\tau;t)|$ has a Rice distribution, resulting in what is called a Rician fading channel. Rayleigh fading appears to be realistic for mobile radio [Proakis, 1983].

It is useful to find correlation functions that define the characteristics of a fading multipath channel. Start with the equivalent low pass impulse response $c(\tau;t)$, which is characterised by a complex-valued zero mean gaussian random process in the t variable. It is assumed that $c(\tau;t)$ is wide sense stationary [Proakis, 1983]. One may define the autocorrelation of $c(\tau;t)$ as

$$\phi_c(\tau_1,\tau_2;\delta t) = \frac{1}{2}E[c^*(\tau_1;t)c(\tau_2;t+\triangle t)] \tag{3.6}$$

Often the attenuation and phase shift of the channel associated with path delay τ_1 is uncorrelated with the attenuation and phase shift associated with the path delay τ_2, which is termed *uncorrelated scattering* . In this case the autocorrelation becomes

$$\frac{1}{2}E[c^*(\tau_1;t)c(\tau_2;t+\triangle t)] = \phi_c(\tau_1;\triangle t)\delta(\tau_1-\tau_2) \tag{3.7}$$

If the difference $\triangle t$ in observation time is made zero, the resulting autocorrelation function $\phi_c(\tau_1;0) \equiv \phi_c(\tau)$ is simply the average power output of the channel as a function of the time delay τ. For this reason, $\phi_c(\tau)$ is called the multipath intensity profile or power delay profile of the channel. A multipath channel is often modelled by an average multipath power delay profile.

In order to make quantitative comparisons of systems in multipath channels, one needs a numerical measure of the temporal extent of a multipath channel. A useful measure of the temporal extent of the multipath delay profile of a channel is the standard deviation or root-mean-squared (rms) delay spread of the delay power profile, which is defined for a continuous channel as

$$\sigma_\tau = \left[\int_{-\infty}^{\infty}(\tau-\overline{\tau})^2\phi_c(\tau)d\tau\right]^{\frac{1}{2}} \tag{3.8}$$

where $\overline{\tau} = \int_{-\infty}^{\infty}\tau\phi_c(\tau)d\tau$.

When a channel is described by L discrete paths with an average gain β_l and delay τ_l, the rms delay spread is given by [Saleh and Valenzuela, 1987]

$$\sigma_\tau \equiv \sqrt{\overline{\tau^2}-(\overline{\tau})^2} \tag{3.9}$$

where

$$\overline{\tau^n} \equiv \frac{\sum_{l=1}^{L}\tau_l^n\beta_l^2}{\sum_{l=1}^{L}\beta_l^2}, \qquad n=1,2. \tag{3.10}$$

3.2 Measured Indoor Radio Channel Characteristics

In this section methods for the measurement of indoor radio channels are discussed, and indoor radio channel measurements made internationally and at the University of Canterbury are summarised.

The indoor radio channel has been investigated by various means including continuous wave [Alexander, 1982; Bultitude, 1987], pseudonoise sequences [Devasirvatham, 1984; Bultitude *et al.*, 1989] and pulsed carrier [Saleh and Valenzuela, 1987; Pahlavan *et al.*, 1989; Rappaport and McGillem, 1989; Cowl, 1990] systems.

3.2.1 Continuous Wave Measurements

Alexander [Alexander, 1982; Alexander, 1983] presented the first continuous wave measurements, investigated attenuation characteristics and showed that the power law describing the signal attenuation as a function of distance varies greatly from building to building and seems to be related to the physical layout. Office buildings typically saw the signal strength proportional to D^{-3} to D^{-4}, with factors as high as D^{-6} in extreme cases [Alexander, 1983], where D is the distance between the transmitter and receiver.

Continuous wave measurements have also been used to investigate the temporal fading characteristics of the indoor radio channel [Bultitude, 1987; Rappaport and McGillem, 1989]. Bultitude's results indicate that a typical indoor channel may be considered to be statistically stationary over a period of 1–4 seconds [Bultitude, 1987]. The temporal statistics of the fading indicate that measurements for many locations correspond well with Rician curves for K ratios between -6 dB and -12 dB, the others having Rayleigh distributions [Bultitude, 1987]. The overall statistics of the fading indicate that the Rayleigh fading model fits the data well for most signal levels [Rappaport and McGillem, 1989].

3.2.2 Pseudonoise Sequence Measurements

The other two measurement methods, pseudonoise sequence and pulsed carrier techniques, provided information about the spread of energy caused by reflections from objects and walls.

In a pseudonoise channel measurement system, the transmitter emits a high rate pseudonoise code modulated onto a carrier. The signal suffers attenuation and time-smear in the propagation channel, due to the multiple paths. The signal is correlated at the receiver with a pseudonoise code identical to that of the transmitter, but at a slightly slower rate. As the codes sweep past each other, the receiver traces out the correlation function, and therefore the power-delay profile of the channel.

Devasirvatham [Devasirvatham, 1984; Devasirvatham, 1987b] presented results found using a pseudonoise measurement system in which a 1023 bit maximal length code at 40 Mb/s was bi-phase modulated onto a 850 MHz carrier in the transmitter.

The receiver correlated using the same maximal length code, but running 4 kHz slower than the transmitter.

An advantage of the pseudonoise sequence technique is that the information comes out of the receiver only as fast as the codes slip past each other, allowing low data recording rates. The resolution is determined by the code rate. The effective data recording rate is increased by the ratio of the code rate over the code slip rate. In the system presented by Devasirvatham, a 1 microsecond time frame would be displayed over a 10 millisecond time period.

3.2.3 Pulsed Carrier Measurements

An alternative to the pseudonoise measurement system is a simple pulse modulated carrier system. In a pulsed carrier measurement system, short radar-like pulses on a high frequency carrier are used to measure the indoor radio channel response. The receiver is time-locked to the transmitter and typically uses an envelope detector to demodulate the received signal.

Such a system was constructed by the author, and is described in detail in Appendix B. The system described features a 5 nanosecond pulse amplitude modulated onto a 1 GHz carrier. The receiver uses a square-law envelope detector to demodulate the multiple versions of the transmitted pulse, due to the multipath propagation. The power-delay profile of the channel is displayed directly, in real time, which requires higher bandwidth instrumentation compared to the pseudonoise measurement system.

3.2.4 Indoor Channel Delay Spread Measurements

Devasirvatham [Devasirvatham, 1984] presented measurements made in a six floor office building, using a pseudonoise channel measurement system with an 850 MHz carrier frequency. The statistics of the results presented indicated that the rms delay spread in this building has a median value of about 125 nanoseconds and a maximum value of about 200 nanoseconds.

Saleh [Saleh and Valenzuela, 1987] presented measurements made in a medium-size two-storey office building, using a pulsed carrier system with a 1.5 GHz carrier frequency. These results indicated that the rms delay spread has a median value of about 25 nanoseconds and a maximum value of about 50 nanoseconds. It was noted that these measurements were made in a building similar to that measured by Devasirvatham [Devasirvatham, 1984], though smaller. Although Saleh's statistics were typically a factor of five times smaller than Devasirvatham's results, this was explained by the fact that the larger rms delay spread results presented by Devasirvatham occurred when the received signal levels were extremely low. When the data was truncated to a subset having a path loss of less than 100 dB, the results obtained were similar to Saleh's results.

Bultitude [Bultitude *et al.*, 1989] presented a comparison of the indoor radio propagation at 900 MHz and 1.7 GHz, using a pseudonoise channel measurement system.

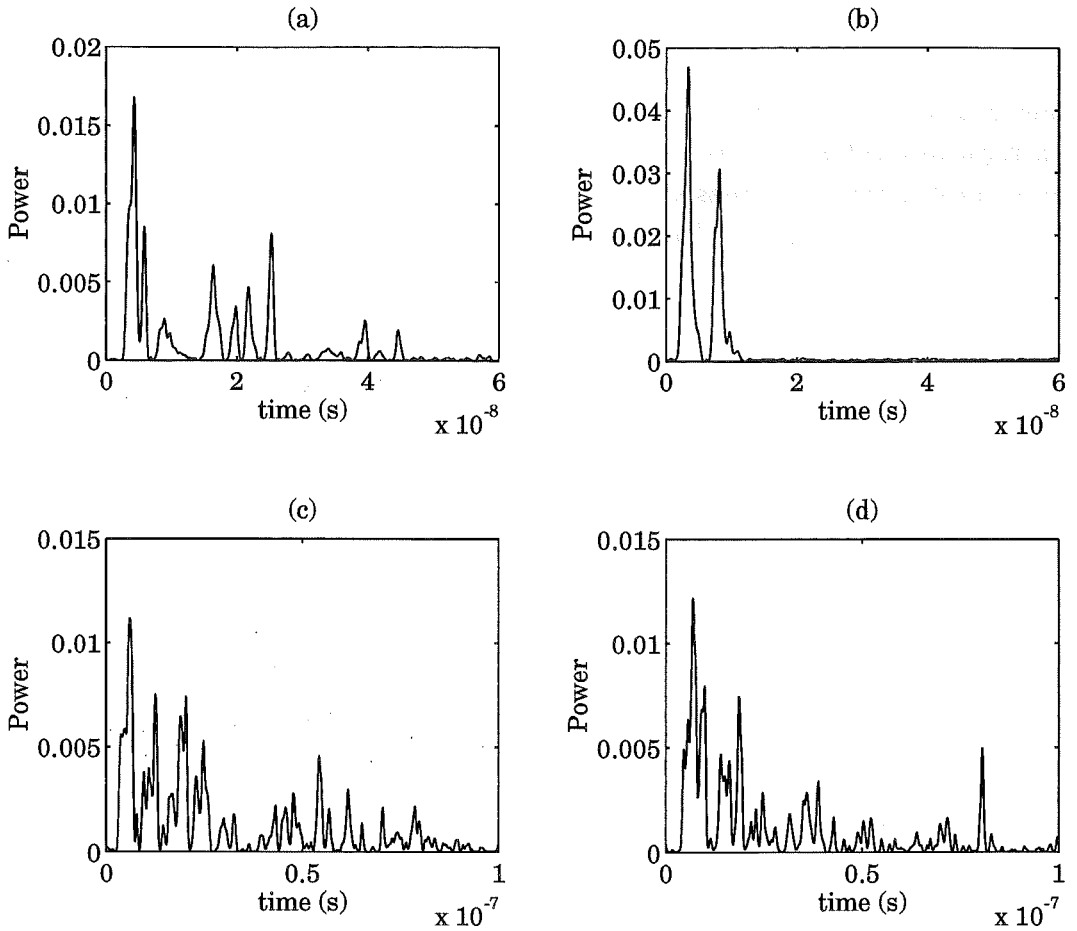

Figure 3.1 A set of four interesting examples of power delay profile measurements taken in a laboratory at the University of Canterbury. (a) A typical power delay profile. (b) A strong signal, with two major paths between the transmitter and receiver. (c) Low signal levels resulting in a large delay spread. Clustering of paths is evident. (d) A large delay spread, with a significantly delayed path of notable signal level.

The measurements were made in two different office buildings. The statistics for both frequencies were similar, and compared well to Saleh's results [Saleh and Valenzuela, 1987]. In one building, the 900 MHz frequency band median rms delay spread was 26 nanoseconds and the 1.7 GHz band rms delay spread was 28 nanoseconds. In the second building, the 900 MHz band median rms delay spread was 30 nanoseconds and the 1.7 GHz band rms delay spread was 29 nanoseconds.

Pahlavan [Pahlavan *et al.*, 1989] presented results for multipath propagation on manufacturing floors at 910 MHz, using a pulsed carrier measurement system. The locations investigated ranged from a typical electronics shop floor to heavy machine floors and car assembly plant locations. The measurements presented showed a maximum rms delay spread of 40 nanoseconds for the electronics workshop and a typical maximum rms delay spread of 150 nanoseconds for the locations with heavier machines and larger floor spaces.

Measurements have also been made in a laboratory at the University of Canterbury and in a Telecom office building Christchurch [Cowl, 1990]. A pulsed carrier measurement system with a 1 GHz carrier frequency was used. The median rms delay spread was approximately 24 nanoseconds in the laboratory and approximately 18 nanoseconds in the Telecom office building. These values are somewhat less than other presented results, which is believed to be due to dynamic range problems in the measurement system, especially in the Telecom office building.

Typical power delay profile measurements from a pulsed carrier measurement system may be seen in figure 3.1.

3.2.5 Other Indoor Channel Measurements

In addition to the typical power delay profile measurements, other aspects of the indoor channels have been investigated and measured. These include comparisons of measurements at various frequencies [Zaghloul *et al.*, 1991b; Hawbaker and Rappaport, 1990], dopper spread measurements [Howard and Pahlavan, 1990], frequency response and path loss measurements [Pahlavan and Howard, 1989a; Zaghloul *et al.*, 1991a], the effects of traffic on the multipath characteristics [Ganesh and Pahlavan, 1990] and experimental evaluation of space, frequency and polarisation diversity in the indoor wireless channel [Lemieux *et al.*, 1991].

3.3 Models Proposed for Indoor Multipath Channels

Saleh [Saleh and Valenzuela, 1987] proposed a discrete channel model for the indoor multipath channel, where each path has a gain $\{\beta_k\}$ and arrival time $\{\tau_k\}$. The arrival times $\{\tau_k\}$ are initially assumed to be a Poisson arrival sequence with some mean arrival rate λ. The path gains β_k associated with every τ_k are chosen from a probability distribution whose mean and mean square are a function of τ_k, and vanishes for large values of τ_k.

This simple model was shown to be inconsistent with measured results, which indicated that paths tended to arrive in clusters, which was clearly not a simple Poisson arrival-time with constant arrival rate λ.

The proposed modification to improve the validity of the model involves the addition of a cluster concept to the model. The arrival times of the clusters are modelled as a Poisson arrival process with some fixed rate Λ. Within each cluster, subsequent rays arrive according to another Poisson process with fixed rate λ. Typically there are many rays within a cluster, i.e., $\lambda \gg \Lambda$. The arrival time of the lth cluster is denoted by T_l, and the arrival time of the kth ray of the lth cluster by τ_{kl}.

The gain of the kth ray of the lth cluster becomes β_{kl}, and the mean square of the gain values $\{\overline{\beta_{kl}^2}\}$ are the monotonically decreasing functions

$$\begin{aligned}\overline{\beta_{kl}^2} &\equiv \overline{\beta^2(T_l, \tau_{kl})} \\ &= \overline{\beta^2(0,0)}\, e^{-T_l/\Gamma} e^{-\tau_{kl}/\gamma},\end{aligned} \tag{3.11}$$

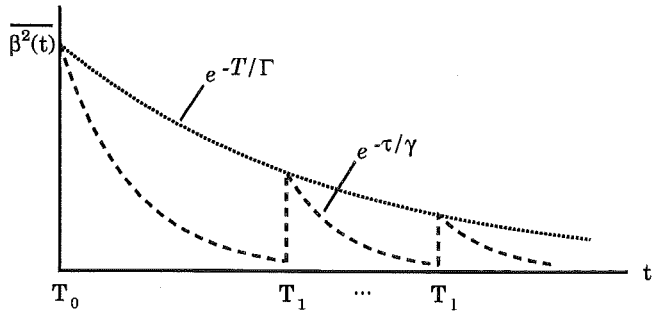

Figure 3.2 A graphical representation of the average power delay profile model for the indoor channel proposed by Saleh.

where $\overline{\beta^2(0,0)} = \overline{\beta_{00}^2}$ is the average power gain of the first ray of the first cluster, and Γ and γ are power delay time constants for the clusters and the rays respectively. A graphical representation of the mean square of the gain values of this model may be seen in figure 3.2.

Ganesh [Ganesh and Pahlavan, 1989] also noted that a simple Poisson arrival time model with a fixed rate was inadequate to model measured results. A modified Poisson model was proposed, where if a path was observed in a given time frame, the mean path arrival rate for the next time frame would be altered by a factor K. Depending on whether K was greater than or less than 1, the probability that there would be another path within the next time frame increases or decreases respectively. The optimum value of K was determined for manufacturing floors and college laboratories, based on empirical data [Ganesh and Pahlavan, 1989].

3.4 The Effects of Multipath on Digital Communications

Knowledge of the nature of the multipath channel is necessary in order to determine the effect the channel could have on the performance of communications systems. The effect of the channel characteristics on digital communication systems, in particular spread spectrum systems, is of specific interest to us.

In a typical digital communication system, the multipath propagation causes a time spread in the received signal, due to the time delay between the arrival times of the different propagation paths between the transmitter and receiver. This time spread causes symbols from one symbol time period to smear into later symbol time periods, an effect called inter-symbol interference (ISI). The greater the delay between the arrival time of the first path and the arrival time of the last significant path with respect to the symbol time, the greater the ISI. As the inter-symbol interference is caused by delayed versions of the transmitted signal, increasing the signal power also increases the power in the delayed signal. Hence, there is no advantage to be gained by increasing the signal level when a system's performance is predominantly ISI limited.

3.4.1 Spread Spectrum on Multipath Channels

The effect of dispersive multipath on direct sequence spread spectrum communications systems differs from standard digital transmission, giving an "inherent diversity in multipath fading channels" [Kavehrad and McLane, 1987].

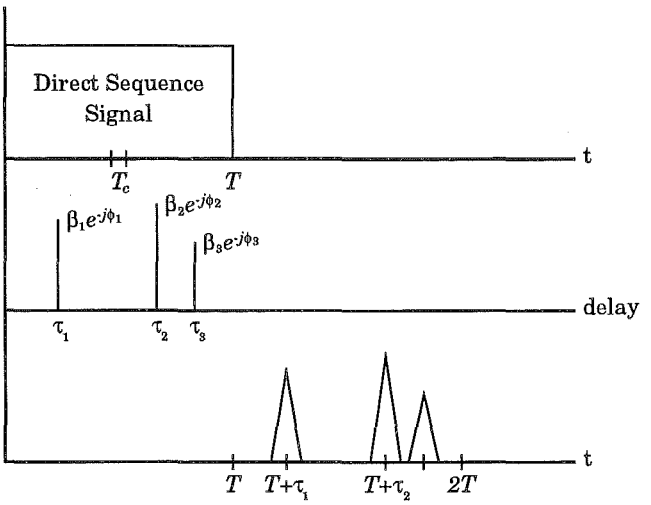

Figure 3.3 Signal transmission model for a direct sequence spread spectrum system and a discrete multipath model.

This inherent diversity is illustrated in figure 3.3. Here a spread spectrum signal and a discrete multipath channel [Turin, 1980] are graphically represented. The third graph shows the output from the correlator in the spread spectrum receiver, assuming that a maximal length spreading code was used. One can see that there are three resolvable signals for a single transmitted signal, giving an effective diversity. This is advantageous over the symbol smearing or inter-symbol interference seen in conventional digital transmission systems with dispersive multipath channels. In general, in a direct sequence spread spectrum system, any signal travelling via a path which has a delay greater than one chip duration of the spreading code is treated by the correlator in the receiver in the same way as any other uncorrelated signal at the receiver [Haykin, 1988].

When multiple receivers are used, paths which can be resolved may be detected or combined using a variety of algorithms, such as selection diversity, simple combining or maximum ratio combining. In this thesis selection diversity is assumed, where the maximum strength resolvable path at any given time is selected by the receiver.

Chapter 4

ANALYSIS OF SIMPLE SYSTEM MODELS

This chapter introduces an analytical investigation of the performance of a Code Division Multiple Access (CDMA) communications system that uses direct sequence spread spectrum signalling on fading channels which exhibit multipath propagation. The system model for the analysis is presented, and the system performance for two cases with simplified channel models is presented. The performance measure in this investigation is the average probability of error. In this system there are K users which each have a mobile transmitter, and a base station which receives the signals from all K users. Each user occupies the same bandwidth, using direct sequence spread spectrum (DSSS) techniques to separate the users' signals. An analytical method for finding the average probability of error for the inbound signals in such a system is presented. A block diagram of this system may be seen in figure 4.1.

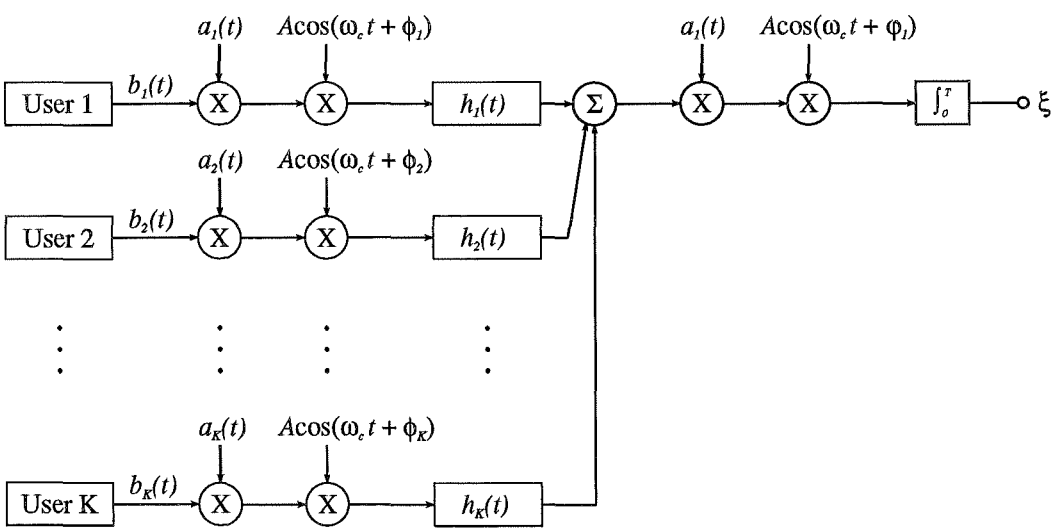

Figure 4.1 System model block diagram.

The use of spread spectrum radio over fading mobile or indoor channels has drawn great interest in recent years, reflected in the possibility that spread spectrum techniques may be employed for later generation digital cellular radio systems [Viterbi *et al.*, 1992]. It is, therefore, of interest to evaluate the performance of such a system. Such performance evaluations [Turin, 1984; Xiang, 1985; Kavehrad

and Ramamurthi, 1987; Stuber and Kchao, 1992; Wang and Milstein, 1992; Eng and Milstein, 1992] have been presented for a variety of scenarios, including differing multipath models and cellular environments. These analyses have employed approximations, bounds or Monte Carlo simulation techniques to incorporate the multipath and multi-user interference.

An analytical technique to evaluate CDMA performance on a channel with an arbitrary multipath power delay profile, without resorting to approximations to represent the multi-user interference is presented. Unlike previous analyses [Kavehrad, 1985; Lam and Steele, 1991], multipath models where there is dependence between path arrival times are utilised, which allows evaluation of arbitrary multipath power delay profiles and permits investigation of realistic models of multipath channels. The resulting average probability of error may be used as a yardstick for less complicated approximate methods.

The system model used in this analysis (see figure 4.1) is similar to that presented in [Pursley, 1977; Pursley and Sarwate, 1977], with the exception that the channel is assumed to be a multipath fading channel. In a direct sequence spread spectrum system, the entire bandwidth is assumed to be utilised by all users of the system at all times. A user spreads the spectrum of his data signal by modulating the data bits with a high-rate binary chipping sequence. The chipping sequence utilised by each user must be selected from a set of near orthogonal codes, where any given code pair has low cross-correlation properties so as to achieve a low level of interference between users. Delayed signals from the desired user due to the multipath channel also add to the interference, so it is also important for the spreading codes to have low even and odd auto correlation values [Sarwate and Pursley, 1980].

The system performance measure analysed in this paper is the average probability of error. This is a function of the multi user interference (MUI) and the desired user's signal strength, which varies due to the multipath channel. Each of these may be considered to be a random variable, and for a complete analysis, one must find their respective probability density functions (pdf's). For the system under investigation, the MUI is a function of several random variables, including the code cross-correlation function evaluated at the random delay between users, the random phase delay, and the random gain of the multiple paths in the channel for the interferer. One uses the probability density of each of these factors to find the probability density of the MUI from any given user. The desired user's signal strength has a Rayleigh probability distribution in the flat fading case. Once the various required probability density functions are found, one finds the probability density function of the total interference. This is achieved by finding the characteristic functions of the interference random variables, and calculating the product to give the characteristic function of the sum of the random variables [Papoulis, 1984]. The probability of error for any given desired signal level is the probability that the interference is greater than the desired signal level, which is the complimentary distribution function of the interference evaluated at the given desired signal level. The average probability of error is the expected value of the probability of error given all possible received signal

strengths.

4.1 The System Model and Description

The system model is described in more detail in this section. The model presented in this section is applicable to an arbitrary multipath channel case, however this chapter covers only the single non-fading channel case and the single flat fading path case. The arbitrary channel case is discussed in the subsequent chapters.

4.1.1 The Transmitted Signal Model

The system in question consists of K users, denoted by the subscript k, $k = 1, 2, \ldots, K$. The user signal to be detected is assumed to be user $k = 1$, and all others are considered to be interferers.

Each user has an information signal $b_k(t)$, which is a series of rectangular pulses with amplitudes of ± 1 and bit duration T s. The jth data bit of this bit stream is represented by b_j^k, thus

$$b_k(t) = \sum_{j=-\infty}^{+\infty} b_j^k P_T(t - jT) \tag{4.1}$$

where $P_T(.)$ is a rectangular waveform of T seconds duration.

Each user also has a unique spreading code $a_k(t)$, which is a periodic sequence of N rectangular chips a_i^k, with amplitudes of ± 1 and duration of T_c s.

$$a_k(t) = \sum_{i=-\infty}^{+\infty} a_i^k P_{T_c}(t - iT) \tag{4.2}$$

where $P_{T_c}(.)$ is a rectangular waveform of T_c seconds duration. The data bit period $T = NT_c$, so that there is one complete period of the spreading code for each data bit and $a_i^k = a_{i+N}^k$. The spreading codes used in this investigation are Gold codes [Gold, 1967].

The carrier frequency ω_c is assumed the same for all users, and the carrier phase for each user is denoted by ϕ_k. The transmitted signal $s_k(t)$ for user k is the product of the data sequence and the spreading sequence, biphase modulated at the carrier of angular frequency ω_c, so that

$$s_k(t) = A a_k(t) b_k(t) \cos(\omega_c t + \phi_k). \tag{4.3}$$

4.1.2 The Channel Model

The specific channel modelled in this study was an indoor wireless channel, where the transmitted signals travel to the base station via a multipath channel, which is assumed to exhibit Rayleigh fading [Proakis, 1983; Saleh and Valenzuela, 1987]. Although the statistics of measurements for many indoor locations correspond well with Rician curves [Bultitude, 1987], the overall statistics of the fading indicate

that the Rayleigh fading model fits the data well for most signal levels [Rappaport and McGillem, 1989]. A slow fading environment is assumed, where the random parameters associated with the channel do not vary significantly over consecutive data bit periods. The model may be applied to a slow varying urban mobile channel, though it should be noted that no attempt is made to model doppler effects, rapidly changing fading statistics, or shadowing effects which may be present in mobile and cellular radio.

The user signals are assumed to be asynchronous, and the relative time delay between the signal from user 1 and the signal from user k is represented by the random variable τ_k, which is assumed to be uniformly distributed in the interval $[0,T]$ for $k = 2,3,\ldots,K$ and $\tau_1 = 0$. In a spread spectrum system, channel paths separated by less than a chip period cannot be resolved [Kavehrad and McLane, 1985]. Here it is assumed that all paths within any given chip period sum to give one effective path, resulting in a model where the paths are spaced at chip-period intervals. The path response for the kth user $h_k(t)$ consists of L impulses with delay τ_{lk} ($\tau_{lk} = \tau_k + (l-1)T_c$), each multiplied by a Rayleigh distributed gain sample $\mathbf{V}_{lk}$ and an effective phase delay Φ_{lk}, which is assumed to be uniformly distributed in the interval $[-\pi,\pi]$. This results in the complex low pass equivalent impulse response $h_k(t)$, where

$$h_k(t) = \sum_{l=1}^{L} \mathbf{V}_{lk}\delta(t-\tau_{lk})e^{j\theta_{lk}} \qquad ;k = 1,2,\ldots,K. \tag{4.4}$$

The total effective phase for user k on path l is $\Phi_{lk} = \theta_{lk} + \phi_k$, which is also uniformly distributed in the interval $[-\pi,\pi]$.

It is assumed for ease of analysis that the number of effective paths L is deterministic and specified by the chosen average gain-delay profile. The average gain-delay profile specifies the average value of the Rayleigh distributed gains $\mathbf{V}_{lk}$. Note that the average power delay profile is proportional to the square of the average gain-delay profile.

The average gain-delay profile is assumed to be the same for all users. It would be more realistic to assign each user a random gain-delay profile, and to take an average performance over all possible profile combinations. Although it is theoretically possible to do this using this analysis technique, the computational expense required to find an average result is currently prohibitive.

The total signal which reaches the base station receiver, $r(t)$, is the sum over the L paths for the K transmitted signals and may be written as

$$r(t) = A\sum_{k=1}^{K}\sum_{l=1}^{L}\mathbf{V}_{lk}a_k(t-\tau_{lk})b_k(t-\tau_{lk})\cos(\omega_c t + \Phi_{lk}) + n(t) \tag{4.5}$$

where $n(t)$ is white Gaussian noise with spectral height $N_0/2$ W/Hz.

4.1.3 Correlation and Demodulation of the Received Signal

It is assumed that the receiver is locked to the strongest signal path, has achieved both carrier and spreading code synchronisation, and is operating in steady state. The

receiver coherently demodulates and despreads the received signal by integrating the product $r(t)a_1(t)\cos(\omega_c t)$ over one bit period T and sampling at time T. The resulting sample is the decision variable ξ. The detector decides that b_0^1 is $+1$ if the decision variable ξ is positive and that b_0^1 is -1 if the decision variable ξ is negative. The decision variable, after coherent demodulation and filtering, may be written as

$$\begin{aligned}\xi &= \int_0^T r(t)a_1(t)\cos(\omega_c t)dt \\ &= \int_0^T A\sum_{k=1}^{K}\sum_{l=1}^{L}\mathbf{V}_{lk}a_k(t-\tau_{lk})a_1(t)b_k(t-\tau_{lk})\cos(\omega_c t+\Phi_{lk})\cos(\omega_c t)dt+\eta \end{aligned} \quad (4.6)$$

where η is a sample of the Gaussian noise with zero mean and variance $(N_0T)/2$.

The integration of the product $[a_k(t-\tau_{lk})a_1(t)b_k(t-\tau_{lk})]$ over one bit-period T is the cross-correlation function of the spreading codes for user 1 and user k evaluated at a relative delay τ_{lk}, which is represented by $\chi_{1k}(\tau_{lk})$, as

$$\chi_{1k}(\tau_{lk}) = \int_0^T a_k(t-\tau_{lk})a_1(t)b_k(t-\tau_{lk})dt \quad (4.7)$$

so that the decision variable may be written in the compact form

$$\xi = \frac{A}{2}\sum_{k=1}^{K}\sum_{l=1}^{L}\mathbf{V}_{lk}\chi_{1k}(\tau_{lk})\cos(\Phi_{lk})+\eta. \quad (4.8)$$

Cross-Correlation Definitions

This section presents simplifications which may be made, due to the assumption that rectangular shaped chips are used. If rectangular pulses of unity amplitude are used, the following equations hold [Kavehrad, 1985].

The discrete periodic cross-correlation function $\theta_{k,1}(\tau)$ and the discrete aperiodic cross-correlation function $\hat{\theta}_{k,1}(\tau)$ are defined as

$$\theta_{k,1}(\tau) = \frac{1}{p}\sum_{l=1}^{p}a_j^k a_{j+\tau}^1 \quad (4.9)$$

$$\hat{\theta}_{k,1}(\tau) = \frac{1}{p}\left[\sum_{j=1}^{p-\tau}a_j^k a_{j+\tau}^1 - \sum_{j=p-\tau+1}^{p}a_j^k a_{j+\tau}^1\right] \quad (4.10)$$

where τ is an integer and p is the number of chips in one period of the spreading code.

It is useful to split the cross correlation functions into two parts,

$$A_{k,1}(\tau) = \frac{1}{p}\sum_{j=1}^{p-\tau}a_j^k a_{j+\tau}^1$$

$$B_{k,1}(\tau) = \frac{1}{p}\sum_{j=p-\tau+1}^{p}a_j^k a_{j+\tau}^1 \quad (4.11)$$

(4.12)

and thus

$$\theta_{k,1}(\tau) = A_{k,1}(\tau) + B_{k,1}(\tau) \tag{4.13}$$

$$\hat{\theta}_{k,1}(\tau) = A_{k,1}(\tau) - B_{k,1}(\tau). \tag{4.14}$$

From these discrete equations one derives an expression for the continuous-time partial cross correlation equations [Pursley, 1977] defined by

$$R_{k,1}(\tau_k) = \int_0^{\tau_k} a_k(t-\tau_k)a_1(t)dt$$

$$\hat{R}_{k,1}(\tau_k) = \int_{\tau_k}^{T} a_k(t-\tau_k)a_1(t)dt. \tag{4.15}$$

The integer number of whole chips of width T_c spanned by τ_k is defined to be n, where $0 \leq nT_c \leq \tau_k \leq (n+1)T_c \leq T$, and due to the rectangular shaped pulses,

$$R_{k,1}(\tau_k) = A_{k,1}(n) \times (\tau_k - nT_c) + A_{k,1}(n+1) \times ((n+1)T_c - \tau_k) \tag{4.16}$$

$$\hat{R}_{k,1}(\tau_k) = B_{k,1}(n) \times (\tau_k - nT_c) + B_{k,1}(n+1) \times ((n+1)T_c - \tau_k). \tag{4.17}$$

If it is assumed that the data bits $b_k(t)$ are also rectangular, $\chi_{1k}(\tau_k)$ can be expressed as

$$\chi_{1k}(\tau_k) = [b^k_{-1}R_{k,1}(\tau_k) + b^k_0\hat{R}_{k,1}(\tau_k)] \tag{4.18}$$

where b^k_{-1} and b^k_0 are the previous and current data bits from the interferer k.

4.2 Calculating The System Performance

The decision variable of equation 4.8 includes both the desired signal and interference resulting from other users and noise. In order to find the performance of a given system, statistical representations of the terms involved in the decision variable are employed. Statistical descriptions are used to determine the statistical characteristics of both the interference and the desired user's signal, from which the average probability of error is calculated.

The random variable $\mathbf{z}_k$ represents the interference from user k, where in general

$$\mathbf{z}_k = \frac{A}{2}\sum_{l=1}^{L} \mathbf{V}_{lk}\chi_{1k}(\tau_{lk})\cos(\Phi_{lk}) \tag{4.19}$$

for $k = 2, 3, \ldots, K$. The probability density function $f_{\mathbf{z}_k}(z_k)$ is determined from the probability density functions of the random path gains $\mathbf{V}_{lk}$, the cross-correlation functions of the spreading codes at the random delays $\chi_{1k}(\tau_{lk})$ and the cosine of the random phases Φ_{lk}. The interference $\mathbf{z}_1$ from user 1, being the desired user, is due to delayed signals caused by the multipath channel. This interference generally is a function of the path gains, the autocorrelation function of the spreading codes, the random phase and the selection diversity algorithm, which is described in section 5.1.

The total interference, represented by the random variable $\mathbf{z}$, is simply the sum of the noise and interference from the K users,

$$\mathbf{z} = \sum_{k=1}^{K} \mathbf{z}_k + \eta. \tag{4.20}$$

The interference from each of the users is independent, and the probability density function of $\mathbf{z}$ is the convolution of the K interference probability density functions $f_{\mathbf{z}_k}(z_k)$ and the probability density function of the noise [Papoulis, 1984]. The characteristic function property that the product of the characteristic functions of a given set of random variables is equivalent to the convolution of the probability density functions of the respective random variables [Papoulis, 1984] is applied. The characteristic function of $\mathbf{z}_k$ is denoted using $\varphi_{\mathbf{z}_k}(\nu)$ where $\varphi_{\mathbf{z}_k}(\nu) = E\left[e^{j\nu\mathbf{z}_k}\right]$. The characteristic function $\varphi_{\mathbf{z}}(\nu)$ of the total interference $\mathbf{z}$ is therefore

$$\varphi_{\mathbf{z}}(\nu) = \varphi_{\eta}(\nu) \prod_{k=1}^{K} \varphi_{\mathbf{z}_k}(\nu) \tag{4.21}$$

where $\varphi_{\eta}(\nu) = E\left[e^{j\nu\eta}\right]$ is the characteristic function of the noise. The characteristic function of $\mathbf{z}$ may be transformed back to the probability density function $f_{\mathbf{z}}(z)$, or used directly to find the complementary distribution function which is used to find the average probability of error, as described in section 4.3.5.

The desired user's signal level, represented by the random variable $\mathbf{X}$, is determined by the chosen delay profile, which specifies the probability density functions of the path gains. The probability density function $f_{\mathbf{X}}(X)$ of the desired user's signal level is in general derived from the probability density functions of the path gains according to the selection diversity algorithm.

The average probability of error is the expected value of the probability of error given all possible received signal levels. The complementary distribution function of the total interference $\mathbf{z}$, $G_{\mathbf{z}}(X) = \int_X^{\infty} f_{\mathbf{z}}(z)dz$, can be used to find the probability that the interference is greater than a given signal level, and therefore the probability of error for the given signal level. The average probability of error is the expected value of the interference complementary distribution function evaluated at the random received signal level $\mathbf{X}$, and hence

$$P_e = E[G_{\mathbf{z}}(X)] = \int_{-\infty}^{\infty} G_{\mathbf{z}}(X) f_{\mathbf{X}}(X) dX. \tag{4.22}$$

4.2.1 The Cross Correlation Function Distribution

In order to find the statistical description of the received signal, it is necessary to find the probability density functions of the terms which contribute to the decision variable ξ. The probability density functions of the path gains and phases specified by the multipath models are well known, though this is not the case for the cross-correlation function of the spreading codes, evaluated at a uniformly distributed random time delay. The probability density function of the cross-correlation function is investigated in this section.

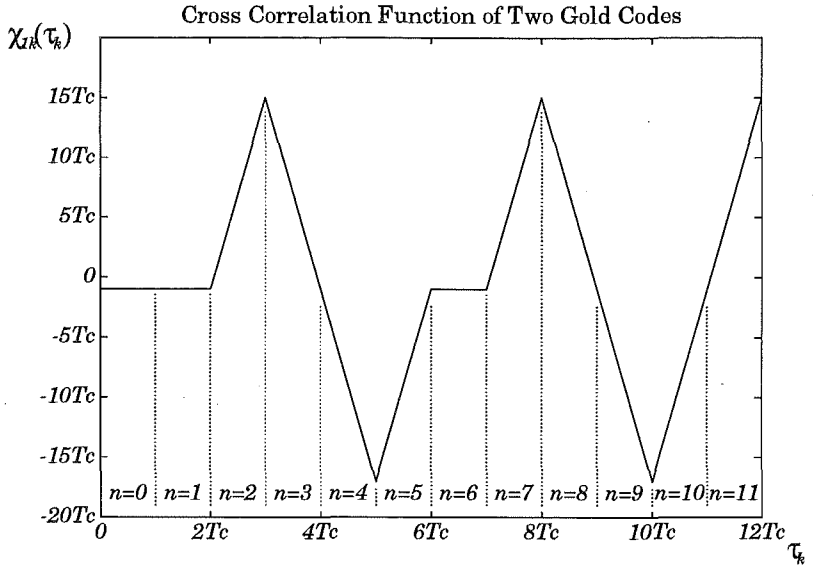

Figure 4.2 Part of the cross-correlation function of two Gold codes.

One begins by considering the random time delay τ_k, which is uniformly distributed in the interval $[0, T]$, the period of the data bit. It is useful to consider this time delay to be equivalent to an integer number of chip periods plus a remainder. A random variable $\mathbf{n}$ is defined to be a function of τ_k, such that $\mathbf{n} = \lfloor \tau_k / T_c \rfloor$, where T_c is the chip period and $\lfloor u \rfloor$ is the largest integer less than or equal to u. Thus, $\mathbf{n}$ is the integer number of chips spanned by τ_k (see figure 4.2). The random variable $\mathbf{n}$ has a discrete distribution where $\mathbf{n}$ takes a value from the set $\{0, 1, \ldots, p-1\}$ with equal probability $1/p$. If $\mathbf{n}$ is given, τ_k has a value in the interval $[\mathbf{n}T_c, (\mathbf{n}+1)T_c]$.

For $\mathbf{n}$ given, the cross correlation function $\chi_{1k}(\tau_k)$ is simply a linear function of τ_k (see figure 4.2). This follows from the definition of the cross correlation function definition,

$$\begin{aligned}
\chi_{1k}(\tau_k) &= [b^k_{-1} R_{k,1}(\tau_k) + b^k_0 \hat{R}_{k,1}(\tau_k)] \\
R_{k,1}(\tau_k) &= A_{k,1}(\mathbf{n}) \times (\tau_k - \mathbf{n}T_c) + A_{k,1}(\mathbf{n}+1) \times ((\mathbf{n}+1)T_c - \tau_k) \\
\hat{R}_{k,1}(\tau_k) &= B_{k,1}(\mathbf{n}) \times (\tau_k - \mathbf{n}T_c) + B_{k,1}(\mathbf{n}+1) \times ((\mathbf{n}+1)T_c - \tau_k)
\end{aligned} \tag{4.23}$$

where it is evident that if $\mathbf{n}$ is given, then $A_{k,1}(\mathbf{n})$, $A_{k,1}(\mathbf{n}+1)$, $B_{k,1}(\mathbf{n})$ and $B_{k,1}(\mathbf{n}+1)$ are all given constants, and that $\hat{R}_{k,1}(\tau_k)$ and $R_{k,1}(\tau_k)$ are linear functions of τ_k. Note that if b^k_{-1} and b^k_0 are also given, then $\chi_{1k}(\tau_k)$ is also a linear function of τ_k.

Thus, for $\mathbf{n}$, b^k_{-1} and b^k_0 given, the conditional pdf of $\chi_{1k}(\tau_k)$ is uniform in the interval $[\chi_{1k}(\mathbf{n}T_c), \chi_{1k}((\mathbf{n}+1)T_c)]$. For notational convenience one defines $\mathbf{y}_k = \chi_{1k}(\tau_k)$.

$$f_{\mathbf{y}_k}(y_k | \mathbf{n}, b^k_{-1}, b^k_0) = \frac{1}{b-a} \qquad \text{for } a < y_k < b, \text{ 0 elsewhere} \tag{4.24}$$

where $a = \max[\chi_{1k}(\mathbf{n}T_c), \chi_{1k}((\mathbf{n}+1)T_c)]$, and $b = \min[\chi_{1k}(\mathbf{n}T_c), \chi_{1k}((\mathbf{n}+1)T_c)]$. For example, where $\mathbf{n} = 2$ in figure 4.2, the cross-correlation function is uniformly distributed on the interval $[-T_c, 15T_c]$.

An exception is where for a given $\mathbf{n}$, b_{-1}^k and b_0^k the cross correlation function value at $\mathbf{n}T_c$ is equal to the cross correlation function value at $(\mathbf{n}+1)T_c$ (such as where $\mathbf{n} = 6$ in figure 4.2). In this case, the cross correlation function has the same value for all τ_k in the interval $[\mathbf{n}T_c, (\mathbf{n}+1)T_c]$, and the conditional pdf is an impulse.

$$f_{y_k}(y_k|\mathbf{n}, b_{-1}^k, b_0^k) = \delta(y_k - \chi_{1k}(\mathbf{n}T_c)) \tag{4.25}$$

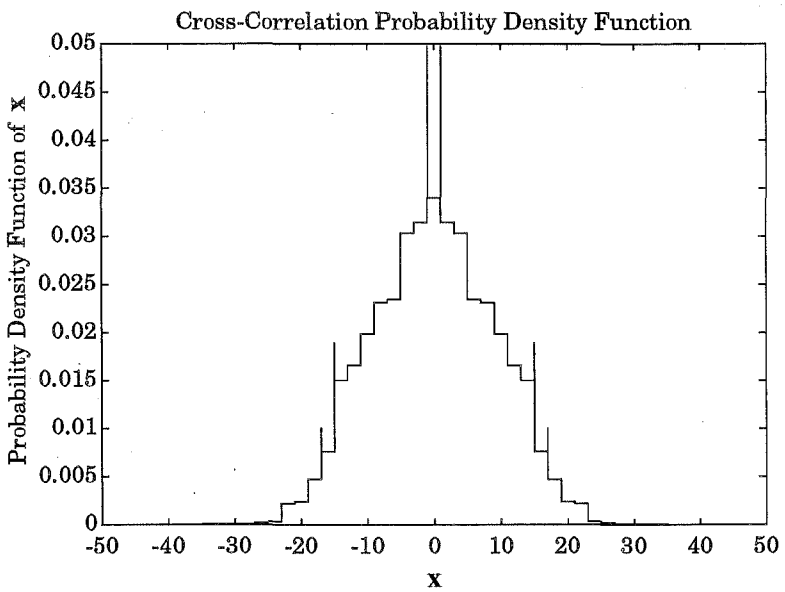

Figure 4.3 An example of the probability density function of the cross-correlation of two 127 chip Gold codes.

Note that b_{-1}^k takes one of 2 values with equal probability, and b_0^k takes one of 2 values with equal probability. This results in 4 possible different combinations, each with equal probability. Thus,

$$f_{y_k}(y_k|\mathbf{n}) = \frac{1}{4}\,[\, f_{y_k}(y_k|\mathbf{n}, b_{-1}^k = 1, b_0^k = 1) + f_{y_k}(y_k|\mathbf{n}, b_{-1}^k = -1, b_0^k = 1) + f_{y_k}(y_k|\mathbf{n}, b_{-1}^k = 1, b_0^k = -1) + f_{y_k}(y_k|\mathbf{n}, b_{-1}^k = -1, b_0^k = -1)]. \tag{4.26}$$

Note also that $\mathbf{n}$ takes one of p values with equal probability. The unconditional pdf of the cross correlation function for a given pair of spreading codes is simply $\frac{1}{p}$ times the sum of the p conditional distributions.

$$f_{y_k}(y_k) = \frac{1}{p}\sum_{\mathbf{n}=0}^{p-1} f_{y_k}(y_k|\mathbf{n}). \tag{4.27}$$

The summation of the various uniform and delta function conditional probability density functions for each $\mathbf{n}$, b_{-1}^k and b_0^k combination results in a staircase-like piecewise constant function, with a finite number of delta functions (see figure 4.3).

An overall average density function for the gold code set is found by averaging the probability densities for each code pair, assuming that each pair is equally likely.

The average probability density for the code set has the same form as the probability density of the cross-correlation function of a pair of codes, with delta functions overlaid on a staircase-like piecewise constant function. This may be mathematically represented as a weighted sum of uniform probability densities, and delta function probability densities. In sections 4.3 and 4.4, for calculations involving the cross-correlation variable general results are initially derived, first replacing the cross-correlation variable with a uniform random variable, and second replacing the cross-correlation variable with a constant. The result for the cross-correlation function probability density is found by summing the general results using the required weights and parameters specified by the average cross-correlation probability density. This provides a per-user interference probability density function $f_{z_k}(z_k)$.

Due to the linear properties of the Fourier transform, the characteristic function of z_k is also found by finding transforms for the two general results, and summing these transforms using the required weights and parameters specified by the average cross-correlation probability density.

4.3 The Ideal Channel Case

The first simplified channel model under investigation is the case where there is no multipath interference or shadowing effects. This case has been studied extensively using a generally accepted approximation method where the multi-user interference is modelled as Gaussian noise [Pursley, 1977]. Improvements to this approximation have also been presented [Morrow, Jr. and Lehnert, 1989; Holtzman, 1992a]. A method involving a combination of exact multi-user interference probability density functions and bounding techniques was presented by Lam [Lam and Özlütürk, 1992]. The analysis method presented here involves exact multi-user interference probability density functions without any need for bounding techniques.

In the single non-fading channel case, the contribution to the decision variable ξ from user k is the product of the cross correlation sample $\chi_{1k}(\tau_k)$ and the cosine of the uniformly distributed random variable ϕ_k. Noting that $\chi_{1,1}(\tau_1) = T$ and $\cos(\phi_1) = 1$,

$$\xi = \frac{A}{2}\sum_{k=1}^{K}\chi_{1k}(\tau_k)\cos(\phi_k) = \frac{AT}{2} + \frac{A}{2}\sum_{k=2}^{K}\chi_{1k}(\tau_k)\cos(\phi_k). \tag{4.28}$$

The system is assumed to be interference limited, so noise terms are omitted. The interference from user k is denoted by $\mathbf{z}_k$, where

$$\mathbf{z}_k = \frac{A}{2}\chi_{1k}(\tau_k)\cos(\phi_k) \tag{4.29}$$

and the total interference $\mathbf{z}$ where

$$\mathbf{z} = \sum_{k=2}^{K}\mathbf{z}_k. \tag{4.30}$$

The approach taken here is to find a generalised result for each of the possible conditional probability density function forms which make up the probability density function of the cross correlation function. The result for the cross-correlation function probability density is found by summing the general results using the required weights and parameters specified by the average cross-correlation probability density.

4.3.1 The Phase Variable

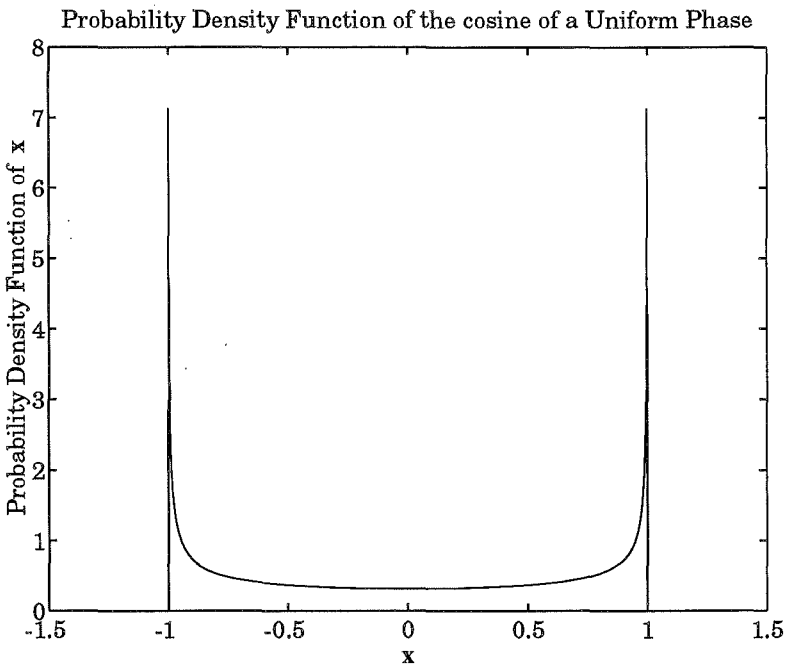

Figure 4.4 The probability density function of the cosine of a uniformly distributed phase variable.

One can see that for each interfering user, the interference $\mathbf{z}_k$ is a function of $\chi_{1k}(\tau_k)$ and $\cos(\phi_k)$. The probability density function of $\chi_{1k}(\tau_k)$ is described in section 4.2.1. The probability density function of the cosine of the uniform phase ϕ_k is found in Papoulis [Papoulis, 1984] (see figure 4.4). If $\mathbf{y}_1 = a\cos(\mathbf{x}_1)$, where $\mathbf{x}_1$ is uniformly distributed in the interval $[0, 2\pi]$ and a is a constant, then

$$f_{\mathbf{y}_1}(y_1) = \frac{1}{\pi a\sqrt{a^2 - y_1^2}} \quad \text{for } |y_1| \leq a, \ 0 \text{ elsewhere.} \tag{4.31}$$

In section 4.2.1 it is noted that, given $\mathbf{n}$, b_{-1}^k and b_0^k, the cross-correlation function $\chi_{1k}(\tau_k)$ is either a uniformly distributed random variable or has a constant. A general result for the probability density function of the product $\chi_{1k}(\tau_k)\cos(\phi_k)$ is found for each of these cases.

4.3.2 The First General Case

For the delta function parts of the average cross-correlation probability density function, which correspond to the cases where the conditional cross-correlation function has a constant value, $\mathbf{z}_k$ is the cosine of a uniform phase variable, scaled by $\frac{A}{2}$ and the constant conditional cross-correlation function value. Thus, for the delta function parts of the average cross-correlation probability density function, the conditional pdf of $\mathbf{z}_k$ takes the form of equation 4.31.

4.3.3 The Second General Case

In the cases where the conditional cross-correlation function has a uniformly distributed value, the interference $\mathbf{z}_k$ is the cosine of a uniformly distributed random variable scaled by $\frac{A}{2}$ and multiplied the uniformly distributed conditional cross-correlation function value. Hence, for a general solution in this case one find the probability density function of the product $\mathbf{y}_2 = \mathbf{x}_1\mathbf{x}_2$, where $\mathbf{x}_1$ is uniformly distributed and $\mathbf{x}_2$ is the cosine of a uniformly distributed phase variable

$$f_{\mathbf{x}_1}(x_1) = \frac{1}{b-a} \quad \text{for } a \le x_1 \le b, \ 0 \text{ elsewhere} \tag{4.32}$$

$$f_{\mathbf{x}_2}(x_2) = \frac{1}{\pi\sqrt{1-x_2^2}} \quad \text{for } |x_2| < 1, \ 0 \text{ elsewhere.} \tag{4.33}$$

The Mellin Convolution method described in Appendix A, Section 5 is used to find the probability density function of the product for this case. Note that

$$\mathbf{y}_2 = \mathbf{x}_1\mathbf{x}_2 \qquad \mathbf{x}_2 = \mathbf{x}_2 \tag{4.34}$$

which may be inversely written

$$\mathbf{x}_1 = \frac{\mathbf{y}_2}{\mathbf{x}_2} \qquad \mathbf{x}_2 = \mathbf{x}_2. \tag{4.35}$$

The derivation of the probability density function of the product differs slightly, depending on the interval of the uniform random variable — more specifically, whether a and b have positive or negative values. The case where $a < 0$ and $b > 0$ is initially considered. In this case, both of the probability density functions have values for both positive and negative arguments, and the probability density functions need to be split into two parts — one to describe the pdf for positive arguments, and one to describe the pdf for negative arguments,

$$f_{\mathbf{x}_1}(x_1) = f^+_{\mathbf{x}_1}(x_1) + f^-_{\mathbf{x}_1}(x_1), \qquad f_{\mathbf{x}_2}(x_2) = f^+_{\mathbf{x}_2}(x_2) + f^-_{\mathbf{x}_2}(x_2). \tag{4.36}$$

It follows from equations 4.32 and 4.33 that

$$f^+_{\mathbf{x}_1}(x_1) = \frac{1}{b-a} \quad \text{for } 0 \le x_1 \le b, \ 0 \text{ elsewhere} \tag{4.37}$$

$$f^-_{\mathbf{x}_1}(x_1) = \frac{1}{b-a} \quad \text{for } a \le x_1 \le 0, \ 0 \text{ elsewhere} \tag{4.38}$$

$$f^{+}_{\mathrm{x}_2}(x_2) = \frac{1}{\pi\sqrt{1-x_2^2}} \quad \text{for } 0 \le x_2 \le 1,\ 0 \text{ elsewhere} \tag{4.39}$$

$$f^{-}_{\mathrm{x}_2}(x_2) = \frac{1}{\pi\sqrt{1-x_2^2}} \quad \text{for } -1 \le x_2 \le 0,\ 0 \text{ elsewhere.} \tag{4.40}$$

In order to have the correct limits in the Mellin convolution integral, one needs to determine the extent of the random variable x_2. For the case when x_1 and x_2 are positive, the maximum value of x_2 is 1 (as defined in equation 4.33). The minimum value of of x_2 is y_2/b, as the maximum value of x_1 id b, and $\mathrm{x}_2 = \mathrm{y}_2/\mathrm{x}_1$. When x_1 and x_2 are negative, the maximum value of x_2 is y_2/a (noting that a has a negative value), and the minimum value is -1. For the case when x_1 is positive and x_2 is negative, the maximum value of x_2 is y_2/b (noting that y_2 has a negative value), and the minimum value is -1. When x_1 is negative and x_2 is positive, the maximum value of x_2 is 1, and the minimum value is y_2/a. Applying these limits, the integrals become

$$\begin{aligned} h^{+}_{\mathrm{y}_2}(y_2) &= \int_0^\infty \frac{1}{x_2} f^{+}_{\mathrm{x}_1}\left(\frac{y_2}{x_2}\right) f^{+}_{\mathrm{x}_2}(x_2)dx_2 + \int_0^\infty \frac{1}{x_2} f^{-}_{\mathrm{x}_1}\left(\frac{y_2}{-x_2}\right) f^{-}_{\mathrm{x}_2}(-x_2)dx_2 \\ &= \frac{1}{\pi(b-a)}\int_{y_2/b}^1 \frac{1}{x_2}\frac{1}{\sqrt{1-x_2^2}}dx_2 + \frac{1}{\pi(b-a)}\int_{-y_2/a}^1 \frac{1}{x_2}\frac{1}{\sqrt{1-x_2^2}}dx_2 \end{aligned} \tag{4.41}$$

$$\begin{aligned} h^{-}_{\mathrm{y}_2}(-y_2) &= \int_0^\infty \frac{1}{x_2} f^{-}_{\mathrm{x}_1}\left(\frac{y_2}{x_2}\right) f^{+}_{\mathrm{x}_2}(x_2)dx_2 + \int_0^\infty \frac{1}{x_2} f^{+}_{\mathrm{x}_1}\left(\frac{y_2}{-x_2}\right) f^{-}_{\mathrm{x}_2}(-x_2)dx_2 \\ &= \frac{1}{\pi(b-a)}\int_{-y_2/a}^1 \frac{1}{x_2}\frac{1}{\sqrt{1-x_2^2}}dx_2 + \frac{1}{\pi(b-a)}\int_{y_2/b}^1 \frac{1}{x_2}\frac{1}{\sqrt{1-x_2^2}}dx_2. \end{aligned} \tag{4.42}$$

The general solution to the integral is given by

$$\int \frac{1}{u}\frac{1}{\sqrt{1-u^2}}du = -\frac{1}{2}\ln\frac{1-\sqrt{1-u^2}}{1+\sqrt{1-u^2}} \quad \text{for } |u| \le 1,\ 0 \text{ elsewhere} \tag{4.43}$$

and thus

$$\int_{y_2/b}^1 \frac{1}{x_2}\frac{1}{\sqrt{1-x_2^2}}dx_2 = -\frac{1}{2}\ln\frac{1-\sqrt{1-\frac{y_2^2}{b^2}}}{1+\sqrt{1-\frac{y_2^2}{b^2}}} \quad \text{for } |y_2| \le |b|,\ 0 \text{ elsewhere} \tag{4.44}$$

$$\int_{-y_2/a}^1 \frac{1}{x_2}\frac{1}{\sqrt{1-x_2^2}}dx_2 = -\frac{1}{2}\ln\frac{1-\sqrt{1-\frac{y_2^2}{a^2}}}{1+\sqrt{1-\frac{y_2^2}{a^2}}} \quad \text{for } |y_2| \le |a|,\ 0 \text{ elsewhere.} \tag{4.45}$$

A graphical representation of equation 4.43 may be seen in figure 4.5.

Secondly consider the case where $a > 0$, $b > 0$ and $a < b$. In this case, the density of x_2 has values for positive and negative arguments, so this density function needs to be split into two parts — one to describe the pdf for positive arguments, and one to describe the pdf for negative arguments.

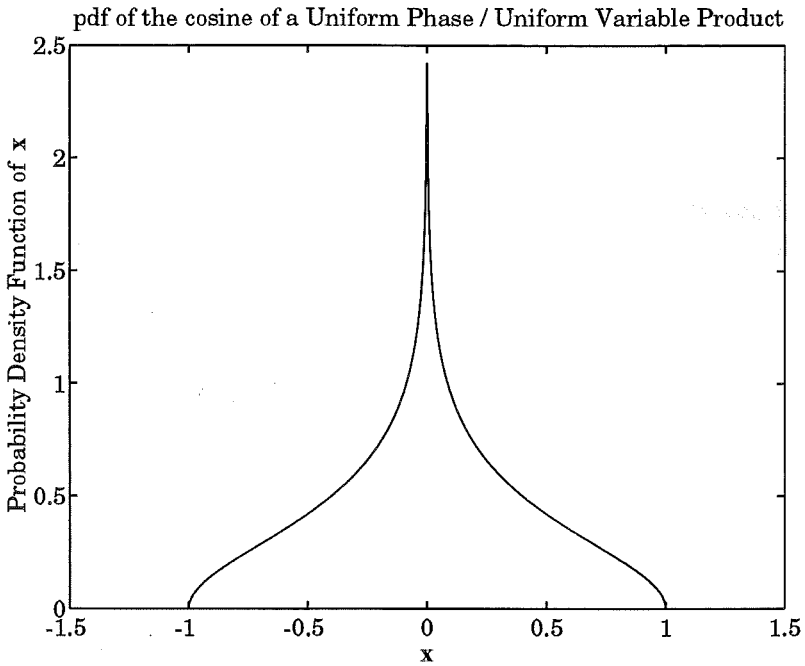

Figure 4.5 The probability density function of the product of a uniformly distributed random variable and the cosine of a uniformly distributed phase variable.

It follows from equations 4.32 and 4.33 that

$$f^{+}_{\mathbf{x}_2}(x_2) = \frac{1}{\pi\sqrt{1-x_2^2}} \quad \text{for } 0 \le x_2 \le 1,\ 0 \text{ elsewhere} \tag{4.46}$$

$$f^{-}_{\mathbf{x}_2}(x_2) = \frac{1}{\pi\sqrt{1-x_2^2}} \quad \text{for } -1 \le x_2 \le 0,\ 0 \text{ elsewhere.} \tag{4.47}$$

Again the extent of the random variable $\mathbf{x}_2$ is determined. When $\mathbf{x}_2$ is positive, the maximum value of $\mathbf{x}_2$ is y_2/a and the minimum value of $\mathbf{x}_2$ is y_2/b. When $\mathbf{x}_2$ is negative, the maximum value of $\mathbf{x}_2$ is y_2/a (noting that y_2 has a negative value), and the minimum value is y_2/b. Applying these limits, one finds that

$$h^{+}_{\mathbf{y}_2}(y_2) = \frac{1}{\pi(b-a)} \int_{y_2/b}^{y_2/a} \frac{1}{x_2} \frac{1}{\sqrt{1-x_2^2}} dx_2 \tag{4.48}$$

$$h^{-}_{\mathbf{y}_2}(-y_2) = \frac{1}{\pi(b-a)} \int_{y_2/b}^{y_2/a} \frac{1}{x_2} \frac{1}{\sqrt{1-x_2^2}} dx_2. \tag{4.49}$$

Solving and combining these integrals gives

$$h_{\mathbf{y}_2}(y_2) = \int_{y_2/b}^{y_2/a} \frac{1}{x_2} \frac{1}{\sqrt{1-x_2^2}} dx_2$$

$$= \frac{1}{2} \ln \frac{1-\sqrt{1-\frac{y_2^2}{b^2}}}{1+\sqrt{1-\frac{y_2^2}{b^2}}} \quad \text{for } |y_2| \le |b|,\ 0 \text{ elsewhere}$$

$$-\frac{1}{2}\ln\frac{1-\sqrt{1-\frac{y_2^2}{a^2}}}{1+\sqrt{1-\frac{y_2^2}{a^2}}} \quad \text{for } |y_2| \leq |a|,\ 0 \text{ elsewhere.} \tag{4.50}$$

A similar result is derived for $a < 0, b < 0$ and $a < b$. To summarise:

$$h_{y_2}(y_2) = \frac{1}{\pi(b-a)}[g_1(a,y_2) + g_1(b,y_2)] \quad \text{for } a < 0, b > 0 \tag{4.51}$$

$$h_{y_2}(y_2) = \frac{1}{\pi(b-a)}[g_1(b,y_2) - g_1(a,y_2)] \quad \text{for } a > 0, b > 0, a < b \tag{4.52}$$

$$h_{y_2}(y_2) = \frac{1}{\pi(b-a)}[g_1(a,y_2) - g_1(b,y_2)] \quad \text{for } a < 0, b < 0, a < b \tag{4.53}$$

where

$$g_1(u,v) = -\frac{1}{2}\ln\frac{1-\sqrt{1-\frac{v^2}{u^2}}}{1+\sqrt{1-\frac{v^2}{u^2}}} \quad \text{for } |v| \leq |u|,\ 0 \text{ elsewhere.} \tag{4.54}$$

Thus, for the uniformly distributed parts of the probability density function of the cross-correlation function, the conditional probability density function of $\mathbf{z}_k$ takes the form of one of equations 4.51, 4.52 or 4.53. The values of a and b are derived from the arbitrary scaling $\frac{A}{2}$ and the limits of the uniformly distributed part in question.

4.3.4 The Received Signal from the Desired User

For the case where there is no multipath, the received signal for the desired user is a constant, $\mathbf{X} = ATb_0^1/2$. Thus, the average probability of error is simply the complementary distribution function of the total interference evaluated at $ATb_0^1/2$.

4.3.5 Numerical Calculation of the Probability of Error

Now that the analytical framework has been described, a suitable method for obtaining numerical results is presented. The main considerations in this undertaking are simplicity and computational efficiency.

Firstly, the characteristic function of the per-user interference (see section 4.2) is found. The method employed to numerically calculate the average probability of error, described later in this section, only requires that the characteristic function of the per-user interference is known at equally spaced points.

Where an analytical Fourier transform is available for the general result, it is used to numerically calculate equally spaced transform values. In cases where there is no analytical Fourier transform available for the general result, probability density function values are numerically calculated using the analytical form of the general result, and equally spaced transform values are determined using a discrete Fourier transform. For the single non-fading channel case, the Fourier transform of the general result of equation 4.31 is given by [Oberhettinger, 1973]

$$\frac{1}{\pi a\sqrt{a^2-t^2}} \rightleftharpoons J_0(af) \tag{4.55}$$

where $J_0(af)$ is the zero order Bessel function, and

$$J_0(u) = \sum_{n=1}^{\infty}(-1)^n[n!\Gamma(n+1)]^{-1}\left(\frac{u}{2}\right)^{2n} \tag{4.56}$$

Equation 4.55 describes the characteristic function for the first general result. For the second general result, the form of the conditional probability density function is more complicated and a discrete Fourier transform is used. A vector of equally spaced transform values is calculated for each part of the average probability density function for the code set. These numerical values are summed using the required weights specified by the average cross-correlation probability density, giving equally spaced values for the characteristic function of the per-user interference $\varphi_{\mathbf{z}_k}(\nu)$.

For the single non-fading channel case, the average probability of error described in equation 4.22 becomes

$$P_e = P\left\{\mathbf{z} > \frac{AT}{2}\right\} = \int_{\frac{AT}{2}}^{-\infty} f_{\mathbf{z}}(z)dz \tag{4.57}$$

which is equivalent to the complementary distribution function of the interference $\mathbf{z}$, evaluated at $\frac{AT}{2}$.

A numerical series expansion technique is used to determine the complementary distribution function $G_{\mathbf{z}}(z)$ of $\mathbf{z}$ from the equally spaced characteristic function points [Beaulieu, 1990], also described in Appendix A, section 6. This gives

$$G_{\mathbf{z}}(z) = \frac{1}{2} + \sum_{n=1}^{\infty}\frac{\exp\left(-j\frac{2\pi nz}{T}\right)\prod_{k=2}^{K}\varphi_{\mathbf{z}_k}\left(\frac{2\pi n}{T}\right) - \exp\left(j\frac{2\pi nz}{T}\right)\prod_{k=2}^{K}\varphi_{\mathbf{z}_k}\left(\frac{-2\pi n}{T}\right)}{n\pi j} \tag{4.58}$$

where $\varphi_{\mathbf{z}_k}(\nu) = E\left[e^{j\nu\mathbf{z}_k}\right]$ is the characteristic function of the random variable $\mathbf{z}_k$. For inclusion of a noise term, the characteristic function of the noise would be included in the characteristic function products in equation 4.58.

The number of characteristic function terms required for the summation in equation 4.58 to ensure good accuracy depends on the value of z and how smooth the probability density function is. This method can require many terms for spiky probability density functions or where z is large, and therefore $G_{\mathbf{z}}(z)$ is very small. Fortunately, once the number of users is greater than 4, only a few hundred terms are required for good accuracy. Generally, the complementary distribution function calculation is computationally much more efficient than the initial calculation of the probability density functions.

4.3.6 Comparisons with Previously Published Approximations

The single non-fading channel case has been studied much already, and it is useful to compare the analytical result with various approximations.

A common approximation [Pursley, 1977] assumes that the inter user interference has a Gaussian distribution. The error performance for this approximation is given

by

$$P_e = Q\left[\sqrt{\frac{3p}{K-1}}\right] \tag{4.59}$$

where K is the number of users, and p is the number of chips in one period of the spreading sequence and

$$Q(x) = \frac{1}{2\pi}\int_x^\infty e^{u^2/2}du.$$

This approximation was found to be close for large numbers of users, but optimistic for small numbers of users.

Morrow presented an improved Gaussian approximation [Morrow, Jr. and Lehnert, 1989] which is based on the observation that the multiple access interference is approximately Gaussian, conditioned on certain random variables. An accurate approximation to the bit error probability is given by

$$P_e = \int_0^\infty Q\left[\frac{p}{\sqrt{\Psi}}\right] f_\Psi(\Psi)d\Psi \tag{4.60}$$

where Ψ is the conditional variance of the multiple access interference. The integration over the probability density function $f_\Psi(\Psi)$ removes the conditioning. Significant improvement in accuracy is shown, though this method is computationally expensive.

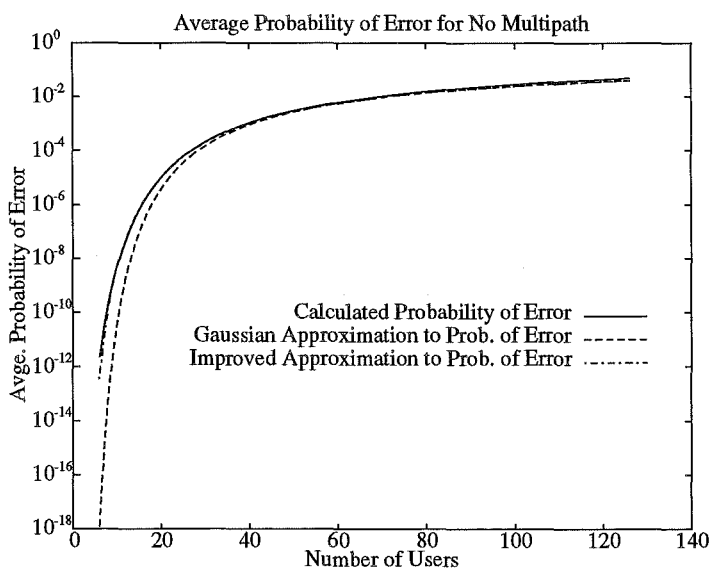

Figure 4.6 Average probability of error for case where there is no multipath and $p = 127$. The standard Gaussian approximation, and an improved approximation are plotted for comparison.

Holtzman [Holtzman, 1992a] published a simpler improved approximation, which retains much of the accuracy, without the computational expense. This was achieved by noting that equation 4.60 is an expected value calculation and replacing it with an approximation to the expected value. Further simplifications were published in

[Holtzman, 1992b]. The resultant approximate average probability of error is given by

$$P_e = \frac{2}{3}Q\left[\sqrt{\frac{3p}{K-1}}\right] + \frac{1}{6}Q\left[\frac{3p}{\sqrt{(K-1)p/3+\sqrt{3}\sigma}}\right] + \frac{1}{6}Q\left[\frac{3p}{\sqrt{(K-1)p/3-\sqrt{3}\sigma}}\right] \tag{4.61}$$

where $\sigma = p\sqrt{(23/360)(K-1)}$.

In figure 4.6, the standard Gaussian approximation (equation 4.59) and the simplified improved approximation (equation 4.61) were plotted against the analytical result. The simplified improved approximation is seen to be very close to the analytical result.

4.4 The Flat Fading Channel Case

The second simplified channel model case is the flat fading multipath case. In this case the maximum difference in arrival time between the first path from user k and the last path from user k is less than one chip period, T_c s, so that all the paths arrive within one chip period. The result is a single effective complex Gaussian path with a Rayleigh distributed gain and a phase offset uniformly distributed in the interval $[-\pi, \pi]$. The contribution to the decision variable ξ from the kth interfering user is the product of the cross correlation function $\chi_{1k}(\tau_k)$ and a random variable with a Gaussian distribution $\mathbf{G}_k$, so that

$$\xi = \frac{A}{2}\sum_{k=1}^{K}\mathbf{V}_{1k}\chi_{1k}(\tau_{1k})\cos(\Phi_{1k}) = \frac{A}{2}\left[\mathbf{V}_{1,1}b_0^1 T + \sum_{k=2}^{K}\mathbf{G}_{1k}\chi_{1k}(\tau_{1k})\right] \tag{4.62}$$

where $\mathbf{G}_{1k} = \mathbf{V}_{1k}\cos(\Phi_{1k})$ [Papoulis, 1984].

For the desired user 1, the autocorrelation $\chi_{1,1}(\tau_{1,1}) = NT_c = T$, and $\Phi_{1,1} = 0$. Thus, the signal from user 1 is $\frac{AT}{2}\mathbf{V}_{1,1}b_0^1$.

$$\xi = \frac{AT}{2}\mathbf{V}_{1,1}b_0^1 + \frac{A}{2}\sum_{k=2}^{K}\mathbf{G}_{1k}\chi_{1k}(\tau_{1k}) = \frac{AT}{2}\mathbf{V}_{1,1}b_0^1 + \sum_{k=2}^{K}\mathbf{z}_k \tag{4.63}$$

where $\mathbf{z}_k = \frac{A}{2}\mathbf{G}_{1k}\chi_{1k}(\tau_{1k})$.

Following a method similar to that used in the non-fading channel case, general results for the uniformly distributed and constant valued parts of the cross-correlation function are derived.

4.4.1 The First General Case

For the delta function parts of the average cross-correlation probability density function, which correspond to the cases where the conditional cross-correlation function has a constant value, the interference $\mathbf{z}_k$ is a Gaussian random variable $\mathbf{G}_{1k}$ scaled by $\frac{A}{2}$ and the constant conditional cross-correlation function value. Thus, for the delta function parts of the average cross-correlation probability density function, the conditional pdf of $\mathbf{z}_k$ has a Gaussian probability density function.

4.4.2 The Second General Case

The second general case is where the conditional cross-correlation function has a uniformly distributed value. In this case, the interference $\mathbf{z}_k$ is a Gaussian random variable $\mathbf{G}_{1k}$ scaled by $\frac{A}{2}$ and multiplied by the uniformly distributed conditional cross-correlation function value. Thus the probability density function of the product $\mathbf{y}_3 = \mathbf{x}_1\mathbf{x}_3$ is derived, where $\mathbf{x}_3$ has a Gaussian distribution with variance σ^2 and $\mathbf{x}_1$ is uniformly distributed in the interval $[a, b]$

$$f_{\mathbf{x}_1}(x_1) = \frac{1}{b-a} \qquad \text{for } a \le x \le b, \text{ 0 elsewhere} \tag{4.64}$$

$$f_{\mathbf{x}_3}(x_3) = \frac{1}{\sigma\sqrt{2\pi}} e^{-x_3^2/2\sigma^2}. \tag{4.65}$$

Again the Mellin convolution method is used to find the probability density function of the product, as noted in section 5 of Appendix A. The density function is divided into its positive and negative parts, the product density derived for each part, and these combined to give the complete product density. Results are initially derived for the case where $a < 0$ and $b > 0$.

$$f^+_{\mathbf{x}_1}(x_1) = \frac{1}{b-a} \qquad \text{where } 0 \le x_1 \le b, \text{ 0 elsewhere} \tag{4.66}$$

$$f^-_{\mathbf{x}_1}(x_1) = \frac{1}{b-a} \qquad \text{where } a \le x_1 \le 0, \text{ 0 elsewhere} \tag{4.67}$$

$$f^+_{\mathbf{x}_3}(x_3) = \frac{1}{\sigma\sqrt{2\pi}} e^{-x_3^2/2\sigma^2} \qquad \text{where } 0 \le x_3 \le \infty, \quad \text{0 elsewhere} \tag{4.68}$$

$$f^-_{\mathbf{x}_3}(x_3) = \frac{1}{\sigma\sqrt{2\pi}} e^{-x_3^2/2\sigma^2} \qquad \text{where } -\infty \le x_3 \le 0, \quad \text{0 elsewhere} \tag{4.69}$$

Firstly the result for the positive part of the probability density function of the product is derived,

$$h^+_{\mathbf{y}_3}(y_3) = \int_0^\infty \frac{1}{x_3} f^+_{\mathbf{x}_1}\left(\frac{y_3}{x_3}\right) f^+_{\mathbf{x}_3}(x_3)dx_3 + \int_0^\infty \frac{1}{x_3} f^-_{\mathbf{x}_1}\left(\frac{y_3}{-x_3}\right) f^-_{\mathbf{x}_3}(-x_3)dx_3. \tag{4.70}$$

Consider the limits of the integration for the first integral in equation 4.70 in the case where $a < 0$ and $b > 0$. The maximum value $\mathbf{x}_3$ can take is ∞. The minimum value $\mathbf{x}_3$ can take is $\mathbf{y}_3/b$, due to the fact that the maximum value of $\mathbf{x}_1$ is b and $\mathbf{x}_3 = \mathbf{y}_3/\mathbf{x}_1$. Similarly, one finds the limits of the integration for the second integral in equation 4.70. The maximum value $-\mathbf{x}_3$ can take is ∞ and the minimum value $-\mathbf{x}_3$ can take is $-\mathbf{y}_3/a$, due to the fact that the maximum value of $-\mathbf{x}_1$ is $-a$ and $\mathbf{x}_3 = \mathbf{y}_3/\mathbf{x}_1$. Substituting these values results in

$$h^+_{\mathbf{y}_3}(y_3) = \frac{1}{(b-a)\sigma\sqrt{2\pi}} \left[\int_{\frac{y_3}{b}}^\infty \frac{e^{-x_3^2/2\sigma^2}}{x_3} dx_3 + \int_{-\frac{y_3}{a}}^\infty \frac{e^{-x_3^2/2\sigma^2}}{x_3} dx_3 \right]. \tag{4.71}$$

In order to simplify the expression, one defines $u_1 = x_3^2/2\sigma^2$, so that $x_3 = \sigma\sqrt{2u_1}$ and $dx_3 = (\sigma/\sqrt{2u_1})du_1$, and finds the integrals in terms of u_1.

$$\frac{1}{(b-a)\sigma\sqrt{2\pi}} \int_{\frac{y_3}{b}}^\infty \frac{e^{-x_3^2/2\sigma^2}}{x_3} dx_3 = \frac{1}{(b-a)\sigma\sqrt{2\pi}} \int_{\frac{1}{2}\left(\frac{y_3}{b\sigma}\right)^2}^\infty \frac{e^{-u_1}}{\sigma\sqrt{2u_1}} \frac{\sigma}{\sqrt{2u_1}} du_1$$

$$= \frac{1}{(b-a)2\sigma\sqrt{2\pi}} \int_{\frac{1}{2}\left(\frac{y_3}{b\sigma}\right)^2}^{\infty} \frac{e^{-u_1}}{u_1} du_1$$

$$= \frac{1}{(b-a)2\sigma\sqrt{2\pi}} E_1\left[\frac{1}{2}\left(\frac{y_3}{b\sigma}\right)^2\right] \tag{4.72}$$

where $E_1(x)$ is the exponential integral, defined by

$$E_1(x) = \int_x^{\infty} \frac{e^{-u}}{u} du.$$

Similarly

$$\frac{1}{(b-a)\sigma\sqrt{2\pi}} \int_{\frac{y_3}{-a}}^{\infty} \frac{e^{-x_3^2/2\sigma^2}}{x_3} dx_3 = \frac{1}{(b-a)2\sigma\sqrt{2\pi}} E_1\left[\frac{1}{2}\left(\frac{y_3}{a\sigma}\right)^2\right] \tag{4.73}$$

and hence

$$h^+_{y_3}(y_3) = \frac{1}{(b-a)2\sigma\sqrt{2\pi}} \left(E_1\left[\frac{1}{2}\left(\frac{y_3}{b\sigma}\right)^2\right] + E_1\left[\frac{1}{2}\left(\frac{y_3}{a\sigma}\right)^2\right]\right) \begin{matrix} \text{where } y_3 \geq 0, \\ 0 \text{ elsewhere.} \end{matrix} \tag{4.74}$$

A similar derivation is followed for the negative values of y_3, which leads to

$$h^-_{\mathbf{y}}(-y_3) = \frac{1}{(b-a)\sigma\sqrt{2\pi}} \left[\int_{\frac{y_3}{b}}^{\infty} \frac{e^{-x_3^2/2\sigma^2}}{x_3} dx_3 + \int_{-\frac{y_3}{a}}^{\infty} \frac{e^{-x_3^2/2\sigma^2}}{x_3} dx_3\right]$$

$$= \frac{1}{(b-a)2\sigma\sqrt{2\pi}} \left(E_1\left[\frac{1}{2}\left(\frac{y_3}{b\sigma}\right)^2\right] + E_1\left[\frac{1}{2}\left(\frac{y_3}{a\sigma}\right)^2\right]\right) \begin{matrix} \text{where } -y_3 \geq 0, \\ 0 \text{ elsewhere} \end{matrix}$$

or equivalently

$$h^-_{y_3}(y_3) = \frac{1}{(b-a)2\sigma\sqrt{2\pi}} \left(E_1\left[\frac{1}{2}\left(\frac{y_3}{b\sigma}\right)^2\right] + E_1\left[\frac{1}{2}\left(\frac{y_3}{a\sigma}\right)^2\right]\right) \begin{matrix} \text{where } y_3 \leq 0, \\ 0 \text{ elsewhere.} \end{matrix} \tag{4.75}$$

To find the overall probability density function of $\mathbf{y}_3$ $h^+_{y_3}(y_3)$ and $h^-_{\mathbf{y}}(-y)$ from equations 4.74 and 4.75 are combined giving

$$h_{y_3}(y_3) = \frac{1}{(b-a)2\sigma\sqrt{2\pi}} \left(E_1\left[\frac{1}{2}\left(\frac{y_3}{b\sigma}\right)^2\right] + E_1\left[\frac{1}{2}\left(\frac{y_3}{a\sigma}\right)^2\right]\right). \tag{4.76}$$

Similar derivations are performed for $a < 0, b < 0$ and $a > 0, b > 0$. Where $a > 0, b > 0, a < b$,

$$h_{y_3}(y_3) = \frac{1}{(b-a)2\sigma\sqrt{2\pi}} \left(E_1\left[\frac{1}{2}\left(\frac{y_3}{b\sigma}\right)^2\right] - E_1\left[\frac{1}{2}\left(\frac{y_3}{a\sigma}\right)^2\right]\right) \tag{4.77}$$

and where $a < 0, b < 0, a < b$,

$$h_{y_3}(y_3) = \frac{1}{(b-a)2\sigma\sqrt{2\pi}} \left(E_1\left[\frac{1}{2}\left(\frac{y_3}{a\sigma}\right)^2\right] - E_1\left[\frac{1}{2}\left(\frac{y_3}{b\sigma}\right)^2\right]\right). \tag{4.78}$$

Thus, for the uniformly distributed parts of the probability density function of the cross-correlation function, the conditional probability density function of $\mathbf{z}_k$ takes the form of one of equations 4.76, 4.77 or 4.78. The values of a and b are derived from the arbitrary scaling $\frac{A}{2}$ and the limits of the uniformly distributed part in question. The value of σ is derived from the variance of $\mathbf{G}_{1k}$.

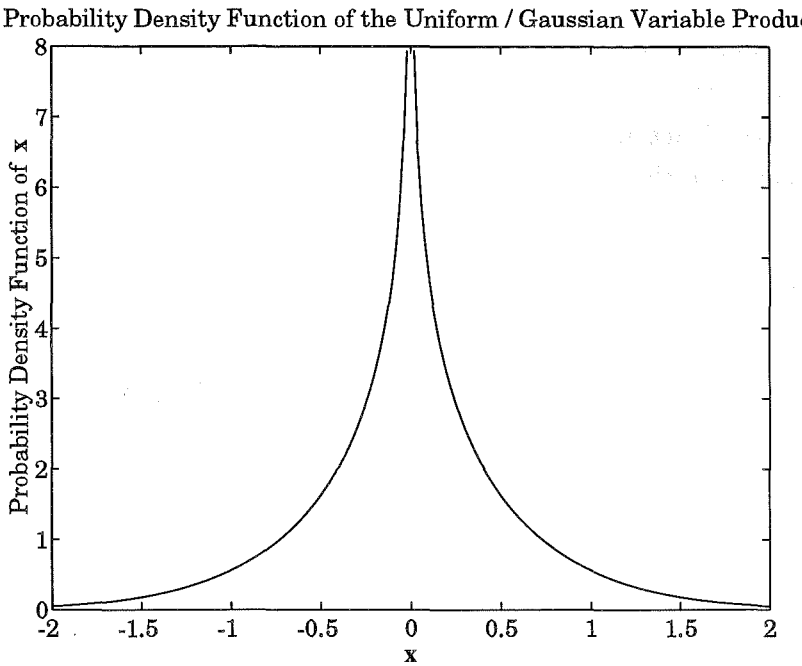

Figure 4.7 Probability density function of a the product of a random variable which is uniformly distributed in the interval [0, 1] multiplied by a random variable which has a Gaussian distribution.

4.4.3 The Received Signal from the Desired User

In the flat fading case, the desired signal from user 1 travels via a flat fading channel, and thus the received signal level, $\mathbf{X} = \frac{AT}{2}\mathbf{V}_{1,1}$ (assuming $b_0^1 = +1$), is a random variable with a Rayleigh distribution. To calculate the average probability of error one finds the average probability that the interference is greater than the desired signal, noting that both the interference and the desired received signal are random variables (see equation 4.22).

4.4.4 Numerical Calculation of the Probability of Error

As in the single non-fading channel case, the of characteristic function is used to efficiently calculate convolution of probability density functions of the interfering users. Once again one begins by finding the characteristic function for each of the general results.

For the case where the conditional cross-correlation function has a constant value, the conditional probability density function is a Gaussian probability density function. The characteristic function of a Gaussian random variable also has a Gaussian form [Oberhettinger, 1973].

The Characteristic Function for the Second General Case

For the second general case, the form of the conditional probability density function is more complicated, though an analytical solution may be found. For initial simplicity, the characteristic function is derived for the case where the conditional probability density function is in the form of equation 4.76, and $a = 0$. Thus

$$f_1(x_1) = \frac{1}{b}, \text{ for } 0 \leq x_1 \leq b$$
$$f_3(x_3) = \frac{1}{\sqrt{2\pi}\sigma} e^{-x_3^2/2\sigma^2} \tag{4.79}$$

and

$$h(y_3) = \frac{1}{b} \int_{y_3/b}^{\infty} \frac{1}{x_3} \cdot \frac{e^{-x_3^2/2\sigma^2}}{\sigma\sqrt{2\pi}} dx_3 \tag{4.80}$$

One needs to find the Fourier transform of the integral in equation 4.80. One begins this process with the Fourier transforms of the terms within the integral:

$$\frac{e^{-t^2/2\sigma^2}}{\sigma\sqrt{2\pi}} \rightleftharpoons e^{-f^2\sigma^2/2} \tag{4.81}$$

$$\frac{1}{t} \rightleftharpoons -j\pi \text{sgn} f \tag{4.82}$$

Next the Fourier transform of the product of the two functions is found. The Fourier transform of the product is equivalent to the convolution the two Fourier transforms [Papoulis, 1984].

$$\begin{aligned}
\frac{e^{-t^2/2\sigma^2}}{t\sigma\sqrt{2\pi}} &\rightleftharpoons \int_{-\infty}^{\infty} -j\pi \text{sgn}(f-\lambda).e^{-\lambda^2\sigma^2/2} d\lambda \\
&= -j\pi \left[\int_{-\infty}^{f} e^{-\lambda^2\sigma^2/2} d\lambda - \int_{f}^{\infty} e^{-\lambda^2\sigma^2/2} d\lambda \right] \\
&= -j\pi \left[\int_{-\infty}^{f} e^{-\lambda^2\sigma^2/2} d\lambda - \int_{-\infty}^{-f} e^{-\lambda^2\sigma^2/2} d\lambda \right] \\
&= -j\pi \left[\int_{-f}^{f} e^{-\lambda^2\sigma^2/2} d\lambda \right] \\
&= -j2\pi \left[\int_{0}^{f} e^{-\lambda^2\sigma^2/2} d\lambda \right] \\
&= -j2\pi . \frac{\sqrt{2\pi}}{2\sigma} \text{erf}\left(\frac{f\sigma}{\sqrt{2}} \right)
\end{aligned} \tag{4.83}$$

where

$$\text{erf}(u) = \frac{2}{\sqrt{\pi}} \int_0^u e^{-t^2} dt.$$

Finally the integration from equation 4.80 is included. Using the Fourier integral property stated as

$$\int_{-\infty}^{t} g(u) du \rightleftharpoons \frac{1}{j2\pi f} G(f) + \frac{G(0)}{2} \delta(f) \tag{4.84}$$

one finds that

$$\int_{-\infty}^{t} \frac{e^{-u^2/2\sigma^2}}{u\sigma\sqrt{2\pi}} du \rightleftharpoons \frac{1}{j2\pi f} \cdot -j2\pi \cdot \frac{\sqrt{2\pi}}{2\sigma} \text{erf}\left(\frac{f\sigma}{\sqrt{2}}\right)$$
$$= -\frac{\sqrt{2\pi}}{f2\sigma} \text{erf}\left(\frac{f\sigma}{\sqrt{2}}\right) \tag{4.85}$$

noting that $G(0) = 0$ because the function in the integral is odd. Being an odd function,

$$\int_{-\infty}^{t} \frac{e^{-u^2/2\sigma^2}}{u\sigma\sqrt{2\pi}} dt = -\int_{t}^{\infty} \frac{e^{-u^2/2\sigma^2}}{u\sigma\sqrt{2\pi}} du \tag{4.86}$$

giving the result

$$\int_{t}^{\infty} \frac{e^{-u^2/2\sigma^2}}{u\sigma\sqrt{2\pi}} dt \rightleftharpoons \frac{\sqrt{2\pi}}{f2\sigma} \text{erf}\left(\frac{f\sigma}{\sqrt{2}}\right). \tag{4.87}$$

The required parameters values are substituted, giving us

$$\frac{1}{2b\sigma\sqrt{2\pi}} E_1\left[\frac{1}{2}\left(\frac{y}{b\sigma}\right)^2\right] = \frac{1}{b\sigma\sqrt{2\pi}} \int_{y/b}^{\infty} \frac{e^{-t^2/2\sigma^2}}{t} dt \rightleftharpoons \frac{\sqrt{2\pi}}{bf2\sigma} \text{erf}\left(\frac{bf\sigma}{\sqrt{2}}\right). \tag{4.88}$$

Calculation of the Average Probability of Error

Once again, a vector of equally spaced transform values is calculated for each part of the average probability density function for the code set. These numerical values are summed using the required weights specified by the average cross-correlation probability density, giving equally spaced values for the characteristic function of the per-user interference $\varphi_{\mathbf{z}_k}(\nu)$.

For the flat fading channel case, the average probability of error is described in equation 4.22, which is repeated here for convenience,

$$P_e = E[G_{\mathbf{z}}(X)] = \int_{-\infty}^{\infty} G_{\mathbf{z}}(X) f_{\mathbf{X}}(X) dX.$$

Again, a numerical series expansion technique is used to determine the complementary distribution function $G_{\mathbf{z}}(z)$ of $\mathbf{z}$ from the equally spaced characteristic function points [Beaulieu, 1990] (see equation 4.58). The average probability of error integral in equation 4.22 is numerically evaluated, using an adaptive recursive Newton Cotes 8 panel rule.

4.4.5 Results for the Flat Fading Case

The average probability of error for the case of the single flat fading channel may be seen in figure 4.8. The result for the single non-fading channel is also plotted for comparison. One can see a large degradation in performance for smaller numbers of users due to the multipath fading of the desired signal energy.

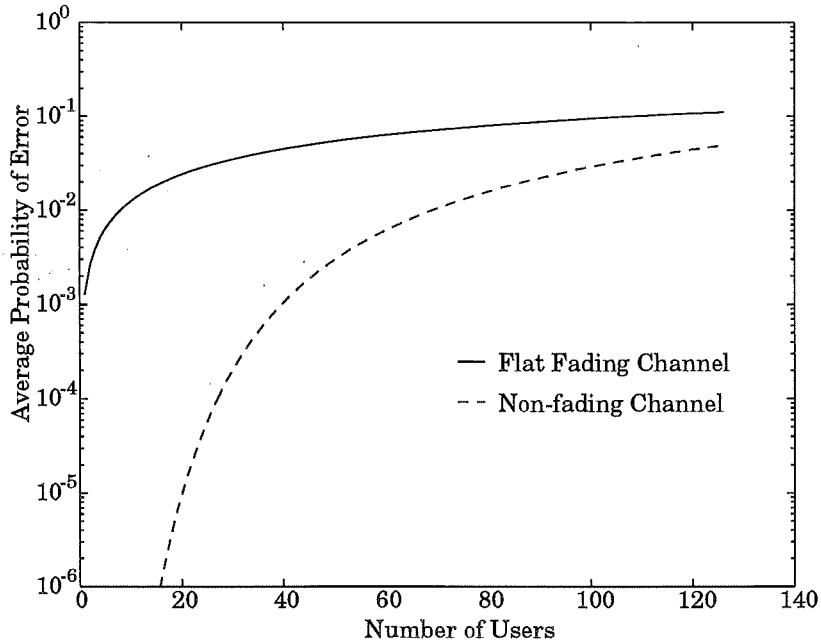

Figure 4.8 A comparison of the average probability of error performance for the flat fading channel case compared with the non-fading channel case, for $p = 127$.

Chapter 5

THE MULTIPLE FADING PATHS CASE

In the previous chapter the system model for the overall analysis and system performance evaluations for the single path non-fading case and a single flat fading path model was presented. In this chapter the system performance evaluation for the multiple fading paths case is presented, using the multipath channel model described in chapter 4. In this channel model the continuous profile of the multiple paths is modelled by a discrete tapped delay line. The taps are spaced in time at the chip period T_c, which is the time resolution of the spread spectrum system. Each of the L taps has a Rayleigh distributed gain, where the average gain of each path is specified by the chosen gain-delay profile. In the multiple fading paths case the receiver sees multiple versions of the signals from each of the users, including the desired user. It is assumed that the system employs an ideal selection diversity algorithm, where at any given moment the receiver is locked to the signal from the desired user which travelled via the path with the maximum gain. As described in equation 4.8, the contribution to the decision variable ξ from the lth path of the kth interfering user is the cross correlation function $\chi_{1k}(\tau_{lk})$ multiplied by a random gain variable $\mathbf{V}_{lk}$ having a Rayleigh distribution and the cosine of the random phase variable Φ_{lk}, and thus

$$\begin{aligned}\xi &= \frac{A}{2}\sum_{k=1}^{K}\sum_{l=1}^{L}\mathbf{V}_{lk}\chi_{1k}(\tau_{lk})\cos(\Phi_{lk}) \\ &= \frac{A}{2}\left[\sum_{l=1}^{L}\mathbf{V}_{l,1}\chi_{1,1}(\tau_{l,1})\cos(\Phi_{l,1}) + \sum_{k=2}^{K}\sum_{l=1}^{L}\mathbf{G}_{lk}\chi_{1k}(\tau_{lk})\right] \end{aligned} \tag{5.1}$$

where $\mathbf{G}_{lk}$ has a Gaussian distribution.

In the multiple fading paths case there are complications not evident in the two simplified channel models. Firstly, due to the multiple paths from the desired user to the receiver and the use of selection diversity, all paths but the path with the maximum gain from the desired user add to the interference. This is a form of Inter-Symbol Interference (ISI), though unlike ISI in TDMA, the interference power from each of the non-maximum paths is much lower than that from the path with the maximum gain, as the signals from the non-maximum paths are not synchronised to the despreading code or the carrier phase at the receiver. These and other issues arising from the selection diversity algorithm are addressed in section 5.1.

Another complication is that the random variables contributing to the interference are no longer all independent. The signals from each effective path are spaced at regular intervals in time, and thus the cross-correlation values for each path are not independent of each other. This implies that for any given user, the signals from each of the paths cannot be simply summed as independent random variables. However, the individual users are still independent of each other.

Statistical descriptions for both the desired and interfering signals from the desired user are derived, followed by derivations for the interference from the other users. The method for finding the average probability of error for the multiple fading paths case is then described. Finally, system performance is presented for a selection of different gain-delay profiles.

5.1 The Signal from the Desired User

In the multiple fading paths case the receiver is assumed to employ an ideal selection diversity algorithm, where at any given moment in time the receiver is locked to the signal from the path with the maximum gain. Signals which travel via the $L-1$ other paths are seen as uncorrelated interference at the receiver.

To calculate the system performance one needs to find the statistical description of the received signal and interference signals due to the multiple paths from the desired user. The probability density function which describes the random signal level seen at the receiver is not Rayleigh as it is in the flat fading case. The selection diversity algorithm selects the maximum gain from a set of paths, each having a Rayleigh distributed gain. Therefore the effective gain for the received signal from the desired user becomes the instantaneous maximum of a set of random variables with Rayleigh distributions.

The selection diversity algorithm also complicates the nature of the interference signals from the multiple paths of the desired user. Any path which does not have the maximum gain contributes to the interference. The signal travelling via any given path may be the desired signal or interference; a decision which depends not only on the instantaneous gain of the given path, but also the instantaneous gain of all the other paths. Note also that the interference is dependent on the gain of the path with the maximum gain, as no interfering path gain can be greater than the maximum path gain.

To find the probability density functions for the received signal and the interference, one needs to find the probability that any given path has the maximum gain. The conditional probability density functions of the gain for each the L paths is found, given that the path has the maximum gain, and given that the path does not have the maximum gain. The probability density function of the effective gain for the desired user is the weighted sum of the conditional probability density functions, given that each path has the maximum gain. Similarly, a set of conditional interference probability density functions is found, given that each path has the maximum gain, and a weighted sum of these conditional interference probability density func-

tions gives the probability density function of the interference from the desired user, given the maximum path gain. The weights in both of these sums are the respective probabilities that each path has the maximum gain.

5.1.1 The Probability that a Given Path has the Maximum Gain

The average gain for each path and the number of paths L are specified in the chosen gain-delay profile, and the gain for each path has a Rayleigh distribution. At any given moment in time, the gain for each of the L paths is a sample from each of the L Rayleigh distributions. The path selected by the receiver is the path whose gain is the maximum of the L path gain samples at that sample time.

Given the L distribution functions, the probability that the lth path will be the path with the maximum gain is calculated. The L path gains are represented by the set of random variables $\mathbf{V}_{1,1}, \mathbf{V}_{2,1}, \ldots, \mathbf{V}_{L,1}$, with respective probability density functions $f_{\mathbf{V}_{1,1}}(V_1), f_{\mathbf{V}_{2,1}}(V_2), \ldots, f_{\mathbf{V}_{L,1}}(V_L)$ and respective distribution functions $F_{\mathbf{V}_{1,1}}(V_1), F_{\mathbf{V}_{2,1}}(V_2), \ldots, F_{\mathbf{V}_{L,1}}(V_L)$. The probability that $\mathbf{V}_{l,1}$ is less than a given value is by definition the distribution function $F_{\mathbf{V}_{l,1}}(V_l)$ evaluated at that value. The probability that a set of random variables are all less than a given value is the product of the respective distribution functions evaluated at that value. To find the probability that all other paths have less gain than the lth path, the product of the respective distribution functions is integrated over the range of values of the lth path gain variable $\mathbf{V}_{l,1}$, and thus the probability p_l that the lth path gain $\mathbf{V}_{l,1}$ is greater than $\mathbf{V}_{i,1}$ for all i, where $i = \{1, 2, \ldots, L\}$ and $i \neq l$, is given by

$$p_l = P\{\mathbf{V}_{l,1} > \mathbf{V}_{i,1}, \forall_i, i \neq l\} = \int_{-\infty}^{\infty} f_{\mathbf{V}_{l,1}}(V_l) \prod_{\substack{i=1 \\ i \neq l}}^{L} F_{\mathbf{V}_{i,1}}(V_l)\ dV_l \tag{5.2}$$

where l has a value from $\{1, 2, \ldots, L\}$. Note that there is always one path with the maximum gain, so the sum of these probabilities is always unity, $\sum_{l=1}^{L} p_l = 1$. Also, the probability that the lth path does not have the maximum gain is $1 - p_l$.

5.1.2 Conditional Distributions Given Path with Maximum Gain

Next the conditional probability density function of the gain of each of the paths, given the path with the maximum path gain, is found. To this end, one considers the set of gain samples from the lth path when the lth path sample $\mathbf{V}_{l,1}$ is the maximum of the L samples, and the sets of samples from the lth path when the lth path sample $\mathbf{V}_{l,1}$ is not the maximum of the L samples.

Firstly, the probability density function for the lth path gain $\mathbf{V}_{l,1}$ is found given that the lth path has the largest gain. The conditional probability that the gain has a given value is the unconditional probability that the gain has that value multiplied by the probability that all the other path gains are less than that value. The probability that all the other paths are less than a given value is the product of the respective distribution functions evaluated at that value. The conditional probability

density function must also be normalised by the probability that the lth path has the maximum gain, giving

$$f_{\mathbf{V}_{l,1}}(V_l|l \text{ has max. gain}) = \left[f_{\mathbf{V}_{l,1}}(V_l) \prod_{\substack{i=1 \\ i \neq l}}^{L} F_{\mathbf{V}_{i,1}}(V_l) \right] / p_l. \tag{5.3}$$

Given equation 5.3, the conditional probability density function of $\mathbf{V}_{l,1}$ is found given that lth path does not have the maximum gain. This conditional probability density function is found by taking $f_{\mathbf{V}_{l,1}}(V_l)$ and excluding the cases when the lth path *does* have the maximum gain, giving

$$f_{\mathbf{V}_{l,1}}(V_l|l \text{ does not have max. gain}) = \frac{f_{\mathbf{V}_{l,1}}(V_l) - p_l f_{\mathbf{V}_{l,1}}(V_l|l \text{ has max. gain})}{1 - p_l}. \tag{5.4}$$

The conditional probability density functions presented in this section have been general, and have not yet considered the form of the probability density functions of the path gain variables. In this investigation each of the L random variables has a Rayleigh distribution,

$$F_{\mathbf{V}_{l,1}}(V_l) = \left\{1 - e^{V_l^2/2\sigma_l^2}\right\} U(V_l) \tag{5.5}$$

$$f_{\mathbf{V}_{l,1}}(V_l) = \frac{V_l}{\sigma_l^2} e^{V_l^2/2\sigma_l^2} U(V_l) \tag{5.6}$$

where $U(V_l)$ is a unit step function. To find the form of the conditional probability density functions of equations 5.3 and 5.4, the form of the product of a Rayleigh density function and a number of Rayleigh distribution functions is found, giving

$$\frac{x}{\sigma_l^2} e^{x^2/2\sigma_m^2} U(x) \prod_{\substack{i=1 \\ i \neq l}}^{L} \left\{1 - e^{x^2/2\sigma_i^2}\right\} U(x) = \sum_{n=1}^{N} \frac{b_n x}{\varsigma_n^2} e^{x^2/2\varsigma_n^2} U(x) \tag{5.7}$$

where the number of terms N in equation 5.7 is 2^{L-1}. Thus, the conditional probability density functions in equations 5.3 and 5.4 are the weighted sums of Rayleigh probability density functions.

5.1.3 The Desired User's Received Signal

The receiver is assumed to employ selection diversity, where the path from the desired user with the maximum signal gain is selected. To evaluate the probability density function of the received signal from the desired user, the probability density function of an equivalent gain variable $\mathbf{V}_m$ is found, where $\mathbf{V}_m$ is the maximum of the L path gains at any given time,

$$\mathbf{V}_m = \max(\mathbf{V}_{1,1}, \mathbf{V}_{2,1}, \ldots, \mathbf{V}_{L,1}). \tag{5.8}$$

The probability density function of the maximum of the path gains $\mathbf{V}_m$ is given by

$$f_{\mathbf{V}_m}(V) = \sum_{l=1}^{L} p_l f_{\mathbf{V}_{l,1}}(V|l \text{ has max. gain}) \tag{5.9}$$

where p_l is the probability that the lth path has the maximum path gain and $f_{V_{l,1}}(V|l \text{ has max. gain})$ is the conditional probability density function of the gain of the lth path given that the lth path has the maximum path gain.

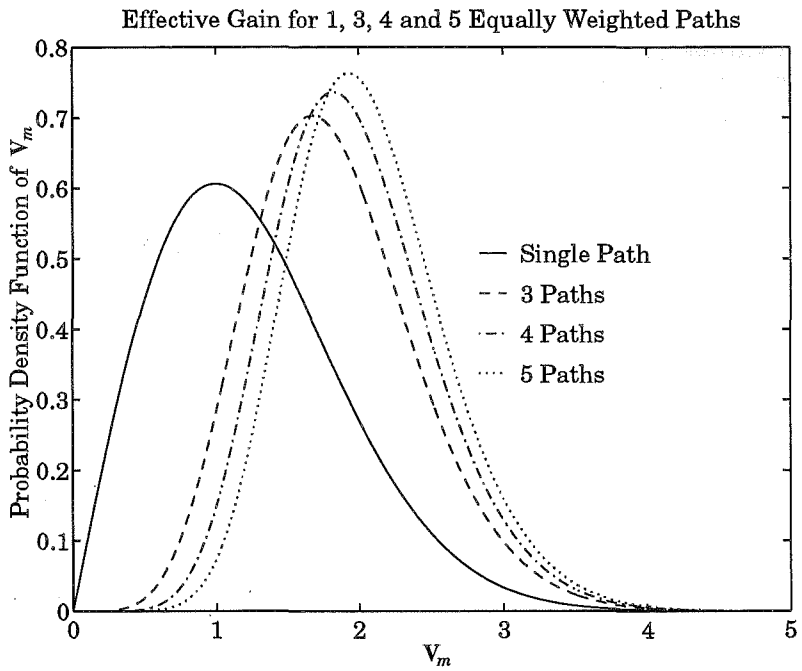

Figure 5.1 Probability density function of the desired signal path gain after selection for a single flat fading path and for three, four and five paths with equal average path gains.

Figure 5.1 shows the probability density function of the desired signal's gain $\mathbf{V}_m$ for some of the multipath models investigated in this study. The single flat fading path model is presented for comparison. The other multipath models are simple models with three, four and five paths of equal average gain. One can see that the more paths there are to select from, the greater the average gain for the desired signal.

An expression for the received signal from the desired user is derived using the effective gain variable $\mathbf{V}_m$. For convenience the mth path is defined to be the path with the maximum gain at any given time. The receiver is assumed to be locked to the mth path, and thus $\tau_{m,1} = 0$ and the autocorrelation $\chi_{1,1}(\tau_{m,1}) = NT_c = T$. The carrier is also assumed to be locked, so that $\Phi_{m,1} = 0$. Thus the received signal from user 1 is represented by $\mathbf{X} = \frac{AT}{2}\mathbf{V}_m b_0^1$.

5.1.4 The Inter-Symbol Interference Distribution

The inter-symbol interference from the desired user comes from all the paths which are not the maximum path. The contribution to the inter-symbol interference from the lth path, where the lth path is not the maximum path, is the product of the autocorrelation value $\chi_{1,1}(\tau_{l,1})$, a sample of the random path gain $\mathbf{V}_{l,1}$ and the cosine

of a sample from the uniform phase distribution of $\Phi_{l,1}$,

$$\mathbf{z}_{l,1} = \mathbf{V}_{l,1}\chi_{1,1}(\tau_{l,1})\cos(\Phi_{l,1}). \tag{5.10}$$

One begins by considering the cross-correlation values $\chi_{1,1}(\tau_{l,1})$. The receiver is locked to the mth path and the effective time delay for the mth path $\tau_{m,1} = 0$. The autocorrelation values $\chi_{1,1}(\tau_{l,1}) = \chi_{1,1}((l-m)T_c)$, as the paths arrive at T_c intervals and $\tau_{m,1} = 0$. This implies that the autocorrelation values for a the lth path depend only on m, the path with the maximum gain. If it is assumed that m is given, then the autocorrelation values $\chi_{1,1}(\tau_{l,1}) = \chi_{1,1}((l-m)T_c)$ are given also, and are simply constants.

Next the gain and phase variables are considered. We begin by noting that no path can have a gain greater than the gain of the path with the maximum gain. Therefore the conditional probability density function of the gain of a non-maximum path is dependent on the gain $\mathbf{V}_m$ of the maximum gain path. Note that the gain of the path with the maximum gain $\mathbf{V}_m$ is also the effective gain of the desired user's received signal. The gain of a non-maximum path, given the path with the maximum gain m and its gain V_m, is simply the original Rayleigh probability density function of the path gain, limited to take values less than V_m and scaled so that the total conditional probability is unity.

$$f_{\mathbf{V}_{l,1}}(V_l|V_m, m, l \text{ does not have max. gain}) = \begin{cases} \dfrac{\frac{V_l}{\sigma_l^2}e^{V_l^2/2\sigma_l^2}}{P\{\mathbf{V}_{l,1} \le V_m\}} & 0 \le V_l \le V_m, \\ 0 \text{ elsewhere.} \end{cases} \tag{5.11}$$

When including the phase variable we must find the probability density function of the product of a random variable with a truncated Rayleigh pdf and a uniformly random phase variable. By following the techniques used in previous chapters, the form of the product pdf is given by

$$h_y(y) = \int \frac{1}{x_2} f_{\mathbf{x}_1}\left(\frac{y_2}{x_2}\right) f_{\mathbf{x}_2}(x_2)dx_2 = \int \frac{1}{\sqrt{1-1/x^2}} \frac{e^{-x/2\sigma^2}}{\sigma^2} dx_2 \tag{5.12}$$

The limits of equation 5.12 need to be found. The lower limit of x_2 is y, due to the maximum value of the phase variable x_1 being unity, and $x_2 = y/x_1$. The maximum value of x_2 is simply the value where the Rayleigh pdf is truncated, which is derived from the given maximum gain of the desired signal V_m. This equation describes the positive values of $h_y(y)$, and the pdf is symmetrical.

Therefore, under the condition that the path with the maximum gain m and its gain $\mathbf{V}_m$ are given, the probability density function of the inter-symbol interference from path l has the form of equation 5.12,

$$f_{\mathbf{z}_{l,1}}(z|V_m, m, l \text{ does not have max. gain}) = \begin{cases} a_{ml}\displaystyle\int_{\mathbf{z}_{l,1}}^{z_{ml}} \frac{e^{-x/2\sigma_l^2}}{\sigma_l^2\sqrt{1-1/x^2}} dx_2 & -z_{ml} \le z \le z_{ml}, \\ 0 \text{ elsewhere} \end{cases} \tag{5.13}$$

where $\mathbf{z}_{l,1}$ represents the interference from the lth path from user 1, a_{ml} is a normalising constant and $\mathbf{z}_{ml} = \chi_{1,1}(\tau_{l,1})\mathbf{V}_m$, which is a constant when $\mathbf{V}_m$ is given.

The total self interference when a given path m has the maximum gain V_m is the sum of the interference from all of the paths which do not have the maximum gain. The conditional probability density function of this sum is the convolution of all the conditional probability density functions for the $L-1$ paths which do not have the maximum gain. This conditional probability density function is the conditional inter-symbol interference, given that the mth path has the maximum path gain V_m,

$$f_{z_1}(z|V_m, m \text{ has max. gain}) = \bigodot_{\substack{l=1 \\ l \neq m}}^{L} f_{z_{l,1}}(z|V_m, m, l \text{ does not have max. gain}) \quad (5.14)$$

where $\odot$ represents the convolution of a range of terms.

The conditioning on m is removed to find the conditional probability density function of the inter-symbol interference $f_{z_1}(z)$ given the gain of the desired user's received signal $\mathbf{V}_m$. To achieve this the weighted sum of the L conditional interference probability density functions $f_{z_1}(z|V_m, m \text{ has max. gain})$ is found. The weight for each conditional probability density function is p_m, the probability that the mth path has the maximum gain. Thus:

$$f_{z_1}(z|V_m) = \sum_{m=1}^{L} p_m f_{z_1}(z|V_m, m \text{ has max. gain}). \quad (5.15)$$

Finally it is noted that the received signal from the desired user $\mathbf{X}$ is the effective path gain of the desired user's received signal $\mathbf{V}_m$ multiplied by $\frac{AT}{2} b_0^1$. Therefore, when $\mathbf{V}_m$ is given and b_0^1 is assumed to be 1, $\mathbf{X}$ is given and equation 5.15 can be rewritten as

$$f_{z_1}(z|X) = f_{z_1}(z|V_m). \quad (5.16)$$

5.2 The Multi-User Interference

In this section the multi-user interference from the other users in the spread spectrum system is considered. The users' signals travel via multipath channels similar to those seen by the desired user. The continuous multipath delay profile is modelled by a tapped delay line where the taps are spaced at intervals of the spreading code chip period T_c. One effect of having the effective paths at regular time intervals is that for any given interfering user the cross-correlation values for each path are not independent of each other. This implies that the signals from each of the paths cannot be simply summed as independent random variables. This complication is handled by initially finding the probability density function for the sum of the interference over the L paths when the relative delay τ_{1k} between user 1 and user k is given. Once the sum over the paths has been taken into account, the condition on the relative delay τ_{1k} is removed.

5.2.1 The Multi-User Interference Given the Delay

Conditional probability density functions are initially found, applying the condition that the relative delay τ_{1k} between user k and the desired user is given. The paths

are spaced at T_c intervals, so specifying τ_{1k} also specifies the delays τ_{lk} for all l, and therefore the cross-correlation function values $\chi_{1k}(\tau_{lk})$ for all l.

Under the condition that τ_{1k} is given, where $\chi_{1k}(\tau_{lk})$ are given constants, the interference term $\chi_{1k}(\tau_{lk})\mathbf{G}_{lk}$ associated with the lth path from user k is a random variable with a Gaussian distribution. The variance ς_{lk}^2 of $\mathbf{G}_{lk}$ is specified by the chosen multipath gain profile. The variance of the product $\chi_{1k}(\tau_{lk})\mathbf{G}_{lk}$ is defined to be w_{lk}^2, where $w_{lk}^2 = [\chi_{1k}(\tau_{lk})\varsigma_{lk}]^2$.

Following from this, when τ_{1k} is given, the total interference from user k is a sum of l independent Gaussian random variables, and has a Gaussian distribution with variance $w_k^2 = \sum_{l=1}^{L} w_{lk}^2$ [Papoulis, 1984]. This is equivalent to a zero mean unity variance Gaussian random variable $\mathbf{G}_k$, multiplied by w_k, where w_k is a constant if τ_{1k} is given. The interference from user $k, k = 2, 3, \ldots, K$ becomes

$$\mathbf{z}_k = \sum_{l=1}^{L} \chi_{1k}(\tau_{lk})\mathbf{G}_{lk} = w_k\mathbf{G}_k. \tag{5.17}$$

5.2.2 Removing the Conditioning on Delay

Now that the sum over the L paths is resolved, the condition that τ_{1k} is given is removed. When this condition is removed, w_k is no longer constant and becomes a random variable $\mathbf{w}_k$, which is a function of the cross-correlation function value, which is in turn a function of the random delay variable τ_{1k}.

To find the relationship between $\mathbf{w}_k$ and τ_{1k}, it is again useful to consider the case where τ_{1k} is conditioned to lie on a chip-length section where $nT_c \leq \tau_{1k} \leq (n+1)T_c$ and $0 \leq n < N$ is an integer. Due to the chip-period spacing of the paths, if the first path lies on a given chip-length section of the cross-correlation function, the following paths lie on consecutive chip-length sections, and hence the delay for the lth path is in the interval $(n+l-1)T_c \leq \tau_{lk} \leq (n+l)T_c$ when $nT_c \leq \tau_{1k} \leq (n+1)T_c$. For example, if the first path delay τ_{1k} lies within the region where $n = 3$ on figure 4.2, then $\tau_{2k} = \tau_{1k} + T_c$ lies within the region where $n = 4$, τ_{3k} lies within the region where $n = 5$, and so on. Given that the chips and data bits have rectangular pulse shapes, when $nT_c \leq \tau_{1k} \leq (n+1)T_c$, the cross-correlation function for each path $\chi_{1k}(\tau_{lk})$ is a linear function of τ_{lk}, such that

$$\chi_{1k}(\tau_{lk}) = a_{lk}\tau_{lk} + b_{lk}. \tag{5.18}$$

Note that $\tau_{lk} = \tau_{1k} + (l-1)T_c$ and that $(l-1)T_c$ is a constant for each l, allowing equation 5.18 to be expressed in terms of τ_{1k}, giving

$$a_{lk}\tau_{lk} + b_{lk} = A_{lk}\tau_{1k} + B_{lk}. \tag{5.19}$$

Applying these equations to the expression for $\mathbf{w}_{lk}$ gives

$$\mathbf{w}_{lk}^2 = [\chi_{1k}(\tau_{lk})\varsigma_{lk}]^2 = (A_{lk}\tau_{1k} + B_{lk})^2\varsigma_{lk}^2, \tag{5.20}$$

$$\mathbf{w}_k^2 = \sum_{l=1}^{L}(A_{lk}\tau_{1k} + B_{lk})^2\varsigma_{lk}^2. \tag{5.21}$$

Therefore, given that $nT_c \leq \tau_{1k} \leq (n+1)T_c$, $\mathbf{w}_k$ has the form

$$\mathbf{w}_k = \sqrt{\alpha\tau_{1k}^2 + 2\beta\tau_{1k} + \gamma} \tag{5.22}$$

where $\alpha = \sum_{l=1}^{L} \varsigma_{lk}^2 A_{lk}^2$, $\beta = \sum_{l=1}^{L} 2\varsigma_{lk}^2 A_{lk}B_{lk}$ and $\gamma = \sum_{l=1}^{L} \varsigma_{lk}^2 B_{lk}^2$.

Transformation techniques [Papoulis, 1984] are used to find the probability density function of $\mathbf{w}_k$ in terms of the pdf of τ_{1k}. For notational convenience, the probability density function of $\mathbf{y}_4$ is found, where

$$\mathbf{y}_4 = g_2(\mathbf{x}_4) = \sqrt{\alpha\mathbf{x}_4^2 + 2\beta\mathbf{x}_4 + \gamma}.$$

Firstly one solves $y_4 = g_2(x_4)$. In this case, there are generally 2 solutions for every y_4. The real roots of $g_2(x_4)$ are denoted by x_{4a} and x_{4b}, such that $y_4 = g_2(x_{4a}) = g_2(x_{4b})$. Solving the equation

$$\begin{aligned} y_4^2 &= \alpha {x_4}^2 + 2\beta x_4 + \gamma \\ \Rightarrow 0 &= \alpha {x_4}^2 + 2\beta x_4 + \gamma - {y_4}^2 \\ \Rightarrow x_4 &= \frac{-\beta \pm \sqrt{(\beta)^2 - \alpha(\gamma - {y_4}^2)}}{\alpha}. \end{aligned} \tag{5.23}$$

From Papoulis [Papoulis, 1984] one finds that when $\mathbf{y}_4 = g_2(\mathbf{x}_4)$,

$$f_{\mathbf{y}_4}(y_4) = \frac{f_{\mathbf{x}_4}(x_{4a})}{|g_2'(x_{4a})|} + \frac{f_{\mathbf{x}_4}(x_{4b})}{|g_2'(x_{4b})|} \tag{5.24}$$

where x_{4a} and x_{4b} denote the real roots of $g_2(x_4)$. Thus one needs to find $g_2'(x_4)$, the derivative of $g_2(x_4)$ with respect to x_4, which is given by

$$g_2'(x_4) = \frac{\alpha x_4 + \beta}{\sqrt{\alpha {x_4}^2 + 2\beta x_4 + \gamma}}. \tag{5.25}$$

In the conditional case $\mathbf{x}_4$ is effectively uniformly distributed over a chip length interval, and therefore $f_{\mathbf{x}_4}(x_4)$ is simply a constant $1/T_c$ in that interval and zero elsewhere. Substituting this $f_{\mathbf{x}_4}(x_4)$ and $g_2'(x_4)$ into equation 5.24 gives

$$\begin{aligned} f_{\mathbf{y}_4}(y_4) &= \frac{1/T_c}{\left|\frac{\alpha x_{4a}+\beta}{\sqrt{\alpha x_{4a}^2+2\beta x_{4a}+\gamma}}\right|} + \frac{1/T_c}{\left|\frac{\alpha x_{4b}+\beta}{\sqrt{\alpha x_{4b}^2+2\beta x_{4b}+\gamma}}\right|} \\ &= \left|\frac{\sqrt{\alpha x_{4a}^2 + 2\beta x_{4a} + \gamma}}{T_c[\alpha x_{4a} + \beta]}\right| + \left|\frac{\sqrt{\alpha x_{4b}^2 + 2\beta x_{4b} + \gamma}}{T_c[\alpha x_{4b} + \beta]}\right| \\ &= \left|\frac{y}{T_c[\alpha x_{4a} + \beta]}\right| + \left|\frac{y}{T_c[\alpha x_{4b} + \beta]}\right| \end{aligned} \tag{5.26}$$

where the real roots

$$\begin{aligned} x_{4a} &= \frac{-\beta + \sqrt{\beta^2 - \alpha(\gamma - y_4^2)}}{\alpha} \\ x_{4b} &= \frac{-\beta - \sqrt{\beta^2 - \alpha(\gamma - y_4^2)}}{\alpha}. \end{aligned} \tag{5.27}$$

Finally x_{4a} and x_{4b} from equation 5.27 are substituted into equation 5.26, to give

$$\begin{aligned} f_{y_4}(y_4) &= \left|\frac{y_4}{T_c[\alpha x_{4a}+\beta]}\right| + \left|\frac{y_4}{T_c[\alpha x_{4b}+\beta]}\right| \\ &= \left|\frac{y}{T_c[-\beta+\sqrt{\beta^2-\alpha(\gamma-y_4^2)}+\beta]}\right| + \left|\frac{y_4}{T_c[-\beta-\sqrt{\beta^2-\alpha(\gamma-y_4^2)}+\beta]}\right| \\ &= \left|\frac{y}{T_c\sqrt{\beta^2-\alpha(\gamma-y_4^2)}}\right| + \left|\frac{y_4}{-T_c\sqrt{\beta^2-\alpha(\gamma-y_4^2)}}\right| \end{aligned} \tag{5.28}$$

which is a two part probability density function. So, for a given chip length section of the cross-correlation function, the random variable w_k has a two part probability density function of the form

$$h_{\mathrm{w}_k}(w_k) = M\frac{w_k}{\sqrt{\beta^2-\alpha\gamma+\alpha w_k^2}} \tag{5.29}$$

where M is a normalising constant to make the total area unity. The pdf of the product $\mathbf{z}_k = \mathbf{w}_k\mathbf{G}_k$ is generally a pair of integrals, each of the form

$$h_{\mathbf{z}_k}(z_k|nT_c \le \tau_{1k} \le (n+1)T_c) = M\int_a^b \frac{e^{\frac{z_k^2}{2u^2}}}{\sqrt{\beta^2-\alpha\gamma+\alpha u^2}}du \tag{5.30}$$

where the limits of the integral depend on the range of of w_k. The numerical evaluation of this integral is discussed in section 5.4.

Equation 5.30 describes the conditional probability density function of the interference when τ_{1k} lies within a given chip length section of the cross-correlation function. To remove this condition, the conditional probability density function is found for each chip length section of the odd and even cross-correlation functions. The overall probability density function is the weighted sum of the conditional probability density functions, noting that each chip length section is equally likely. This provides the probability density function for the multi-user interference given a pair of spreading sequences. The probability density function for a large number of sequence pairs is found and the average taken to provide an average multi-user interference probability density function for the multi-user interference $\mathbf{z}_k$ from user k. It is noted that the probability density functions for each spreading sequence pair are very similar for the multiple fading paths case.

5.3 The Average Probability of Error

The interference from the $K-1$ interfering users and the inter-symbol interference given the received signal from the desired user are all independent, so the pdf of the total interference given the desired received signal is the convolution of the interference probability density functions from each user,

$$f_{\mathbf{z}}(z|X) = f_{\mathbf{z}_1}(z_1|X) \odot f_{\mathbf{z}_2}(z_2) \odot \ldots \odot f_{\mathbf{z}_K}(z_K). \tag{5.31}$$

In this case the desired signal from user 1 effectively travels via the path with the maximum gain and has the amplitude $\mathbf{X} = \frac{AT}{2}\mathbf{V}_m b_0^1$ (see section 5.1.3). To calculate the error performance one finds the probability that the interference given X is greater than X, and thus the average probability of error is

$$P_e = \int_{-\infty}^{\infty} P\{\mathbf{z} > X|X\}\ f_{\mathbf{X}}(X)\ dX. \tag{5.32}$$

5.4 Numerical Calculation of the Probability of Error

As for the simplified channel cases, the basic numerical method employed to determine the performance of the system involves finding the characteristic function of the interference and using this to calculate the average probability of error. Thus one needs to find the characteristic function of the per-user multi-user interference, and the characteristic function of the inter-symbol interference. The method employed to find the average probability of error only requires that the characteristic function of the per-user interference is known at equally spaced points.

For this general case, the integral describing the conditional pdf of the multi-user interference in equation 5.30 is solved numerically for each required point on the pdf. It is difficult to attain good accuracy for this numerical integration, as the denominator of equation 5.30 often goes to zero at one of the limits of the integral. To avoid this problem, the exponential in the numerator is approximated by a set of straight line segments, where the number of line segments is adapted to ensure good approximation accuracy. This allows an analytical solution to the integral for each given line segment and results in a more accurate and computationally efficient calculation. This method is used to find a set of equally spaced points on the conditional probability density function, given that the delay lies within a given chip length section of the cross correlation. The conditional characteristic function is then found using a discrete Fourier transform of this set of pdf points. A vector of equally spaced conditional characteristic function values is calculated for each chip length section of the odd and even cross-correlation functions of a given pair of spreading sequences. To obtain equally spaced values of the characteristic function of the per-user multi-user interference, the weighted sum of the conditional characteristic function values is found, noting that each chip length section is equally likely. This process is followed for a large number of spreading code pairs, and an average taken to give an average per-user interference characteristic function $\varphi_{\mathbf{z}_k}(\nu)$.

The form of the conditional probability density functions which form the statistical description of the inter-symbol interference (see equation 5.13) is very similar to the form for the multi-user interference. Equally spaced values on the conditional pdf are found using the same method as for the multi-user interference. The conditional characteristic function is found using a discrete Fourier transform of these values. With characteristic functions in place of probability density functions, the convolution in equation 5.14 becomes a product, and the characteristic function of the inter-symbol interference conditioned on X is then given by a weighted sum of

the conditional characteristic functions, equivalent to that of equation 5.15.

A further complication of the general case is that the interference is conditioned on the desired received signal. Note that only the inter-symbol interference is dependent on the received signal. This problem is numerically solved using a look-up table of inter-symbol interference characteristic functions, where each characteristic function in the table is calculated for a different given received signal X. This look-up table is large to ensure a good coverage of the possible received signal range.

For the multiple fading paths case, the average probability of error is described in equation 5.31. A numerical series expansion technique is used to determine the probability $P\{\mathbf{z} > X|X\}$ for any given X from the equally spaced characteristic function points [Beaulieu, 1990] (see equation 4.58). The characteristic function of the interference for any given X is calculated by selecting the most suitable inter-symbol interference characteristic function from the look-up table and multiplying by the multi-user interference characteristic function. The average probability of error integral in equation 4.22 is numerically evaluated, using an adaptive recursive Newton Cotes 8 panel rule.

5.5 Results for the Multiple Fading Paths Cases

In this section the performance results for a selection of multipath gain-delay profiles is presented. Firstly the results for a set of multipath profiles with a number of paths with equal average gains are presented. Next the results for a range of profiles with five paths with different profile shapes are presented. Finally the performance for three different multipath models is compared, and the effects of the selection diversity observed.

5.5.1 Equally Weighted Path Models

We begin our study of the results with set of simple multipath models, varying only the number of effective paths in the model. The probability density function of the per-user interference is shown in figure 5.2 for multipath models with three, four and five paths of equal average gain. The probability density functions are even and only the positive values are shown. This figure shows that the variance of the per-user interference increases with the number of paths, as one would expect.

Based on figure 5.2, one would expect the system performance to degrade with the increasing number of effective paths. Figure 5.3 indicates that this is not the case for small numbers of users. It is evident that the improved gain for the larger numbers of paths (see figure 5.1) due to the selection diversity almost completely counteracts the increase in the interference. The effect of the selection diversity is less for larger numbers of users, and degraded performance due to the greater interference is evident.

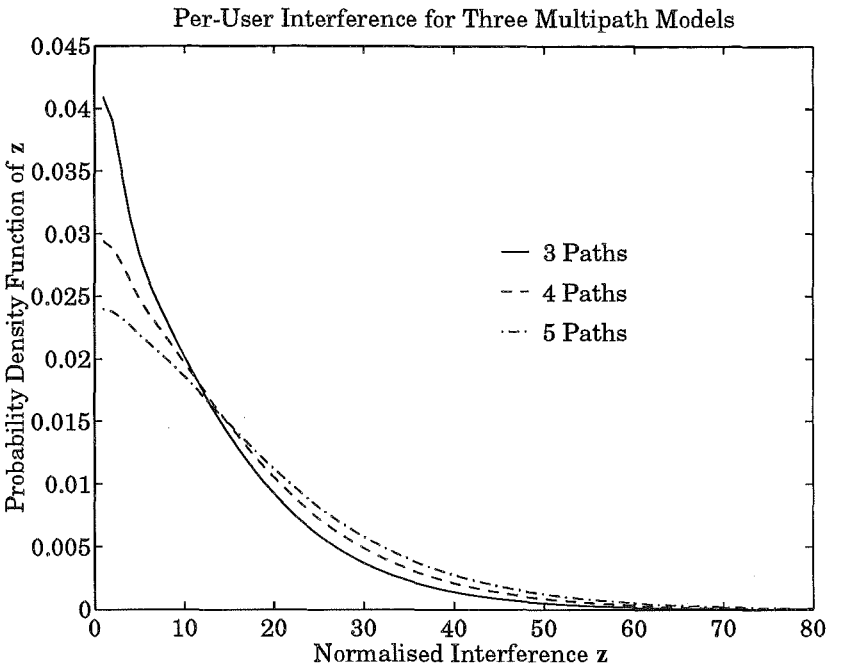

Figure 5.2 The average per-user interference probability density function for three, four and five equal path multipath profiles. For each case, the normalised interference $\mathbf{z} = \sum_{l=1}^{L} \mathbf{G}_{lk}\chi_{1k}(\tau_{lk})$.

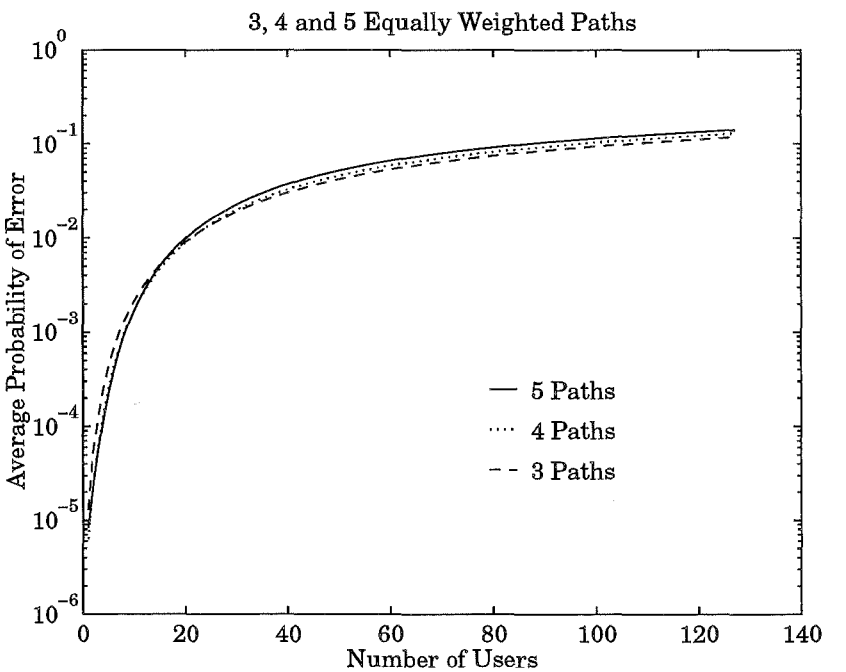

Figure 5.3 Average probability of error for the equal gain multipath models.

5.5.2 Five Path Multipath Models

A factor of interest is the complexity of the multipath model required to accurately represent a real multipath channel, where the signal strength typically decays with

Shape	Weights
Triangular	1, 0.8, 0.6, 0.4, 0.2
Exponential	1 0.74 0.55 0.41 0.3
Gaussian	0.28 0.72 1 0.72 0.28
Random	0.63 0.76 1 0.37 0.24

Table 5.1 Table of the gain weights for the profile shape performance comparison.

time. To this end, we compare the performance results for a set of five path multipath models, where the shape of each profile is different. The first model has five paths with average gains weighted (1, 0.8, 0.6, 0.4, 0.2), resulting in a quadratic shaped average power delay profile, which is a simple approximation to a typical decay of signal strength with time. For comparison with this simple approximation, results for an exponentially decaying profile, a Gaussian shaped profile and a profile based on a set of uniformly random numbers (see table 5.1) are presented.

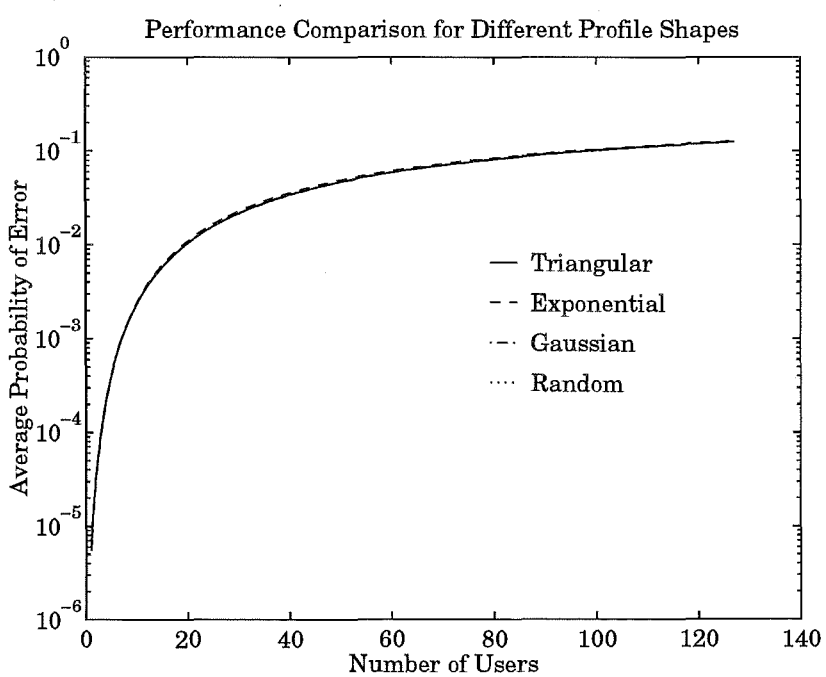

Figure 5.4 Average probability of error for four different multipath delay profile shapes.

The performance curves shown in figure 5.4 indicate that the performance for the four different profile shapes is very similar, and that any of these, including the simple triangular shaped gain profile, could be used to model a multipath channel where the signal strength typically decays with time.

5.5.3 Multipath Models and Selection Diversity

In order to better observe the effects of selection diversity, the performance for three different multipath models is compared. The effective gains and performance for the single path flat fading model, the five equal average gain model and the five triangularly weighted average gain model are presented and compared.

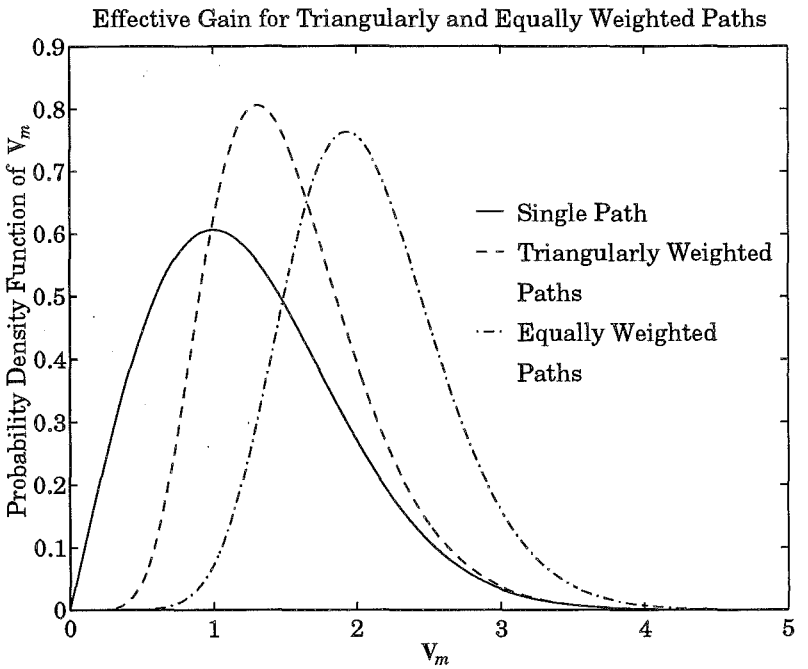

Figure 5.5 Probability density function of the desired signal path gain after selection for single path flat fading, five triangularly weighted average gain and five equal average gain multipath models.

When the effective path gains for the three multipath models are compared (see figure 5.5) it is clear that the five equal average gain model has the greatest average effective gain, and therefore is expected to have better selection diversity performance. However, it should also be noted that the variance of the per-user multi-user interference for the five equal average gain model is greater than for the triangular average gain model, which is in turn greater than that for the single flat fading path model.

The system performance for these three multipath models gives good insight into the effects of the selection diversity algorithm. For small numbers of users, the selection diversity has a large effect, and the equal average gain model shows the best performance. The single effective flat fading path model offers no diversity and relatively poor performance is evident.

Also of interest is the case where there is only one interfering user. In this case the system performance is dominated by the inter-symbol interference. One notes

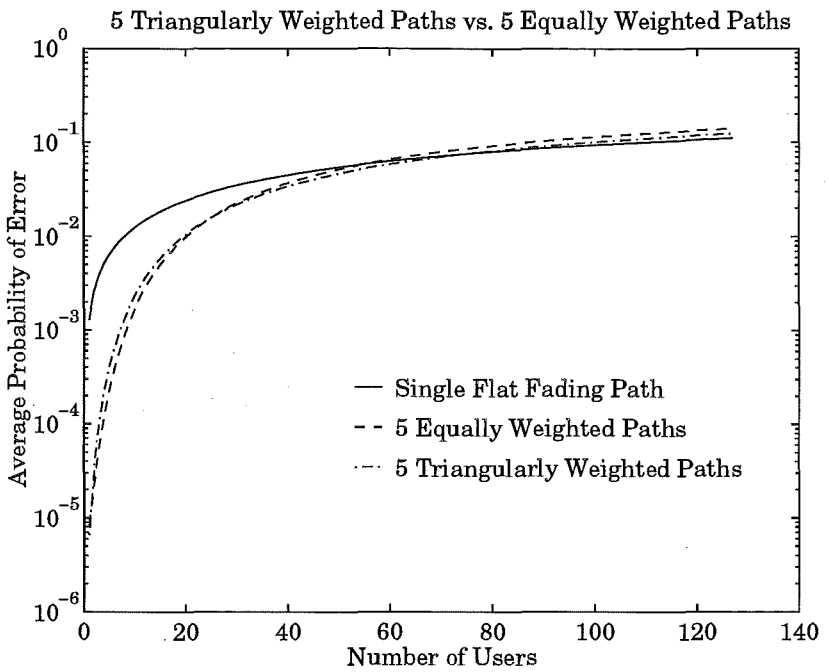

Figure 5.6 Average probability of error for the single path flat fading, five equal average gain and five triangularly weighted average gain multipath models.

from figure 5.6 that the five triangularly weighted average gain multipath model has a slightly better system performance than the five equal average gain model. The explanation lies in the dominance of the inter-symbol interference. For a given received signal path gain V_m, we have noted that due to selection diversity the inter-symbol interference path gains will be less than V_m. For the five equal average path gains, the interference path gains can all be quite close to V_m, but due to the decreasing average path gain with increasing time in the triangularly weighted case, the average gains of paths 3, 4 and 5 are likely to be significantly less than V_m. Thus the total inter-symbol interference for the triangularly weighted paths is less on average, and the system performance better when the performance is dominated by the inter-symbol interference.

As the number of users increases, the gain offered by the selection diversity decreases and the performance curves for the triangular average gain and equal average gain models cross. As the number of users increases further, the gain of the selection diversity for the multiple path models is offset by the increase in interference, and the single flat fading path model offers the best performance.

These findings indicate that selection diversity has a significant effect on performance for spread spectrum systems over multipath channels. In the single flat fading channel model case, there is only one resolvable path which has a Rayleigh distributed gain. In the multiple paths case there is more than one path available for selection, and a deep fade in the desired signal occurs only when all the paths are fading simultaneously. The probability that all the paths fade simultaneously is

small, and hence improved performance over the single effective path case is generally observed.

Chapter 6

THE EFFECTS OF POWER CONTROL

An important consideration in direct sequence spread spectrum is the relative levels of the signals arriving at the receiver. In this chapter the effect of an ideal power control algorithm which ensures that the strongest signals from each of the users have the same power level is considered.

The power control algorithm is assumed to function in the following way. The gain of each of the paths from each user to the base station has a Rayleigh distributed gain, where the average gain is specified by the chosen gain delay profile. At any given moment in time the gain for each of the paths is a sample taken from each respective distribution. The power control algorithm selects the path with the maximum gain, as the selection diversity algorithm does, and alters the power level of the transmitted signal so that the signal at the receiver via the strongest path has a constant power level. It is assumed that the signal level is altered to cancel out the gain of the maximum gain path, so that the effective gain of the maximum gain path becomes unity. It is assumed that the strongest gain can always be found, that the power can be altered by any amount and that the control of the signal level is instantaneous. A real power control system may have difficulty finding the maximum gain path, will have a limited maximum power increase and will have a delay time associated with the algorithm. Therefore this analysis could be considered the best a power control algorithm could achieve and in that sense gives an upper bound on power control performance.

The ideal power control case is mathematically similar to the general multipath case, where the contribution to the decision variable ξ from the lth path of the kth interfering user is the cross correlation function $\chi_{1k}(\tau_{lk})$ multiplied by an effective gain variable V_{lk} and the cosine of the random phase variable Φ_{lk}, and yields

$$\xi = \frac{A}{2} \sum_{k=1}^{K} \sum_{l=1}^{L} \mathrm{V}_{lk} \chi_{1k}(\tau_{lk}) \cos(\Phi_{lk}). \tag{6.1}$$

Note that the effective gain V_{lk} does not have a Rayleigh distribution for the ideal power control case, as this gain variable represents the effective gain after the power control algorithm is applied. The interference from an interfering user k is given by

$$\mathrm{z}_k = \frac{A}{2} \sum_{l=1}^{L} \mathrm{V}_{lk} \chi_{1k}(\tau_{lk}) \cos(\Phi_{lk}). \tag{6.2}$$

In this chapter two channel model cases are considered. The first is the flat fading multipath channel case, and the second is the case where there are three effective paths, each with an equal average gain.

In the flat fading channel model case there is only one effective path for each user to the receiver, and the path gain has a Rayleigh distribution. When ideal power control is applied to such a system, the fading on the path is exactly cancelled out by the power control algorithm, and the resulting performance is therefore the same as that for the single non-fading path case.

It is more interesting to investigate the effect of ideal power control on a system where the multipath channel model for each user has more than one effective path. Here a system is analysed where the channel between each user and the receiver is modelled by three effective paths, each having Rayleigh distributed gains with equal average gain. The results found here can be extended to cover other multipath gain-delay profiles.

In the power control algorithm the maximum path gain is found and the signal level altered so that the effective gain is constant. This is done by increasing the signal level if the maximum gain is small or decreasing the signal level if the maximum gain is large. In effect the signal is divided through by the maximum gain, making the effective gain unity. The signal transmitted over each of the paths is the same, and therefore the gain of all of the paths is effectively divided by the gain of the maximum path. Note that the power control algorithm affects the form of the signals from all of the users, whereas the selection diversity algorithm affected only the desired user's received signal.

To analyse the power control algorithm one needs to derive probability density functions for the effective paths gains $\mathbf{V}_{lk}$, after the original Rayleigh distributed path gains have been divided through by the gain of the maximum path. Once the effective path gain probability density functions have been derived, the cosine of the uniformly distributed phase variable is included, and finally the effects of the data bits and the cross correlation function evaluated at the uniformly distributed delay are included.

6.1 Probability Density Function of the Effective Path Gains

In the multipath model there are three paths spaced T_c s apart, where each path has a Rayleigh distributed gain and equal average gain.

$$f_{\mathbf{x}_5}(x_5) = x_5 e^{-x_5^2/2} \tag{6.3}$$

$$f_{\mathbf{x}_6}(x_6) = x_6 e^{-x_6^2/2} \tag{6.4}$$

$$f_{\mathbf{x}_7}(x_7) = x_7 e^{-x_7^2/2} \tag{6.5}$$

These are the path gains for the multipath model before the power control algorithm is applied. After the power control is applied, the effective path gains no longer have

Rayleigh distributions.

Note that the gains of each of the three paths have equivalent probability density functions, and thus the probability that any of the given paths has the maximum path gain at any given time is $\frac{1}{3}$. Also, the probability that any of the given paths does not have the maximum path gain at any given time is $1 - \frac{1}{3} = \frac{2}{3}$. If a profile with different average gains for each path were analysed, the probability that each path had the maximum path gain would be different for each path. These probabilities are used as weights when summing conditional probability density functions and conditional characteristic functions when removing the conditions.

In the analysis of this system, one needs to find the probability density function of effective path gain $\mathbf{V}_{lk}$, which is equivalent to the path gain divided by the instantaneous maximum path gain. One begins by finding the probability density function of the maximum of two of the paths,

$$f_{\mathbf{x}_5}(x_5|\mathbf{x}_5 \geq \mathbf{x}_6) = f_{\mathbf{x}_5}(x_5)F_{\mathbf{x}_6}(x_5) = 2x_5e^{-x_5^2/2} - 2x_5e^{-x_5^2}. \tag{6.6}$$

For the power control algorithm one divides the gain of each path by the gain of the maximum of the three paths. Consider the case where a random variable $\mathbf{y}_5$ is equal to the gain of the third path $\mathbf{x}_7$ divided by the maximum of the gains of paths 1 and 2, that is $\mathbf{y}_5 = \mathbf{x}_7/\max(\mathbf{x}_5, \mathbf{x}_6)$. The probability density function for $\mathbf{y}_5$ is derived,

$$\begin{aligned}
h_{\mathbf{y}_5}(y_5) &= \int_0^\infty x_5 y_5 x_5 e^{-y_5^2 x_5^2/2}[2x_5e^{-(x_5)^2/2} - 2x_5e^{-(x_5)^2}]dx_5 \\
&= 2y_5\int_0^\infty x_5^3 e^{-y_5^2x_5^2/2}[e^{-x_5^2/2} - e^{-x_5^2}]dx_5 \\
&= 2y_5\int_0^\infty x_5^3 e^{-(y_5^2/2+1/2)x_5^2} - x_5^3e^{-(y_5^2/2+1)x_5^2}dx_5 \\
&= 2y_5\int_0^\infty x_5^3 e^{-(y_5^2/2+1/2)x_5^2}dx_5 - 2y_5\int_0^\infty x_5^3e^{-(y_5^2/2+1)x_5^2}dx_5.
\end{aligned} \tag{6.7}$$

Noting that

$$\int u^3e^{au^2}du = \frac{e^{au^2}}{2}\left[\frac{u^2}{a} - \frac{1}{u^2}\right] \tag{6.8}$$

and substituting into equation 6.7 one finds

$$\begin{aligned}
h_{\mathbf{y}_5}(y_5) &= 2y_5\int_0^\infty x_5^3e^{-(y_5^2/2+1/2)x_5^2}dx_5 - 2y_5\int_0^\infty x_5^3e^{-(y_5^2/2+1)x_5^2}dx_5 \\
&= 2y_5\left[\frac{e^{-(y_5^2/2+1/2)x_5^2}}{2}\left(\frac{x_5^2}{-(y_5^2/2+1/2)} - \frac{1}{(y_5^2/2+1/2)^2}\right)\right]_0^\infty \\
&\quad - 2y_5\left[\frac{e^{-(y_5^2/2+1)x_5^2}}{2}\left(\frac{x_5^2}{-(y_5^2/2+1)} - \frac{1}{(y_5^2/2+1)^2}\right)\right]_0^\infty \\
&= 2y_5\left[0 - \frac{1}{2}\times - \frac{1}{(y_5^2/2+1/2)^2}\right] - 2y_5\left[0 - \frac{1}{2}\times - \frac{1}{(y^2/2+1)^2}\right] \\
&= y_5\left[\frac{1}{(y_5^2/2+1/2)^2} - \frac{1}{(y_5^2/2+1)^2}\right]
\end{aligned}$$

$$= 4y_5 \left[\frac{1}{(y_5^2+1)^2} - \frac{1}{(y_5^2+2)^2} \right]. \tag{6.9}$$

When x_7 is greater than both x_5 and x_6, the value of y_5 will be greater than 1. On the other hand, in the cases where x_7 is less than either x_5 or x_6, the value of y_5 will be less than 1. In these cases one can also say that $x_7/\max(x_5, x_6) = x_7/\max(x_5, x_6, x_7)$, as x_7 is *not* greater than both x_5 and x_6 and therefore cannot be the maximum of the three. Therefore the conditional probability density function of $x_7/\max(x_5, x_6, x_7)$, given that x_7 does not have the maximum value, has the same form as equation 6.9, but only has values for y_5 between 0 and 1, and is zero elsewhere. Note that this condition alters the area under the function in equation 6.9, and the conditional probability function is scaled by $\frac{3}{2}$ to make the area under the conditional pdf unity. The conditional probability density function of y_5, given that x_7 does not have the maximum value is therefore given by

$$h_{y_5}(y_5|\max(x_5, x_6) > x_7) = 6y_5 \left[\frac{1}{(y_5^2+1)^2} - \frac{1}{(y_5^2+2)^2} \right] \text{ for } 0 < y_5 < 1, \text{ 0 elsewhere} \tag{6.10}$$

noting that equation 6.10 describes the form of the conditional probability density function of the effective path gain V_{lk}, given that the path does not have the maximum gain.

When x_7 has the maximum value of the three, the effective gain $x_7/\max(x_5, x_6, x_7)$ is obviously unity. Thus, if one defines $y_6 = x_7/\max(x_5, x_6, x_7)$, the probability density function of y_6 is given by

$$h_{y_6}(y_6) = 4y_6 \left[\frac{1}{(y_6^2+1)^2} - \frac{1}{(y_6^2+2)^2} \right] + \frac{1}{3}\delta(y_6 - 1) \text{ for } 0 < y_6 < 1, \text{ 0 elsewhere} \tag{6.11}$$

noting that equation 6.11 describes the probability density function of the effective path gain V_{lk} for each of the three paths.

6.2 The Effect of the Phase Variable

The next step in the analysis is to include the cosine of the uniformly distributed phase variable. In this section the form of the probability density function of the effective gain of a given path V_{lk} multiplied by the cosine of the random phase Φ_{lk} is derived. Note that one only needs to find this probability density function for the condition that the given path is not the path with the maximum gain. If the given path has the maximum gain, the effective path gain after power control is unity, and thus the conditional probability density function in this case is simply the probability density function of the cosine of a random phase variable.

Due to the complexity of the resulting equations, one initially derives a general result for the basic form of the probability density function in equation 6.10. The parameters of equation 6.10 are then applied to the general result. Note that the

probability density function of the effective gain of any given channel is based on the mathematical form

$$\frac{x_8}{(b+x_8^2)^2}.$$

The random phase variable is included by finding the probability density function of the product of the effective gain described above and the cosine of a random phase variable, which is uniformly distributed on the interval $[-\pi, \pi]$. The probability density function of the cosine of a random phase has the form

$$\frac{1}{\pi\sqrt{1-x_9^2}}.$$

To calculate the probability density function of the product one needs to solve the integral [Springer, 1979]

$$\int \frac{1}{(b+x_8^2)^2\sqrt{1-y_7^2/x_8^2}}dx_8. \tag{6.12}$$

Note that this is not strictly a probability density function, as the normalising constants have not been included at this stage. The integral in equation 6.12 has a solution

$$\frac{1}{4\sqrt{-b}(b+y_7^2)}\left[\begin{array}{l} -\frac{\sqrt{x_8^2-y_7^2}}{(x_8+\sqrt{-b})}+\frac{\sqrt{-b}\arcsin\left[\frac{-x_8\sqrt{-b}-y_7^2}{y_7(x_8+\sqrt{-b})}\right]}{\sqrt{b+y_7^2}} \\ +\frac{\sqrt{x_8^2-y_7^2}}{(x_8-\sqrt{-b})}+\frac{\sqrt{-b}\arcsin\left[\frac{x_8\sqrt{-b}-y_7^2}{y_7(x_8-\sqrt{-b})}\right]}{\sqrt{b+y_7^2}} \end{array}\right]. \tag{6.13}$$

Consider the limits of the integral in equation 6.12, noting that $\mathbf{x}_9$ has values on the interval $[-1, 1]$ and $\mathbf{x}_8$ has values on the interval $[0, 1]$. The minimum value of $\mathbf{x}_8$ is y_7, as the maximum value of $\mathbf{x}_9$ is 1, and $\mathbf{x}_8 = \mathbf{y}_7/\mathbf{x}_9$. The maximum value $\mathbf{x}_8$ can take is 1. The probability density function of the product is found by substituting these limits into the solution and finding the difference.

One begins by substituting the lower limit, $x_8 = y_7$, into the solution of equation 6.13. Two of the terms become zero, and the arguments of the arcsin terms become -1, giving

$$\begin{aligned} &\frac{1}{4\sqrt{-b}(b+y_7^2)}\left[\frac{\sqrt{-b}\arcsin(-1)}{\sqrt{b+y_7^2}}+\frac{\sqrt{-b}\arcsin(-1)}{\sqrt{b+y_7^2}}\right] \\ &=\frac{\arcsin(-1)}{2(b+y_7^2)\sqrt{b+y_7^2}} \\ &=\frac{-\pi}{4(b+y_7^2)\sqrt{b+y_7^2}}. \end{aligned} \tag{6.14}$$

Next consider the upper limit, $x_8 = 1$.

$$\frac{1}{4(b+y_7^2)}\left[-\frac{\sqrt{1-y_7^2}}{\sqrt{-b}(1+\sqrt{-b})}+\frac{\arcsin\left[\frac{-\sqrt{-b}-y_7^2}{y_7(1+\sqrt{-b})}\right]}{\sqrt{b+y_7^2}}\right.$$

$$+\frac{\sqrt{1-y_7^2}}{\sqrt{-b}(1-\sqrt{-b})}+\frac{\arcsin\left[\frac{\sqrt{-b}-y_7^2}{y_7(1-\sqrt{-b})}\right]}{\sqrt{b+y_7^2}}\Bigg]$$

$$=\frac{1}{4(b+y_7^2)}\left[\frac{1}{\sqrt{b+y_7^2}}\left(\arcsin\left[\frac{-\sqrt{-b}-y_7^2}{y_7(1+\sqrt{-b})}\right]+\arcsin\left[\frac{\sqrt{-b}-y_7^2}{y_7(1-\sqrt{-b})}\right]\right)\right.$$

$$\left.-\frac{\sqrt{1-y_7^2}}{\sqrt{-b}(1+\sqrt{-b})}+\frac{\sqrt{1-y_7^2}}{\sqrt{-b}(1-\sqrt{-b})}\right]. \tag{6.15}$$

This equation is simplified further by noting that

$$\frac{\sqrt{1-y_7^2}}{1-\sqrt{-b}}-\frac{\sqrt{1-y_7^2}}{1+\sqrt{-b}}=\frac{\sqrt{1-y_7^2}(1+\sqrt{-b})}{1+b}-\frac{\sqrt{1-y_7^2}(1-\sqrt{-b})}{1+b}$$

$$=\frac{2\sqrt{-b}\sqrt{1-y_7^2}}{1+b} \tag{6.16}$$

and substituting this result into equation 6.16 gives us

$$\frac{1}{4(b+y_7^2)}\left[\frac{1}{\sqrt{b+y_7^2}}\left(\arcsin\left[\frac{-\sqrt{-b}-y_7^2}{y_7(1+\sqrt{-b})}\right]+\arcsin\left[\frac{\sqrt{-b}-y_7^2}{y_7(1-\sqrt{-b})}\right]\right)\right.$$

$$\left.-\frac{\sqrt{1-y_7^2}}{\sqrt{-b}(1+\sqrt{-b})}+\frac{\sqrt{1-y_7^2}}{\sqrt{-b}(1-\sqrt{-b})}\right]$$

$$=\frac{1}{4(b+y_7^2)}\left[\frac{1}{\sqrt{b+y_7^2}}\left(\arcsin\left[\frac{-\sqrt{-b}-y_7^2}{y_7(1+\sqrt{-b})}\right]+\arcsin\left[\frac{\sqrt{-b}-y_7^2}{y_7(1-\sqrt{-b})}\right]\right)\right.$$

$$\left.+\frac{2\sqrt{1-y_7^2}}{1+b}\right]. \tag{6.17}$$

Finally, the general solution is found by taking the solution at the upper limit $x_8 = 1$ less the solution at the lower limit $x_8 = y_7$,

$$g_3(b,u)=\frac{1}{4(b+u^2)}\left[\frac{1}{\sqrt{b+u^2}}\left(\arcsin\left[\frac{-\sqrt{-b}-u^2}{u(1+\sqrt{-b})}\right]+\arcsin\left[\frac{\sqrt{-b}-u^2}{u(1-\sqrt{-b})}\right]+\pi\right)\right.$$

$$\left.+\frac{2\sqrt{1-u^2}}{1+b}\right]. \tag{6.18}$$

The conditional probability density function of the product of the effective gain and the cosine of the random phase variable is the solution to the integral

$$h_{y_8}(y_8)=\frac{6}{\pi}\int_{y_8}^{1}\left[\frac{1}{(1+u^2)^2}-\frac{1}{(2+u^2)^2}\right]\frac{1}{\sqrt{1-y_8^2/u^2}}du \tag{6.19}$$

which, based on the general result, has the solution

$$h_{y_8}(y_8)=\frac{6}{\pi}\left[g_3(1,y_8)-g_3(2,y_8)\right] \tag{6.20}$$

where $g_3(b, y)$ is defined in equation 6.18.

The probability density function described by equations 6.20 and 6.18 is that of the equivalent path gain random variable, multiplied by the cosine of a uniform phase variable. For the ideal power control case, this probability density function is the basis for the probability density function of the multi-user interference and that of the inter-symbol interference from the desired user.

6.3 The Multi-User Interference

The multi-user interference from any given user consists of the sum of the interference from each of the three paths,

$$\mathbf{z}_k = \frac{A}{2}\left[\mathbf{V}_{1,k}\chi_{1k}(\tau_{1,k})\cos(\Phi_{1,k}) + \mathbf{V}_{2,k}\chi_{1k}(\tau_{2,k})\cos(\Phi_{2,k}) + \mathbf{V}_{3,k}\chi_{1k}(\tau_{3,k})\cos(\Phi_{3,k})\right]. \tag{6.21}$$

One begins by finding the probability density function of the multi-user interference, given that the effective delay between the desired user and the interfering user τ_{1k} and the data bits b_{-1}^k and b_0^k are given constants. Under this condition, the effective delay for each path τ_{lk} and the cross-correlation function value $\chi_{1k}(\tau_{lk})$ for each of the three paths are given constants. Once the conditional probability density function is found for this case, the condition is removed and the probability density function for one interfering user is found. The total multi-user interference is simply the sum of the interference from each user over all the interfering users,

$$\mathbf{z} = \sum_{k=1}^{K} \mathbf{z}_k. \tag{6.22}$$

6.3.1 Probability Density Function Given a Constant Effective Delay

One begins by considering the conditional probability density function given that the effective delay between the desired user and the interfering user $\tau_{1,k}$ and the data bits b_{-1}^k and b_0^k are given constants. In this case, the effective delay for each path is also given, due to the multipath model definition:

$$\tau_{1,k} = \tau_{1,k}, \quad \tau_{2,k} = \tau_{1,k} + T_c, \quad \tau_{3,k} = \tau_{1,k} + 2T_c.$$

The data bits b_{-1}^k and b_0^k are given, so the cross-correlation function values at $\tau_{1,k}$, $\tau_{2,k}$ and $\tau_{3,k}$ are given constants also.

With constant cross-correlation function values, the signal from each interfering path is the product of a constant $\frac{A}{2}\chi_{1k}(\tau_{lk})$, the effective gain $\mathbf{V}_{lk}$ for that path and the cosine of the random phase Φ_{lk} (see equation 6.21). The effective gain of a given path is either unity in the case when the given path has the largest gain, or a random variable with a probability density function described in equation 6.10 when the given path does not have the largest gain.

When the given path has the maximum gain, the probability density function of the interference for that path has the form of the probability density function of the

cosine of a random phase variable scaled by the constant. When the given path does not have the maximum gain, the probability density function of the interference for that path is a probability density function of the form of equation 6.20 scaled by a constant.

Given the path that has the maximum gain, the form of the probability density function is known for each of the paths. The total interference from an interfering user is the sum of the interference of each of the three paths from that user (see equation 6.21). The interference from each of the paths is independent (given that the cross-correlation function values are constant), and therefore the probability density function of the total interference is the convolution of the probability density functions of the interference from each of the three paths. This convolution is performed three times, given that each respective path has the maximum gain, giving three conditional interference probability density functions.

The probability density function of the interference is the weighted sum of the three conditional probability density functions, where the weights are the probabilities that each path has the maximum gain. The probability that each of the three paths has the maximum path gain is 1/3, as the paths have equivalent gain distributions, making it equally likely for each path to have the maximum gain. Thus the probability density function for the interference is 1/3 times the sum of the conditional probability density functions, given that each of the paths has the maximum path gain. This gives the probability density function for the interference from one interfering user, given the data bits b^k_{-1}, b^k_0 and the relative delay $\tau_{1,k}$.

6.3.2 Removing the Constant Effective Delay Condition

The final step in finding the probability density function from one interfering user involves removing the condition of having a constant effective delay $\tau_{1,k}$, and also removing the condition on the data bits b^k_{-1} and b^k_0. Removing the condition on the relative time delay includes the effect of the cross-correlation function, as the cross-correlation function values for each path are a function of the random relative delay $\tau_{1,k}$.

To remove the condition of the constant effective delay $\tau_{1,k}$, one sums the probability density function for every possible $\tau_{1,k}$, multiplied by the probability that $\tau_{1,k}$ has that particular value. Note that $\tau_{1,k}$ is continuous and uniformly distributed in the interval $[0, T]$, so this sum becomes

$$f_{z_k}(z_k|b^k_{-1}, b^k_0) = \frac{1}{T}\int_0^T f_{z_k}(z_k|\tau_{1,k}, b^k_{-1}, b^k_0)d\tau_{1,k}. \tag{6.23}$$

Removing the condition on the data bits b^k_{-1} and b^k_0 is simple, assuming that 0 and 1 are equally likely. One finds the probability density functions given each of the four possible combinations of b^k_{-1} and b^k_0, and takes and average to give the unconditional probability density function for the interference from one interfering user,

$$f_{z_k}(z_k) = \frac{1}{4}\sum_{b^k_{-1}, b^k_0} f_{z_k}(z_k|b^k_{-1}, b^k_0) \qquad b^k_{-1}, b^k_0 \in \{0, 1\}. \tag{6.24}$$

6.4 The Inter-Symbol Interference

The inter-symbol interference in this case is very similar to that of the multiple paths case case, in that the inter-symbol interference is caused by the paths which are not the maximum path. One begins by finding the conditional inter-symbol interference, given that the path with the maximum gain is known, and is the mth path. This condition is then removed to give the probability density function of the inter-symbol interference.

The contribution to the interference from the lth path, where the lth path is not the maximum gain path, is the product of the scaled autocorrelation value $\frac{A}{2}\chi_{1,1}(\tau_{l,1})$, the effective gain variable $V_{l,1}$, and the cosine of the random phase $\Phi_{l,1}$. The effective path gain has a conditional probability density function of the form described in equation 6.10.

The receiver is locked to the mth path, as the mth path has the maximum gain. Thus, the effective time delay for the mth path $\tau_{m,1} = 0$. The autocorrelation values $\chi_{1,1}(\tau_{l,1}) = \chi_{1,1}((l-m)T_c)$, as the paths arrive at T_c intervals, and $\tau_{m,1} = 0$. This implies that the autocorrelation values for a given path l depend only on m, the path with the maximum gain. If it is assumed that m is given, then the autocorrelation values $\chi_{1,1}(\tau_{l,1}) = \chi_{1,1}((l-m)T_c)$ are given also, and are constants. Thus the conditional probability density function, given the path with the maximum gain, has the form of equation 6.20 scaled by a constant.

The total self interference when a given path has the maximum gain is the sum of the interference from the other two paths under this condition. The probability density function of this sum is the convolution of the conditional probability density functions for the two paths that do not have the maximum path gain. The resulting probability density function is the conditional inter-symbol interference, given that the mth path has the maximum path gain.

To find the overall probability density function of the inter-symbol interference, one finds the weighted sum of the three conditional interference probability density functions, where the weight for each density is 1/3, the probability that the mth path has the maximum gain,

$$f_{z_1} = \frac{1}{3}\begin{bmatrix} f_{z_{2,1}}(z|m=1) \odot f_{z_{3,1}}(z|m=1) \\ +f_{z_{1,1}}(z|m=2) \odot f_{z_{3,1}}(z|m=2) \\ +f_{z_{1,1}}(z|m=3) \odot f_{z_{2,1}}(z|m=3) \end{bmatrix}. \tag{6.25}$$

6.5 Probability Density Function of the Total Interference

The multi-user interference from the $K-1$ interfering users and the inter-symbol interference from the desired user are independent, so the probability density function of the total interference $f_z(z)$ is the convolution of the probability density functions from each user [Papoulis, 1984] and may be written

$$f_z(z) = f_{z_1}(z_1) \odot f_{z_2}(z_2) \odot \ldots \odot f_{z_K}(z_K) \tag{6.26}$$

where $\odot$ denotes convolution.

6.6 The Received Signal with Ideal Power Control

In this system the selection diversity ensures that the signal that the receiver is locked to the signal on the path with the maximum gain at any given time. In the case where ideal power control is employed, the strongest signal is normalised, making the effective gain on the path for the strongest signal unity. Therefore, the effective gain for the desired user is unity at all times, and the signal strength at the receiver is a constant $\frac{AT}{2}b_0^1$ for the ideal power controlled case.

6.7 Calculating the Average Probability of Error

The interference will cause an error in the symbol decision if the total interference $\mathbf{z}$ is greater than the bit energy $\frac{AT}{2}b_0^1$ of the desired signal from user 1. To calculate the average probability of error one finds the probability that the interference is greater than the received desired signal level

$$P_e = P\left\{\mathbf{z} > \frac{AT}{2}\right\} = \int_{\frac{AT}{2}}^{\infty} f_{\mathbf{z}}(z)dz \tag{6.27}$$

which is equivalent to the complementary distribution function of the interference $\mathbf{z}$, evaluated at $\frac{AT}{2}$.

6.8 Numerical Calculation of the Probability of Error

The method used to numerically calculate results for the ideal power control case is again similar to that presented in chapter 4. Equally spaced points on the characteristic functions of the interference are found and used to calculate the average probability of error. Thus one needs to find the characteristic function of the per-user multi-user interference and the characteristic function of the inter-symbol interference.

6.8.1 The Multi-User Interference

When calculating the characteristic functions for the multi-user interference, initially the conditional characteristic function is found, given the path with the maximum gain, the data bits b_{-1}^k and b_0^k, and given the relative delay $\tau_{1,k}$ is a constant. These conditions are removed following similar methods to those used to remove the conditioning for the probability density functions, to give the per-user characteristic function for the multi-user interference.

There are two possible forms for the conditional density functions of the interference signal on a given path, depending on whether the path has, or does not have, the maximum gain.

For the case where the path has the maximum gain and the power control algorithm makes the effective gain unity, the conditional probability density function has the form

$$f_{z_{lk}}(z_{lk}|l=m,\tau_{lk},b_{-1}^{k},b_{0}^{k})=\frac{1}{\pi a\sqrt{a^{2}-z_{lk}^{2}}}\quad\text{for } |z_{lk}|<a,\ 0 \text{ elsewhere} \tag{6.28}$$

where $a=\frac{A}{2}|\chi_{1k}(\tau_{lk})|$. For this probability density function form there is an analytical expression for the characteristic function. From Oberhettinger's tables [Oberhettinger, 1973] one finds that

$$\frac{1}{\pi a\sqrt{a^{2}-t^{2}}}\rightleftharpoons J_{0}(af) \tag{6.29}$$

where $J_0(af)$ is the zero order Bessel function, and

$$J_{0}(u)=\sum_{n=1}^{\infty}(-1)^{n}[n!\Gamma(n+1)]^{-1}\left(\frac{u}{2}\right)^{2n} \tag{6.30}$$

This gives us the conditional characteristic function for the multi-user interference signal on the path with the maximum gain. Discrete values of the conditional characteristic function are calculated from this analytical expression.

When the path does not have the maximum gain, the form of the conditional probability density function has a more complicated form (see equation 6.20). For these cases a numerical Fourier transform is performed on discrete values found using the analytical conditional probability density function to give discrete values of the conditional characteristic function.

Given the path with the maximum gain, the conditional characteristic function of the sum over the three paths is calculated by taking the product of the three conditional characteristic functions. This calculation is performed three times, given each respective path has the maximum gain, and the weighted sum of the conditional characteristic functions is calculated, noting that each path is equally likely to have the maximum gain. The result is the conditional characteristic function of the multi-user interference from user k, given τ_{1k}, b_{-1}^{k} and b_{0}^{k}.

To remove the conditioning on τ_{1k}, b_{-1}^{k} and b_{0}^{k}, the conditional characteristic function must be found and averaged over all values of τ_{1k}, b_{-1}^{k} and b_{0}^{k}. The relative delay τ_{1k} has a continuous distribution, and the integration over all values of τ_{1k} is performed numerically using a discrete sum over a large number of values of τ_{1k}. Care is taken to ensure that a sufficient number of values of τ_{1k} are used to give accurate results. This process is repeated for each of the four possible combinations of b_{-1}^{k} and b_{0}^{k}, and the average taken. The result is the characteristic function of the multi-user interference from a given user k.

6.8.2 The Inter-Symbol Interference

For the inter-symbol interference on a given path, the form of the conditional probability density function has the same form as that of the multi-user interference case when the given path does not have the maximum gain (see equation 6.20). Again a

numerical Fourier transform is performed on discrete values of the analytical conditional probability density function values to give discrete values of the conditional characteristic function. Note that inter-symbol interference comes only from the two paths which do not have the maximum gain.

Given the path with the maximum gain, the conditional characteristic function of the sum over the two interfering paths is calculated by taking the product of the two conditional characteristic functions. This calculation is performed three times, given each respective path has the maximum gain, and the weighted sum of the conditional characteristic functions is calculated, noting that each path is equally likely to have the maximum gain. The result is the characteristic function of the inter-symbol interference from the desired user.

To gain an average result, the inter-symbol interference characteristic function was found for each of the codes in the Gold code set, and an average characteristic function was calculated to give an average inter-symbol interference characteristic function.

6.8.3 The Total Interference

The characteristic function of the total interference is the product of the $K-1$ multi-user interference characteristic functions and the inter-symbol interference characteristic function.

6.8.4 Numerical Calculation of the Average Probability of Error

As described in section 6.7, the average probability of error is given by

$$P_e = P\left\{\mathbf{z} > \frac{AT}{2}\right\} = \int_{\frac{AT}{2}}^{\infty} f_{\mathbf{z}}(z)dz \tag{6.31}$$

assuming $b_0^1 = +1$, which is the complementary distribution function of the interference $\mathbf{z}$, evaluated at $\frac{AT}{2}$. As for the previous cases, a numerical series expansion technique is used to determine the complementary distribution function $G_{\mathbf{z}}(z)$ of $\mathbf{z}$ from the equally spaced characteristic function points [Beaulieu, 1990] (see equation 4.58).

6.9 Performance Results for the Ideal Power Algorithm

The average probability of error performance for the case with ideal power control on three equal average gain paths may be seen in figure 6.1. The results for the non-fading channel and selection diversity on three equal average gain paths are plotted for comparison. One can see that the power control performance results are an improvement over the performance with selection diversity alone, but are inferior to the non-fading channel case. These results indicate that a good power control algorithm improves performance for spread spectrum multiple access systems with multipath channels.

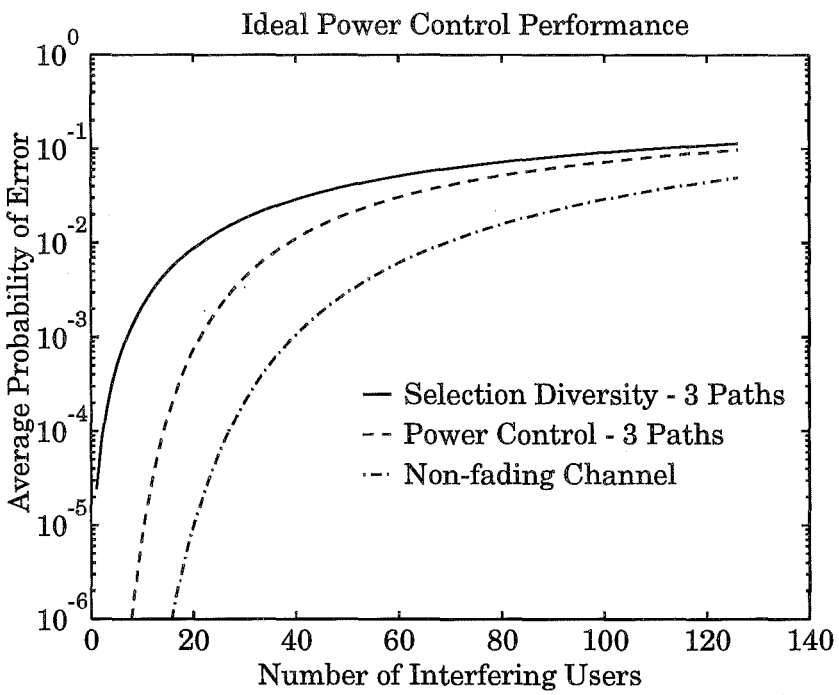

Figure 6.1 The average probability of error performance for the ideal power control case for three equal average gain paths, compared to the non-fading channel case and the selection diversity case for three equal average gain paths.

Chapter 7

DISCUSSION AND CONCLUSIONS

This thesis presents a novel combination of techniques which together have effectively allowed an analytical path for the evaluation of the performance of a spread spectrum CDMA system over non-fading or arbitrary multipath fading channels. In the past, researchers in this area have opted for analytical techniques with simplified channel models, a combination of analytical and bounding techniques, Monte Carlo integration techniques or approximation techniques to investigate performance. Thus the technique presented here, which involves finding the actual empirical probability density functions and characteristic functions, and uses these to calculate the system performance, is an original contribution to the body of knowledge in this area.

This chapter summarises the assumptions made and the method that was employed, and draws conclusions based on the results. Suggestions of some useful extensions for further research are also presented.

7.1 Summary of Method and Assumptions

The exact analysis of the performance a direct sequence spread spectrum multiple access system operating over an arbitrary multipath channel is presented. The performance measure in this analysis is the average probability of error.

The system that is analysed has K users, each with a mobile transmitter, and a base station which receives the signals from all of the K users. Spread spectrum code division multiple access techniques are used to distinguish the signals from each user. The average error probability is determined for one desired user, which is assumed to be user 1.

The users are assumed to transmit a binary data stream, where each level is equally likely. The users each have a spreading sequence, which in this study is a Gold sequence of length 127. Both the spreading code and the binary data are assumed to be represented by rectangular shaped pulses. All users employ the same carrier frequency, and the carrier phase and spreading code timing of all users are assumed to be independent.

The multipath channel is generally modelled by a tapped delay line model, where the taps are spaced at chip period intervals. Each tap is assumed to have a random gain with a Rayleigh distribution. The average gain of each tap is specified by a chosen delay profile. It is assumed that all users have the same average delay profile. A

slow fading environment is assumed, where the random parameters associated with the channel do not vary significantly over consecutive bit periods.

The receiver is assumed to be locked to the carrier and synchronised to the spreading code of the desired user at any given time, and operating in steady state. The receiver coherently demodulates and despreads the signal. The receiver employs a selection diversity algorithm, and is therefore assumed to be locked to the signal on the path with the maximum gain at any given time. Noise terms are omitted, as the system is assumed to be interference limited.

In chapter 6 an ideal power control algorithm is introduced. It is assumed that the transmitted signal level for any given user is altered to cancel out the gain of the maximum gain path from that user, so that the effective gain of the maximum gain path becomes unity. It is assumed that the strongest gain can always be found, that the power can be altered by any amount and that the control of the signal level is instantaneous.

The method employed to calculate the system performance involves the following steps, as described in section 4.2. Firstly, the probability density function of the per-user multi-user interference is found, derived from the probability density functions of each the contributing factors, including the cross-correlation function of the spreading codes. Similarly, the probability density function of the inter-symbol interference from the desired user is found.

The interference probability density functions are transformed to give the characteristic functions of the per-user multi-user interference and the inter-symbol interference. The characteristic function of the total interference is the product of $K-1$ multi-user interference characteristic functions and the inter-symbol interference characteristic function. The complementary distribution function of the interference is found from the total interference characteristic function using a numerical series expansion technique.

The probability density function of the desired signal is determined from the proability density function of the path gains specified in the delay profile, based on the selection diversity algorithm. The average probability of error is the expected value of the complementary distribution function of the total interference over the range of the desired signal.

This method is used to evaluate the performance for a single non-fading path case, a single flat fading path case with one effective fading path, a selection of multiple fading path cases, and finally a three path multipath model with the addition of a power control algorithm.

7.2 Conclusions

The following conclusions were reached based on the results found using this novel method.

7.2.1 Simplified Channel Model

For the single non-fading path case the analytical result is compared with those found using the common Gaussian approximation [Pursley, 1977] and an improved approximation [Holtzman, 1992b]. The results indicate that the Gaussian approximation is optimistic for small numbers of users, and that Holtzman's improved approximation is quite accurate.

7.2.2 Multipath Fading Models

The multipath results show that flat fading multipath has the worst performance for small numbers of users, due to errors caused by the deep fading of the desired user's signal. Selection diversity is shown to improve performance by reducing the effect of deep fades in the desired user's signal. Selection diversity results in better performance for the same number of users, even though the variance of the multiple path interference is greater than the flat fading interference variance.

It is shown that for the multiple fading paths case, the shape of the average delay profile does have some effect on performance when selection diversity is employed. A simple triangular shaped multipath gain-delay profile is adequate to model the typical signal level decay with increasing time, as the performance is almost identical for all of the decaying profile shapes. The simple five equal average gain model has similar yet observably different performance when compared to the other five path models.

7.2.3 The Effects of Power Control

The performance for the three equal average gain multipath model with power control was compared with those for the single non-fading path case and selection diversity on three equal average gain paths. The power control performance results are an improvement over the selection diversity performance, but are inferior to the non-fading channel case, where there is no multipath fading. These results indicate that a good power control algorithm improves performance for spread spectrum multiple access systems with multipath channels. It should be considered, however, that the power control algorithm presented here was ideal, and that a practical power control system would not perform as well.

7.3 Suggestions for Continuing Research

This thesis presents a combination of ideas and techniques which allows an analytical method for finding system performance. The use of these techniques could be extended to be a better representation of the practical case, or to further generalise the procedure to cover other areas of mobile radio, including cellular concepts and fast fading channels. Other proposed extensions include consideration other receiver

structures and investigations of the temporal statistics of the errors observed on the channel.

7.3.1 Practical Considerations

Some of the models that have been used in this analysis have been selected due to mathematical simplicity. Now that the basic technique has been resolved, some of these models may be extended to be more realistic in a practical sense.

- **Rician Fading Statistics**
  While the Rayleigh indoor radio channel models in the current analysis are a good representation of channel gain statistics taken over a wide set of measurement results, it has been shown that individual rooms' fading statistics often have a distribution closer to a Rician distribution than a Rayleigh distribution. Investigating the system performance for a Rician channel model is therefore of interest.

- **Limited Power Control**
  The power control algorithm presented here has a potentially infinite gain. A useful extension would be to consider the effect of having a maximum allowable gain, so that when extreme signal fading occurs, the signal is at most boosted by the maximum allowable gain. This would give a more realistic view of how much performance gain could be achieved with a practical power control algorithm.

7.3.2 Further Generalisations

The basic techniques presented here could also be extended to cover new cases and situations.

- **Mobile Environment Considerations**
  With the possibility of spread spectrum being employed in the mobile environment, it would be interesting to extend the analysis to cover aspects common to the urban mobile environment. These extensions could include cellular radio, fast fading effects and doppler effects.

  - The effects of cellular radio could be included into the analysis using some form of spatial distribution for the desired user, and considering the effects of signal loss and interference from other cells based on the relative position of the user and the base station.
  - The effects of rapid fading, where the signal fading changes quickly with respect to the symbol time of the transmitted data,
  - The effects of doppler shift in the carrier would be a useful extension to the analysis, in order to more accurately model the vehicular mobile environment.

- **Alternative Receiver Structures**
  Further extensions of the analysis could be made to include other receiver structures, such as RAKE receivers with different path-combining algorithms and possibly optimal receiver structures. This would allow comparisons between selection diversity, with or without power control, to RAKE receivers. Systems presented by Qualcomm have included RAKE receiver structures, making this an interesting comparison [Viterbi *et al.*, 1992].

- **Temporal Statistics**
  Currently, the performance measure is the average probability of error. The temporal statistics of the error events is also of interest as some aspects of a communications system, such as error correction codes, are influenced by the nature of the error events. The temporal statistics of errors could be investigated using a simulated temporal multipath model for the desired user.

Appendix A

RANDOM PROCESSES IN COMMUNICATIONS

In many communications systems, some contributions to the received signal are not deterministic, and are the result of stochastic or random processes. Examples of these are thermal noise and interference from other users, where the users transmit independently. To analyse a communications system which involves random processes, it is necessary to know the statistical distribution of the random processes involved.

When there is more than one stochastic process contributing to the received signal, one needs to find the statistical distribution of the total random contribution from all of the random processes involved. This chapter describes some statistical distributions commonly used to describe random processes found in communications, and methods for calculating the overall density function when functions of these random processes are summed or multiplied.

1 The Distribution of the Sum of Random Variables

The received signal in a communications system often involves the sum of several interference terms. If more than one of these terms is a random variable with a known distribution, it is necessary to find the distribution of sums of random variables in order to find the distribution of the received signal.

Thus it is desirable to find the distribution of the sum of two independent random variables with densities $f_{\mathbf{x}_1}(x_1)$, $f_{\mathbf{x}_2}(x_2)$. Papoulis states [Papoulis, 1984] that if the random variables $\mathbf{x}_1$ and $\mathbf{x}_2$ are independant, then the probability density of their sum $\mathbf{y} = \mathbf{x}_1 + \mathbf{x}_2$ is the convolution of their respective probability densities:

$$h_{\mathbf{y}}(y) = \int_{-\infty}^{\infty} f_{\mathbf{x}_1}(y - x_2) f_{\mathbf{x}_2}(x_2) dx_2 = \int_{-\infty}^{\infty} f_{\mathbf{x}_1}(x_1) f_{\mathbf{x}_2}(y - x_1) dx_1 \tag{A.1}$$

2 Characteristic Functions

The *characteristic function* of a random variable is defined to be [Papoulis, 1984]

$$\Phi(\omega) = \int_{-\infty}^{\infty} f(x) e^{j\omega x} dx \tag{A.2}$$

thus [Papoulis, 1984], is also

$$\Phi(\omega) = E\{e^{j\omega \mathbf{x}}\} \tag{A.3}$$

2.1 Independence and Convolution

Note that if two random variables x and y are independent, then the expected values [Papoulis, 1984]

$$E\{e^{j\omega(\mathbf{x}+\mathbf{y})}\} = E\{e^{j\omega\mathbf{x}}\}E\{e^{j\omega\mathbf{y}}\} \tag{A.4}$$

Now, if $\mathbf{z} = \mathbf{x} + \mathbf{y}$, then

$$E\{e^{j\omega\mathbf{z}}\} = E\{e^{j\omega(\mathbf{x}+\mathbf{y})}\} = E\{e^{j\omega\mathbf{x}}\}E\{e^{j\omega\mathbf{y}}\} \tag{A.5}$$

Resulting in

$$\Phi_{\mathbf{z}}(\omega) = \Phi_{\mathbf{x}}(\omega)\Phi_{\mathbf{y}}(\omega) \tag{A.6}$$

We know that the density of z is the convolution of $f_{\mathbf{x}}(x)$ and $f_{\mathbf{y}}(y)$. From this and equation A.6, it follows that the convolution of two densities is equivalent to the product of the two respective characteristic functions.

3 Complex Gaussian Random Variables

In this section it is shown that a complex Gaussian random variable, a complex number whose real and imaginary parts are both independent Gaussian variables, has a Rayleigh distributed modulus and a uniformly distributed argument.

If

$$\begin{aligned} r &= \sqrt{x^2 + y^2} \qquad \text{where } r \geq 0 \\ \Phi &= \arctan\frac{y}{x} \qquad \text{where } -\pi < \Phi \leq \pi \end{aligned} \tag{A.7}$$

then the system has one solution, $x = r\cos\Phi, y = r\sin\Phi$ for $r > 0$. (see figure A.1)

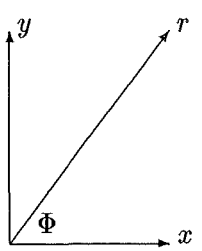

Figure A.1 Relationship of Rayleigh random variables and Gaussian random variables

The Jacobian transformation matrix is

$$J(x,y) = \begin{vmatrix} \cos\Phi & -r\sin\Phi \\ \sin\Phi & r\cos\Phi \end{vmatrix}^{-1} = \frac{1}{r} \tag{A.8}$$

It is concluded that the joint density function

$$f_{r\Phi}(r,\Phi) = r f_{xy}(r\cos\Phi, r\sin\Phi) \qquad \text{where } r > 0 \tag{A.9}$$

Now, if x and y are zero mean Gaussian then the joint density function is

$$f_{xy}(x,y) = \frac{1}{2\pi\sigma^2} e^{-(x^2+y^2)/2\sigma^2} \tag{A.10}$$

which, if $x = r\cos\Phi, y = r\sin\Phi$, yields

$$f_{r\Phi}(r,\Phi) = \frac{r}{2\pi\sigma^2} e^{-r^2/2\sigma^2} \qquad \text{where } r > 0, \qquad |\Phi| < \pi \tag{A.11}$$

and zero otherwise. This is a product of a function of r and a function of Φ. Hence the random variables r and Φ are independent with

$$\begin{aligned} f_r(r) &= \frac{r}{\sigma^2} e^{-r^2/2\sigma^2} \qquad \text{where } r > 0 \\ f_\Phi(\Phi) &= \frac{1}{2\pi} \qquad \text{where } -\pi < \Phi \leq \pi \end{aligned} \tag{A.12}$$

and zero elsewhere. The proportionality factors are chosen so as to make the area of each term 1. (see [Papoulis, 1984], pages 145,146).

4 Distribution of the Sine of a Random Phase Variable

If we have a random phase variable x which is uniformly distributed in the interval $[-\pi, \pi]$, and a function g such that

$$\mathbf{y} = g(\mathbf{x}) = a\sin(\mathbf{x} + \theta) \tag{A.13}$$

we can find the density function of y in terms of the density function of x.

Note that

$$g'(x) = a\cos(x+\theta) = \sqrt{a^2 - y^2} \tag{A.14}$$

For any given constant θ, there are two roots for $\sin(\mathbf{x} + \theta)$ in the interval $[-\pi, \pi]$. At these roots, the density function $f_{\mathrm{x}}(x_n) = 1/2\pi$. Thus, summing the results from the two roots gives [Papoulis, 1984]

$$f_{\mathrm{y}}(y) = \frac{f_{\mathrm{x}}(x_1)}{|g'(x_1)|} + \frac{f_{\mathrm{x}}(x_2)}{|g'(x_2)|} = \frac{2}{2\pi\sqrt{a^2 - y^2}} \qquad \text{for } |y| < a, \text{ 0 elsewhere} \tag{A.15}$$

5 The Distribution of Products of Random Variables

The received signal in a communications system often involves the product of several gain terms. If more than one of these terms is a random variable with a known distribution, then the overall gain is a product of these random variables, and it is therefore necessary to find the distribution of products of random variables in order to find the distribution of the received signal.

We start by finding the distribution of the product of two non-negative independent random variables with densities $f_{\mathrm{x}_1}(x_1)$, $f_{\mathrm{x}_2}(x_2)$ [Springer, 1979]. In order to find this distribution, we use the transformation of variables

$$\mathbf{y} = \mathbf{x}_1\mathbf{x}_2 \qquad \mathbf{x}_2 = \mathbf{x}_2 \tag{A.16}$$

which may be inversely written

$$\mathbf{x}_1 = \frac{\mathbf{y}}{\mathbf{x}_2} \qquad \mathbf{x}_2 = \mathbf{x}_2 \tag{A.17}$$

The transformation (eq. A.16) to transform the joint pdf $f(x_1, x_2) = f_{\mathbf{x}_1}(x_1) f_{\mathbf{x}_2}(x_2)$ into $g(y, x_2)$ gives

$$g(y, x_2) = f_{\mathbf{x}_1}\left(\frac{y}{x_2}\right) f_{\mathbf{x}_2}(x_2)|J| \tag{A.18}$$

where J is the Jacobian of the inverse transformation (eq. A.17):

$$\begin{aligned} J &= \begin{vmatrix} \frac{\partial x_1}{\partial y} & \frac{\partial x_1}{\partial x_2} \\ \frac{\partial x_2}{\partial y} & \frac{\partial x_2}{\partial x_2} \end{vmatrix} \\ &= \begin{vmatrix} \frac{1}{x_2} & \frac{-y}{x_2^2} \\ 0 & 1 \end{vmatrix} \\ &= \frac{1}{x_2} \end{aligned} \tag{A.19}$$

One then integrates out the variable x_2 from equation A.18, to obtain the density of y, namely

$$h_{\mathbf{y}}(y) = \int_0^\infty \frac{1}{x_2} f_{\mathbf{x}_1}\left(\frac{y}{x_2}\right) f_{\mathbf{x}_2}(x_2) dx_2 \tag{A.20}$$

This solution covers only non-negative random variables, but it is possible to extend this solution to cover the more general case where random variables may assume both positive and negative values. This extension is accomplished by partitioning a function $f_{\mathbf{x}_i}(x_i), -\infty < x_i < \infty, i = 1, 2, \ldots, n$, into two parts, being

$$f_{\mathbf{x}_i}(x_i) = f^-_{\mathbf{x}_i}(x_i) + f^+_{\mathbf{x}_i}(x_i) \tag{A.21}$$

where $f^-_{\mathbf{x}_i}(x_i)$ is identically zero except on the interval $-\infty < x_i < 0$, where $f^-_{\mathbf{x}_i}(x_i) = f_{\mathbf{x}_i}(x_i)$. Also $f^+_{\mathbf{x}_i}(x_i)$ is identically zero except on the interval $0 < x_i < \infty$, where $f^+_{\mathbf{x}_i}(x_i) = f_{\mathbf{x}_i}(x_i)$. Using this partitioning, it is possible to express the density $h_{\mathbf{y}}(y)$ of the product $\mathbf{y} = \mathbf{x}_1\mathbf{x}_2$ in terms of pairs of functions defined over the interval $(0, \infty)$.

In view of equation A.21, one may express the density $h_{\mathbf{y}}(y)$ as

$$\begin{aligned} h_{\mathbf{y}}(y) &= \int_{-\infty}^{\infty} \frac{1}{x_2} \left(f^+_{\mathbf{x}_1}\left(\frac{y}{x_2}\right) + f^-_{\mathbf{x}_1}\left(\frac{y}{x_2}\right)\right) (f^+_{\mathbf{x}_2}(x_2) + f^-_{\mathbf{x}_2}(x_2)) dx_2 \\ &= \int_{-\infty}^{\infty} \frac{1}{x_2} f^+_{\mathbf{x}_1}\left(\frac{y}{x_2}\right) f^+_{\mathbf{x}_2}(x_2) dx_2 + \int_{-\infty}^{\infty} \frac{1}{x_2} f^+_{\mathbf{x}_1}\left(\frac{y}{x_2}\right) f^-_{\mathbf{x}_2}(x_2) dx_2 \\ &\quad + \int_{-\infty}^{\infty} \frac{1}{x_2} f^-_{\mathbf{x}_1}\left(\frac{y}{x_2}\right) f^+_{\mathbf{x}_2}(x_2) dx_2 + \int_{-\infty}^{\infty} \frac{1}{x_2} f^-_{\mathbf{x}_1}\left(\frac{y}{x_2}\right) f^-_{\mathbf{x}_2}(x_2) dx_2 \end{aligned} \tag{A.22}$$

Note that when $y < 0$ and $-\infty < x_2 < \infty$,

$$f^+_{\mathbf{x}_1}\left(\frac{y}{x_2}\right) f^+_{\mathbf{x}_2}(x_2) = 0 \qquad \text{and} \qquad f^-_{\mathbf{x}_1}\left(\frac{y}{x_2}\right) f^-_{\mathbf{x}_2}(x_2) = 0 \tag{A.23}$$

so that equation A.22 becomes

$$h_y(y) = \int_{-\infty}^{\infty} \frac{1}{x_2} \left(f_{x_1}^{-}\left(\frac{y}{x_2}\right) f_{x_2}^{+}(x_2) + f_{x_1}^{+}\left(\frac{y}{x_2}\right) f_{x_2}^{-}(x_2) \right) dx_2$$

$$= \int_{0}^{\infty} \frac{1}{x_2} \left[f_{x_1}^{-}\left(\frac{y}{x_2}\right) f_{x_2}^{+}(x_2) + f_{x_1}^{+}\left(\frac{y}{-x_2}\right) f_{x_2}^{-}(-x_2) \right] dx_2, \quad -\infty < y \leq 0 \text{A.24)}$$

Similarly, when $y < 0$ and $-\infty < x_2 < \infty$,

$$f_{x_1}^{+}\left(\frac{y}{x_2}\right) f_{x_2}^{-}(x_2) = 0 \qquad \text{and} \qquad f_{x_1}^{-}\left(\frac{y}{x_2}\right) f_{x_2}^{+}(x_2) = 0 \tag{A.25}$$

and equation A.22 reduces to

$$h_y(y) = \int_{0}^{\infty} \frac{1}{x_2} \left[f_{x_1}^{+}\left(\frac{y}{x_2}\right) f_{x_2}^{+}(x_2) + f_{x_1}^{+}\left(\frac{y}{-x_2}\right) f_{x_2}^{-}(-x_2) \right] dx_2, \quad 0 \leq y < \infty \tag{A.26}$$

If one now defines

$$h_y(y) = h_y^{-}(y) + h_y^{+}(y) \tag{A.27}$$

where

$$h_y^{-}(y) = \begin{cases} h_y(y) & \text{if} \quad -\infty < y \leq 0 \\ 0 & \text{elsewhere} \end{cases} \tag{A.28}$$

and

$$h_y^{+}(y) = \begin{cases} h_y(y) & \text{if} \quad 0 \leq y < \infty \\ 0 & \text{elsewhere} \end{cases} \tag{A.29}$$

then

$$h_y^{-}(-y) = \int_{0}^{\infty} \frac{1}{x_2} f_{x_1}^{-}\left(\frac{y}{x_2}\right) f_{x_2}^{+}(x_2) dx_2 + \int_{0}^{\infty} \frac{1}{x_2} f_{x_1}^{+}\left(\frac{y}{-x_2}\right) f_{x_2}^{-}(-x_2) dx_2 \tag{A.30}$$

and

$$h_y^{+}(y) = \int_{0}^{\infty} \frac{1}{x_2} f_{x_1}^{+}\left(\frac{y}{x_2}\right) f_{x_2}^{+}(x_2) dx_2 + \int_{0}^{\infty} \frac{1}{x_2} f_{x_1}^{-}\left(\frac{y}{-x_2}\right) f_{x_2}^{-}(-x_2) dx_2 \tag{A.31}$$

6 The Distribution Function of a Sum of Random Variables

6.1 Introduction

In our study, it is necessary to find the distribution of the sum of the interference from a large number of users. The distribution of the interference from any given user should be allowed to be arbitrary, and the users are all independent interferers.

As we already know, the density function of the sum of two independent random variables is the convolution of the respective density functions. For the sum of more than two independent random variables, we find [Papoulis, 1984] that

$$f_z(z) = f_{z_2}(z_2) \odot f_{z_3}(z_3) \odot \ldots \odot f_{z_K}(z_K) \tag{A.32}$$

where $\odot$ denotes convolution.

It is possible to calculate this convolution numerically, but it is inefficient computationally, and it is much simpler to work with the characteristic functions (effectively the Fourier transform) of the densities, where the convolutions become products.

The following method uses a similar approach, where Fourier series are used to represent the density functions, so that the product can be used to represent the density function of the sum of the random variables. The density function or complementary distribution function can then be found from this series.

6.2 Description of the Numerical Method

The following method was devised by Beaulieu [Beaulieu, 1990]. This method firstly is derived for bounded random variables, but may be extended to unbounded random variables.

An upper bound on the probability of the sum of independent random variables exceeding a specified value has been given by Chernoff [Wozencraft and Jacobs, 1965]. This probability is first expressed as the expectation of a unit step function, which is then overbounded by a class of exponential functions. The upper bound may then be found by taking the expectation of the overbounding exponential function. This method derives a convergent infinite series for the cdf by representing the unit step function by a Fourier series and taking the expectation of the series.

Let $\mathbf{X}_i, i = 1, \ldots, L$ be bounded independent random variables, each with pdf $f_{\mathbf{X}_i}(x_i)$ such that $f_{\mathbf{X}_i}(x_i) = 0$ for all $x_i < B_i^L$ and for all $x_i > B_i^U$. Denote the sum of the L random variables as $\mathbf{X}$, where $\mathbf{X} = \sum_{i=1}^{L} \mathbf{X}_i$. The complementary distribution of $\mathbf{X}$ is $G_{\mathbf{X}}(x)$ and the pdf of $\mathbf{X}$ is $f_{\mathbf{X}}(x)$. Therefore, $\mathbf{X}$ is lower bounded by $B_L = \sum_{i=1}^{L} B_i^L$ and upper bounded by $B_U = \sum_{i=1}^{L} B_i^U$.

Now, let $S(x)$ be a periodic square wave, where

$$S(x) = \begin{cases} 0, & -T/2 < x < 0 \\ 1, & 0 < x < T/2 \\ \frac{1}{2}, & \pm T/2 \end{cases} \tag{A.33}$$

$$S(x + mT) = S(x), \qquad m = 0, \pm 1, \pm 2, \ldots \tag{A.34}$$

Then, as illustrated in figure A.2,

$$G_{\mathbf{X}}(\varepsilon L) = Pr(\mathbf{X} \geq \varepsilon L) = E\left[S(\mathbf{X} - \varepsilon L)\right] \tag{A.35}$$

where $E[\mathbf{X}]$ is the expected value of $\mathbf{X}$. Equation A.35 holds for $T/2 = \max\{B_U - \varepsilon L, \varepsilon L - B_L\}$, provided that the pdf of $\mathbf{X}$ does not have an impulse at a discontinuity of $S(\mathbf{X} - \varepsilon L)$

The Fourier series representation of $S(x)$ is

$$S(x) = \frac{1}{2} + \sum_{n=-\infty}^{\infty} C_n e^{jn\omega x}, C_n = \frac{1}{\pi n j} \tag{A.36}$$

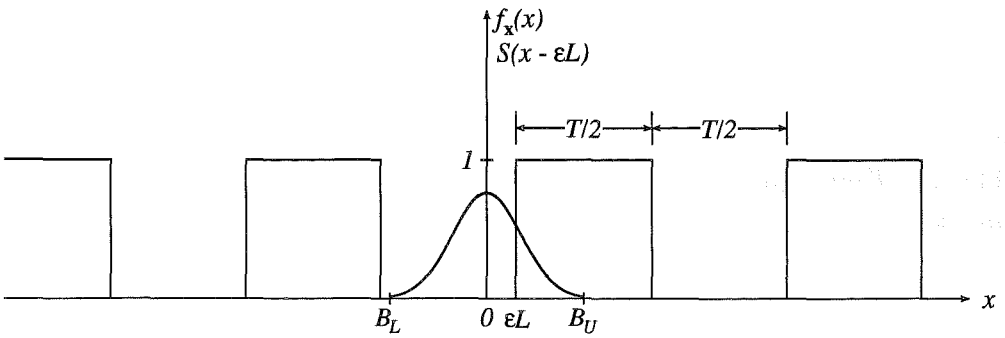

Figure A.2 The pdf of $f_{\mathbf{X}}(x)$ of the bounded sum, **X**, and the periodic square wave, $S(x - \varepsilon L)$. The sum is upper bounded by B_U and lower bounded by B_L

where $\omega = 2\pi/T$. The equality in equation A.36 is in the mean square sense.

Combining equations A.35 and A.36 gives

$$
\begin{aligned}
G_X(\varepsilon L) &= \frac{1}{2} + \sum_{n=-\infty}^{\infty} C_n E\left[e^{jn\omega(X-\varepsilon L)}\right] \\
&= \frac{1}{2} + \sum_{n=1}^{\infty} \frac{E\left[e^{jn\omega(X-\varepsilon L)}\right] - E\left[e^{-jn\omega(X-\varepsilon L)}\right]}{n\pi j} \\
&= \frac{1}{2} + \sum_{n=1}^{\infty} \frac{E\left[\exp\left(jn\omega\left(\sum_{i=1}^{L} X_i - \varepsilon L\right)\right)\right] - E\left[\exp\left(-jn\omega\left(\sum_{i=1}^{L} X_i - \varepsilon L\right)\right)\right]}{n\pi j} \\
&= \frac{1}{2} + \sum_{n=1}^{\infty} \frac{\prod_{i=1}^{L} E\left[e^{jn\omega(X_i-\varepsilon L)}\right] - \prod_{i=1}^{L} E\left[e^{-jn\omega(X_i-\varepsilon L)}\right]}{n\pi j} \\
&= \frac{1}{2} + \sum_{n=1}^{\infty} \frac{\prod_{i=1}^{L} A_{in} e^{j\theta_{in}} - \prod_{i=1}^{L} A_{in} e^{-j\theta_{in}}}{n\pi j} \\
&= \frac{1}{2} + \sum_{n=1}^{\infty} \frac{\exp\left(j\sum_{i=1}^{L}\theta_{in}\right)\prod_{i=1}^{L} A_{in} - \exp\left(-j\sum_{i=1}^{L}\theta_{in}\right)\prod_{i=1}^{L} A_{in}}{n\pi j} \\
&= \frac{1}{2} + \sum_{n=1}^{\infty} \frac{A_n e^{j\theta_n} - A_n e^{-j\theta_n}}{n\pi j} \\
&= \frac{1}{2} + \sum_{n=1}^{\infty} \frac{A_n \sin\theta_n}{n}
\end{aligned}
\tag{A.37}
$$

where

$$A_{in} = \sqrt{\{E\left[\cos(n\omega X_i)\right]\}^2 + \{E\left[\sin(n\omega X_i)\right]\}^2} \tag{A.38}$$

$$\theta_{in} = \tan^{-1}\left\{\frac{E\left[\sin(n\omega(X_i - \varepsilon))\right]}{E\left[\cos(n\omega(X_i - \varepsilon))\right]}\right\} \tag{A.39}$$

$$A_n = \prod_{i=1}^{L} A_{in} \tag{A.40}$$

$$\theta_n = \sum_{i=1}^{L} \theta_{in} \tag{A.41}$$

Let $\Phi_i(\nu) = E\left[e^{j\nu X_i}\right]$ be the characteristic function of the pdf $f_{X_i}(x)$ of the random variable X_i. Then equation A.37 may be expressed in terms of the characteristic function $\Phi_i(\nu)$

$$G_X(\varepsilon L) = \frac{1}{2} + \sum_{n=1}^{\infty} \frac{\exp\left(-j\frac{2\pi n\varepsilon L}{T}\right)\prod_{i=1}^{L}\Phi_i\left(\frac{2\pi n}{T}\right) - \exp\left(j\frac{2\pi n\varepsilon L}{T}\right)\prod_{i=1}^{L}\Phi_i\left(\frac{-2\pi n}{T}\right)}{n\pi j} \tag{A.42}$$

Note that for a symmetrical distribution, $\Phi_i\left(\frac{2\pi n}{T}\right) = \Phi_i\left(\frac{-2\pi n}{T}\right)$, so that

$$G_X(\varepsilon L) = \frac{1}{2} + \sum_{n=1}^{\infty} \frac{\prod_{i=1}^{L}\Phi_i\left(\frac{2\pi n}{T}\right)\sin\left(-j\frac{2\pi n\varepsilon L}{T}\right)}{n} \tag{A.43}$$

6.3 Unbounded Random Variables

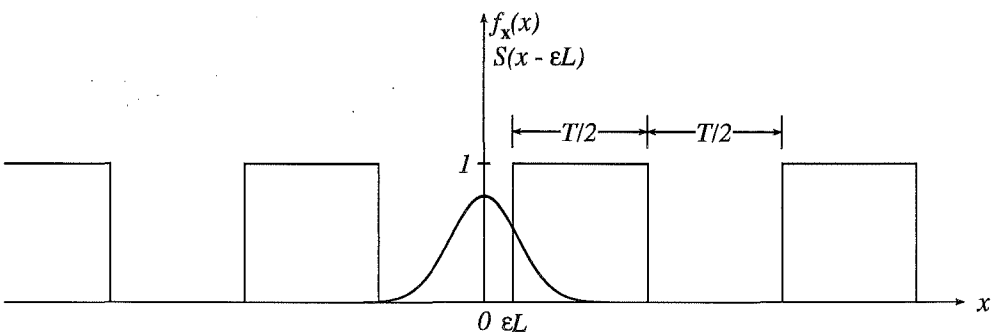

Figure A.3 The pdf of the unbounded sum, **X**, and the periodic square wave, $S(x - \varepsilon L)$.

Now a set of unbounded independent random variables, with an unbounded sum, are considered (see figure A.3). It is assumed that B_L and B_U can be chosen so that $Pr(\mathbf{X} \leq B_L)$ and $Pr(\mathbf{X} \geq B_U)$ are "negligible".

Once B_L and B_U are chosen, one simply follows the same method as for bounded random variables, described above.

Appendix B

INDOOR WIRELESS CHANNEL INVESTIGATIONS

The indoor radio channel measurement system described here was designed by the author to measure the transmission characteristics of low power UHF radio inside buildings. The measurements made with this equipment could be used to examine rms delay spread statistics for any particular room or to see how well the results fit certain models.

The indoor radio channel has been investigated by various methods including continuous wave [Alexander, 1982] [Alexander, 1983], pseudonoise sequences [Devasirvatham, 1984] [Bultitude *et al.*, 1989] and pulsed carrier [Saleh and Valenzuela, 1987] [Pahlavan *et al.*, 1989] [Rappaport and McGillem, 1989] systems. The continuous wave measurements investigated attenuation characteristics and showed that the power law describing the signal attenuation as a function of distance varies greatly from building to building and seems to be related to the physical layout. Office buildings typically saw the signal strength $\alpha\ D^{-3}$ to D^{-4}, with factors as high as D^{-6} in extreme cases [Alexander, 1983]. The other two methods provided information about the spread of energy caused by reflections from objects and walls. The rms measure of the delay spread is given by

$$\tau_{rms} = \left(\frac{\sum_{k=0}^{L} (\tau_k - \bar{\tau})^2 C(\tau_k)}{\sum_{k=0}^{L} C(\tau_k)} \right)^{1/2} \tag{B.1}$$

$$\bar{\tau} = \sum_{k=0}^{L} \tau_k C(\tau_k) \tag{B.2}$$

where τ_k is the kth path arrival time and $C(\tau_k)$ is the amplitude of the kth path [Sexton and Pahlavan, 1989].

We chose to construct a system based on the pulsed carrier system used by Saleh [Saleh and Valenzuela, 1987] as it would give the delay spread information and would be simpler than the pseudonoise system to construct.

The statistics of the spread values and models of the delay profiles are of interest and some models have been proposed [Sexton and Pahlavan, 1989] [Winters and Yeh, 1985] [Chuang, 1987]. These models, shown in Figure B.1, are used in computer simulations and attempt to satisfy the statistics of the path amplitudes.

Saleh [Saleh and Valenzuela, 1987] devised a model which also attempted to describe the path arrival times. The basic envelope of the delay profile was stated to

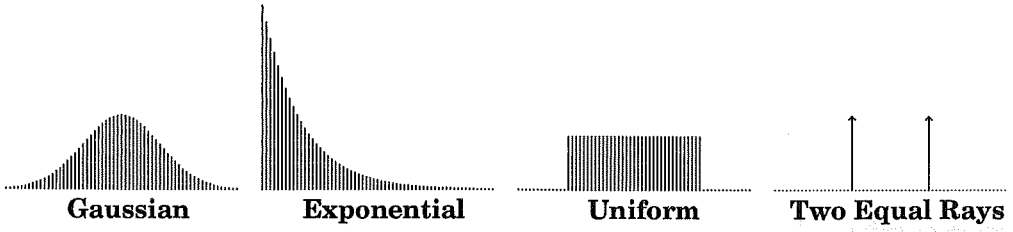

Figure B.1 Graphical representations of channel models — these diagrams are scaled to have the same rms delay spread

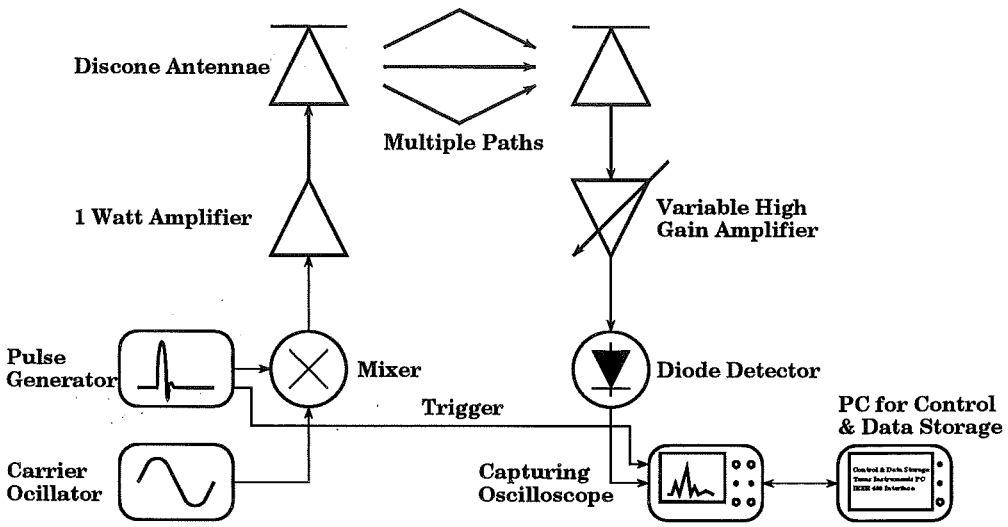

Figure B.2 Block diagram of the hardware

be exponential (see fig. B.1) with clusters of rays arriving with a poisson distribution. These ray clusters are described as being like small exponential delay profiles also with poisson arrival times. Ganesh [Ganesh and Pahlavan, 1989] also noted this cluster effect, but chose to model it by having modified poisson arrival times. In this model, if one ray arrives, the poisson mean arrival rate is altered, generating the "cluster".

A description of the hardware (see fig. B.2) and software used for this project and results from measurements in two different locations are be discussed in this appendix.

1 System Design

Ideally, the impulse response of the multipath indoor channel would be measured by transmitting a single pulse of high power but very short duration (a delta function) and monitoring the spread of arrival times of the pulse reflections at the receiver. In practice, a 2.5 nanosecond pulse modulating a 1000 megahertz carrier was the closest approximation achievable. Narrower pulses would imply increasing bandwidth with correspondingly greater noise at the receiver.

Figure B.2 shows a block diagram of the Channel Sounder, and the following sections describe its design.

1.1 Noise Parameters

The noise floor power was taken to be -174 dBm per Hertz. This figure is derived from the passive irreducible kT noise, where k is Boltzman's constant and T is the temperature in Kelvin. If T is taken to be 290 degrees [Davenport, Jr. and Root, 1958], $kT = 4 \times 10^{-18}$ mW per Hertz which is -174 dBm per Hertz. If an overall receiver bandwidth of 1 GHz is assumed, the bandwidth in decibels is

$$BW(dB) = 10 \log 10^9 = 90dB \tag{B.3}$$

The total noise power is given by the noise power per Hertz multiplied by the bandwidth, which would result in the noise power becoming -174 dBm + 90 dB, giving a noise floor of -84 dBm for a bandwidth of 1 GHz.

The high gain amplifier was estimated to have a noise figure of 9 dB, derived from

$$F = \frac{S_{NO}}{G.S_{NI}} \tag{B.4}$$

where S_{NI} is the input noise power, S_{NO} is the output noise power and G is the gain. This amplifier was constructed from six separate amplifiers in series. The total noise figure was calculated using

$$F_{tot} = F + \frac{F-1}{G} + \frac{F-1}{G^2} + \frac{F-1}{G^3} + \frac{F-1}{G^4} + \frac{F-1}{G^5} \tag{B.5}$$

which was derived from [Haykin, 1983] eqn. (A3.14). The gain (G) was 10 dB and a noise figure (F) was 7 dB, taken from the data book.

This results in an overall input noise power at -75 dBm.

1.2 Path Loss

The attenuation of signals in indoor environments has been shown to be between 40 and 80 dB [Devasirvatham, 1986]. If the measurement system was required to cope with a path loss of 70 dB, the total power transmitted was required to be -75 + 70 + dynamic range. A dynamic range of 30 dB would require transmitter power to be +25 dBm. This is equivalent to 400 mW into 50 ohms. The power amplifiers used in the transmitter were rated at 30 dBm (1 watt) to cope with these requirements.

2 The Hardware Description

2.1 The Transmitter

The transmitter was designed to transmit 2.5 nanosecond pulses modulated onto a 1 gigahertz carrier. The narrowness of the pulses is limited by the amount of bandwidth allowable. If the pulses are narrower, the resolution is finer, but the bandwidth

requirement is greater. Another limiting factor apparent when increasing the bandwidth is the increase in the noise power. The carrier frequency of 1 GHz was chosen as many experiments have been performed in this region of the spectrum [Alexander, 1982] [Bultitude *et al.*, 1989] [Pahlavan *et al.*, 1989] and a similar frequency should be used to get comparable results. This frequency region also seems to be the likely choice for indoor systems [Sexton and Pahlavan, 1989].

The transmitter was composed of a carrier oscillator, a pulse modulator and a mixer, followed by a power amplifier and a discone antenna. The discone antenna was chosen over the dipole because of the greater bandwidth available (see section 2.1).

The Carrier Oscillator

The carrier oscillator used was a manually adjustable General Radio 1218-B Unit Oscillator. This has a range of 900–2000 megahertz, but for the measurements this was permanently set to 1000 megahertz. The carrier level setting was adjusted to where the pulsed output was at its maximum and the carrier feedthrough amplitude (when there was no pulse) was minimal compared to the pulse height, giving maximum dynamic range.

The Pulse Generator

The pulse generator used was a Tektronix Type 111 Pretrigger Pulse Generator. This pulse generator has a pretrigger output for use as a trigger for external devices and the pulse output which provides pulses approximately 2 nanoseconds in length. The time between the pretrigger and the pulse is variable between 25 nanoseconds and 240 nanoseconds. The pulse repetition frequency used was around 100 kHz, which is the maximum with this pulse generator. It would have been desirable to have around 600 nanoseconds [Saleh and Valenzuela, 1987] between pulses (1.66 MHz) which would have resulted in a shorter acquisition time.

It was necessary to attenuate the pretrigger output by 20 dB to ensure that there was no damage to the external trigger input of the oscilloscope (see figure B.2). The oscilloscope inputs are all rated at a maximum of 5 volts rms and the output from the pulse generator has a maximum value of +10 volts. A 20 dB attenuator made it possible to view the trigger pulse or to use the pulse with the external trigger input of the oscilloscope.

The pulse output, which is +10 volts, was attenuated by 17 dB before going into the mixer to give a clean modulated pulse from the power amplifier. This value was determined by observing the pulsed carrier output from the power amplifier (as in section 2.1) and adjusting the height of the pulse using a variable attenuator until the pulse was the maximum height but the ringing was at a minimum. Figure B.3 shows oscilloscope trace plots for the normal 17 dB attenuation of the pulse, as well as a larger pulse input (10 dB attenuation) and a smaller pulse input (22 dB attenuation).

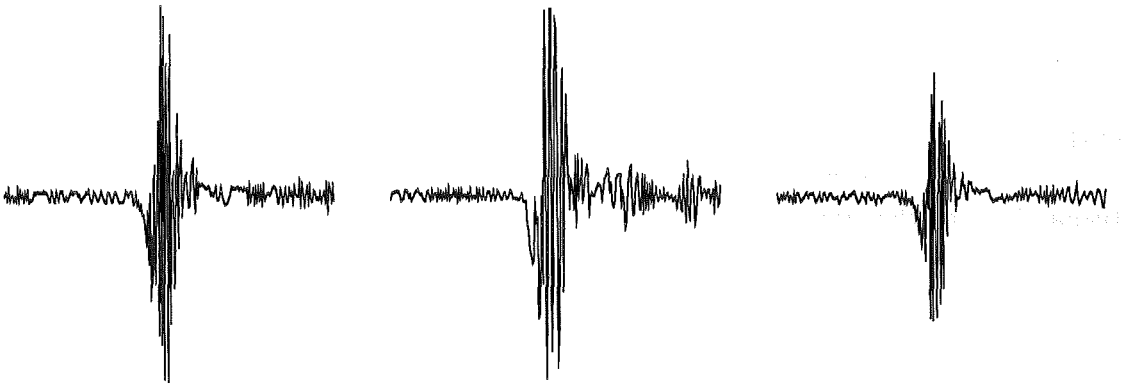

Figure B.3 Oscilloscope trace for various pulse output attenuation settings

The Modulator

The modulator was made up from two double balanced mixers (Mini Circuits SRA-11H - see fig. B.4.

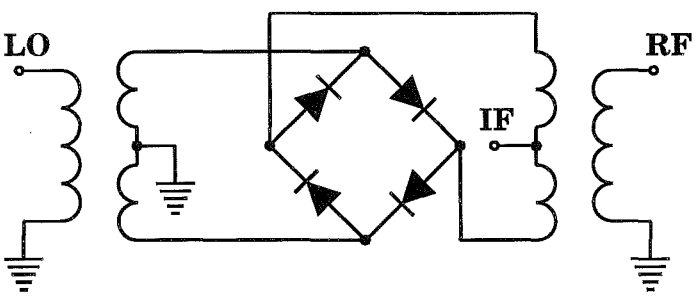

Figure B.4 Circuit diagram for a double balanced mixer

The modulated pulse was generated by creating an imbalance in the diodes by connecting the pulse to the IF input, resulting in a large amount of feed through between the RF and LO ports. Connecting the carrier to one of these ports resulted in the gated carrier appearing at the other port. When using only one mixer it was noticed that the carrier feedthrough level compared to the pulse height was too high, giving a dynamic range limit of around 20 dB. Two mixers in series gave a dynamic range of greater than 30 dB, which was adequate for the system.

Small capacitors (6 pf) were used in series with the mixers to make RC high pass filters to minimize the feedthrough of the pulse onto the output. With the capacitors in circuit, the maximum value of the pulse feedthrough without carrier present is 14 dB lower than the peak pulsed carrier level. Higher order filters may be used to decrease the pulse feedthrough further. Connecting cables were attached directly to the device pins or the capacitors to minimise impedance mismatch.

The Power Amplifier

The power amplifier used was a Mini Circuits ZHL–2–12. This unit has a maximum output power of 28.5 dBm (1 watt) and a gain of 24 dB. The frequency response is 10 – 1200 MHz and noise figure is 10 dB. The noise figure is not important in the transmitter as the signal to noise ratio is large.

The Antenna

A pair of wide band discone antennae [Nail, 1953] were used. The discone antenna has similar gain to a dipole but has a much wider bandwidth, and can be constructed to match the impedance of the system. The antennae constructed had a radius of 220 mm at the base of the cone, a height of 190 mm and the disc had a radius of 155 mm. The spacer was 3 mm thick and 13 mm in diameter. The ratio of disc radius to cone base radius and spacer thickness were taken as the optimum values shown in [Nail, 1953] to give the best match to a 50 ohm line over the largest frequency band. The slant height of 220 mm allows use of the antenna down to f_o = 440 MHz. The normalized field patterns shown in Figure B.5 are for $2f_o$ and $2.5f_o$. The 1 GHz centre frequency used was about $2.25f_o$.

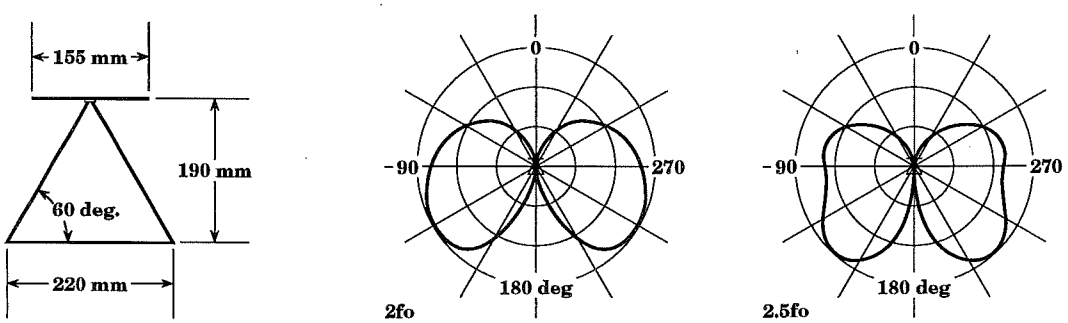

Figure B.5 Antenna dimensions and E-plane normalized field patterns

2.2 The Receiver

The task of the receiver is to amplify the transmitted signals, perform envelope detection and then save the resulting profile for future reference. The receiving equipment resides on a trolley, which allows the receiver to be moved to many different locations in a given room with relative ease. The receiver requires hard wired connections to the transmitter for oscilloscope synchronization and to a 240 volt AC outlet for power.

The Antenna

The receiver antenna is a wide band discone antenna, identical to the transmitter antenna. The receiver antenna was placed on the trolley at the same height from the floor as the transmitter antenna (approximately 1 metre).

The Variable High Gain Amplifier

The high gain amplifier is made from six Motorola MWA0204 10 dB amplifiers connected in series. These devices are capacitively coupled, with a dc current supply connected to the output of each device. The value of the capacitors used sets the low frequency response, with the 3 dB point chosen by $f_{LF}(\text{Hz}) = \frac{1}{100\pi C}$ (assuming R = 50 Ω). This was chosen to be 500 MHz.

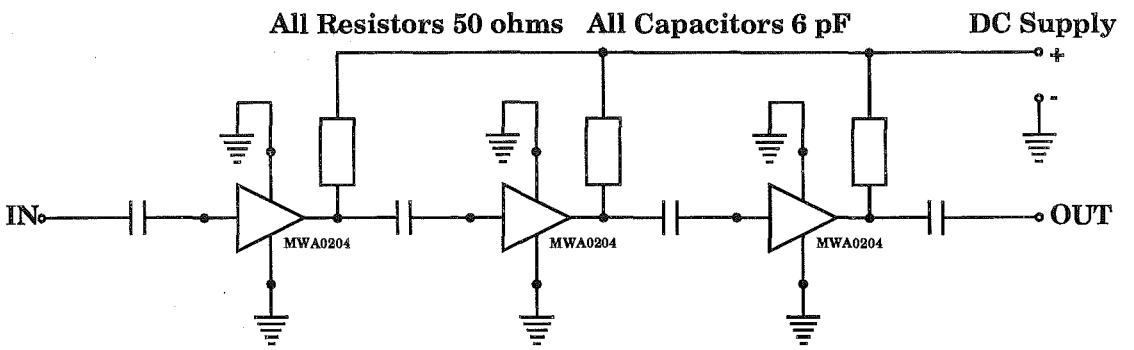

Figure B.6 Circuit diagram of a three stage amplifier

The circuit board was made with two separate circuits with three devices each (see fig. B.6). A circuit made from six amplifiers in series on one board was attempted but it was not possible to ensure stability with this layout. Both circuits were essentially identical, but were the mirror image of each other physically.

The basic layout can be seen in Figure B.7. The 6 pF coupling capacitors and 220 Ω current supply resistors were connected directly to appropriate pins of the amplifier. The two ground pins of the amplifiers were soldered directly to the ground plane. The devices were sunk into the board to keep pin length to a minimum. The input and output coaxial cables were attached to the coupling capacitors for the signal path, and soldered directly to the earth plane for the shield.

The direct current power for the amplifiers is supplied by current limiting resistor connected to the output pin of the amplifier. It is important that no RF energy travels up these resistors as, due to the gain, positive feedback could occur through the common supply. Inductive beads were placed on the leads of the resistors to make the path high in impedance for the high frequency signals. A further precaution was taken by placing 27 pF capacitors to ground close to the power supply resistor of the highest amplitude output amplifier. A second capacitor was placed close to the power dc supply connection to give a low impedance path to ground for any high frequency energy coming from the supply. These measures ensured the stability of the circuit.

The two circuit boards were placed back to back with an earth plane in between. The signal and ground paths were conducted via a short length of coax which was placed in a hole drilled through the circuit boards. The two capacitors, one on each side, connecting to this are 12 pF each as they are in series. This gives the 6 pF

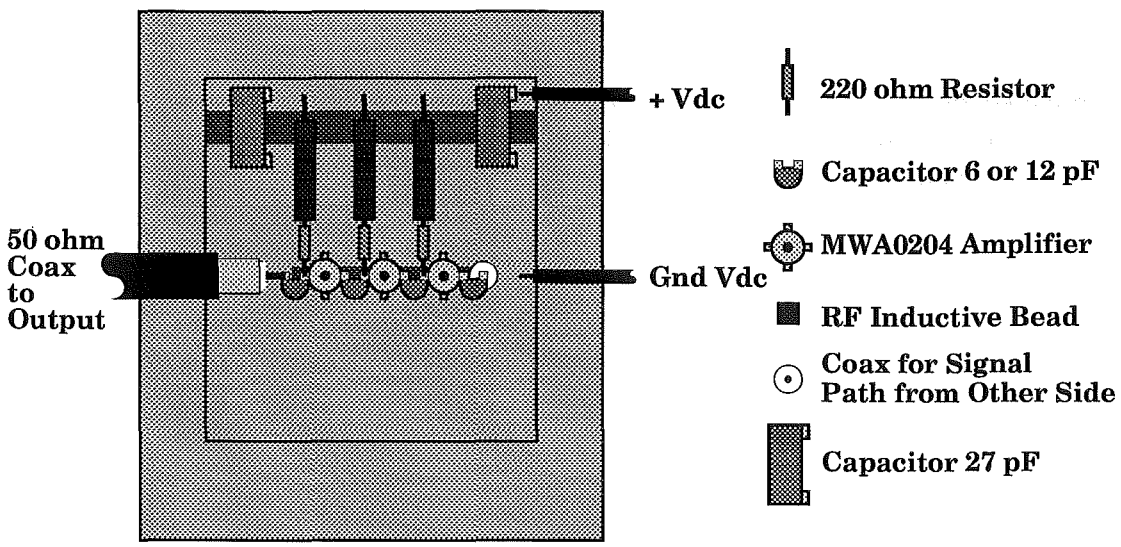

Figure B.7 Physical layout of a three stage amplifier

coupling capacitance.

It was important to ensure that there was only one earth path from input to output as extra paths caused oscillations. The connectors on the front of the case were mounted on perspex to prevent any path between the input and output grounds through the case.

The gain is controlled by a variable voltage power supply. This supply is a simple direct current supply with six selectable settings. It is possible to set the output for each of the six positions to a voltage between 7 and 10 volts. This voltage supply range allows for a wide variation in the gain of the amplifier. The actual voltage levels for each setting were trimmed to provide the gain required for that setting. The voltages were set up to give a gain of 10 dB at 7.34v, 20 dB at 7.83v, 30 dB at 8.00v, 40 dB at 8.22v, 50 dB at 8.63v and 60 dB at 9.76v.

Power Amplifier

A Mini Circuits ZHL–2–12 (see section 2.1) amplifier is used to amplify the signal to a sufficient level for detection by a diode.

Diode Detector

The diode detector consists of a load resistance in parallel with a series diode with a capacitor to ground on the output (see fig. B.8). The output from this is a 50 ohm load provided by the input load of the oscilloscope.

This small circuit was mounted inside an extended female to female BNC connector. An earlier prototype was made simply mounted on a piece of U shaped sheet metal, but this was susceptible to interference. The female to female BNC connector

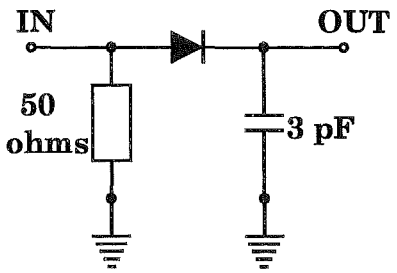

Figure B.8 Circuit diagram of the diode detector

was cut in half, and the diode was placed in between the input and output. A piece of brass tube (see fig. B.9) was added to the connector to allow for this increase in length. The resistor and capacitor were connected to ground and the unit was labelled and sealed. The complete grounded casing eliminated interference problems.

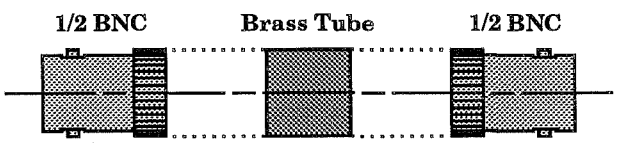

Figure B.9 BNC female to female connector halved with extension brass tube

The Oscilloscope

The oscilloscope used to display and transfer the profile data to the computer was a Phillips PM 3340 2 GHz oscilloscope. The effective bandwidth was used in the development of the high gain amplifier and other devices where it was useful to be able to display the 1 GHz carrier. The bandwidth requirement for an oscilloscope solely for use in the receiver would be determined by the width of the pulses used. For 2.5 nanosecond pulses, it would be desirable to have a bandwidth of at least 400 MHz. If wider pulses were used, the bandwidth requirement would be less.

The PM 3340 is a repetitive sampling oscilloscope. This means that it samples a large number of waveforms in different places and creates a display of one single trace from all the samples. For this method to work, the waveform being displayed must repeat itself exactly each time samples are taken. This was not entirely the case for the profile measurements. The carrier was not synchronised with the pulse, which resulted in the detected waveform changing shape while the repetitive sampling process was operating. This was observable when the output from the transmitter was connected directly to the diode detector, and was even more noticeable when used for taking profile measurements. The averaging function on the oscilloscope was used to lessen the effect, and also lowered the noise level evident on the display. It was possible to average over 64 traces. With the averaging set to 64, the acquisition time was about three seconds.

The final consideration in choosing an oscilloscope, is the control and data transfer options. The PM 3340 has both IEEE–488 and RS–232 options for connection to an external controlling source. The GPIB (IEEE–488) interface was used as it was a parallel interface designed for use with instrumentation. Using this interface would make the system hardware compatible with a greater range of instruments compared with using RS–232.

2.3 Control and Data Capture - The Personal Computer

A Texas Instruments Personal Computer was used to control the oscilloscope settings, measurement timing, data transfer and data storage. This machine is a standard IBM PC-XT clone and operates using the MSDOS disk operating system. A 40 megabyte fixed disk drive unit was installed to allow mass data storage. The data transfer and control for the oscilloscope was achieved using a National Instruments IEEE-488 bus card with associated software and cables.

3 Software Summary

3.1 The GPIB Bus Control Software

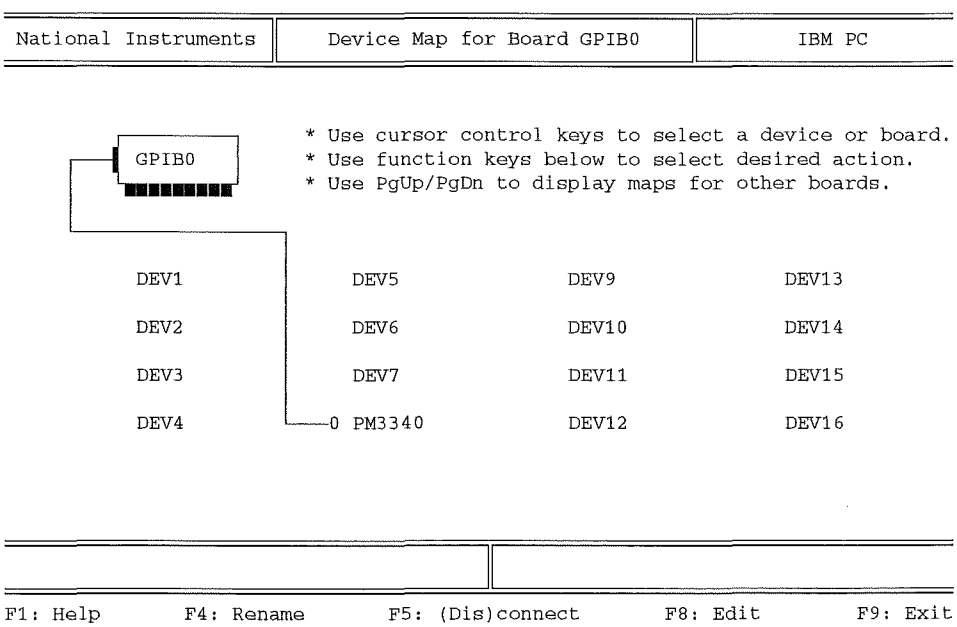

Figure B.10 National Instruments GPIB device map screen

Software obtained from National Instruments was used for setting up the GPIB Bus and interfacing to the bus using Turbo C. The main configuration programme used when setting up the GPIB bus system is IBCONF.EXE, which was used to set up the GPIB device driver by altering the computer's map of the physical layout of the instrument system. The final GPIB device layout can be seen in Figure B.10.

Software was also available for testing the GPIB setup, by allowing interactive communication between the Personal Computer (PC) and the oscilloscope during system development.

3.2 The Control and Data Capturing Software

The software written for the PC was needed to control the oscilloscope during the experiment and capture the data for storage. This software was written in Turbo C and was linked with National Instruments software to operate with the IEEE-488 bus. The main control routine had options allowing control of the oscilloscope settings, measurement timing and labelling for profile storage.

There were two options for making measurements — instantaneous and by delayed timer. The timer allows a number of measurements to be made starting at a set time, with a set time between each measurement. This option could be used to make measurements while the user was absent. For example, one could make a set of seven measurements made from 1:00 am to 7:00 am at one hour spacing. Also, if the measurement location is quite noisy, one may wish to make more than one measurement at each position (see sections 4.2 & 5.1), and take an average. For one noisy location, a set of 8 measurements was made for each position, with an interval of 12 seconds between each measurement.

3.3 Data Processing Software

The Personal Computer is only an IBM XT clone, and is too slow for data processing. This resulted in the processing of the profiles being mainly executed on the departmental VAX. These processing programmes, written in VAX-C, were designed to assist the user to extract the amplitude and arrival times of the paths represented in the measured profiles.

Averaging and Conversion to Voltages

For some of the measurement locations, the noise level was sufficiently high to require several measurements to be made in each position. These measurements needed to be combined in some way. The first programme in the processing chain took input from a number of measurements, averaged them into one profile and converted this profile into a voltage level using the vertical scale and offset information.

The averaging process is not just a simple average. It was found that, due to timing jitter between measurements, the profiles did not line up exactly. This jitter was sometimes as much as ten samples, which corresponds to a time value of half a nanosecond. This timing jitter is due to triggering jitter from the rising edge of the trigger pulse and the repetitive sampling of a signal that is not truly repetitive, as the pulse and carrier are not synchronised. Once the first profile is read in and converted to an integer array, the next profile is read in and a cross correlation is performed on the two profiles before they are added to form one profile. This profile is then

correlated and added with the next, until all the profiles are added into one. This profile is divided by n to reduce it back to the original scale and processed using the oscilloscope vertical scale value and voltage offset to leave an array of 4096 floating point voltage values, representing the original measured profile voltages.

Adding Amplifier Gain Information and Smoothing

The next step in the processing was to incorporate the gain setting of the variable gain amplifier and to smooth out the sharp peaks in the data. It was noted that some of the peaks on the averaged profiles were very sharp where others were quite rounded. The energy in a rounded peak would be much more than the energy in a sharp peak of the same height. If this peak height alone was used to estimate the energy in each path, the two peaks would be considered equal, which was clearly not the case. The example shown in Figure B.11 has the first two peaks near the same height, but the second peak is more narrow than the first.

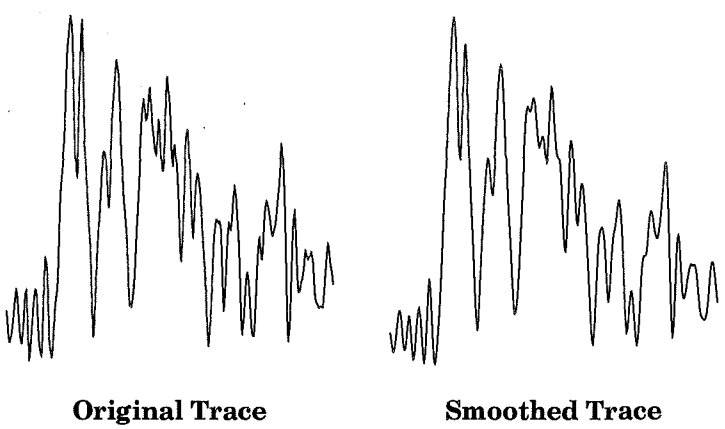

Figure B.11 Part of a measured profile trace before and after smoothing.

A process was needed that would lower the height of a narrow peak but leave the rounded peak as it was. It was decided to convolve the profile with a Kaiser window [Harris, 1978] to smooth out the sharp peaks. The width of the window was chosen to be 15 samples (0.75 nanoseconds) with a 3dB point of approximately 1.28 GHz, which was wide enough to smooth off the sharp peaks but narrow enough so as not to smear two peaks into one (see fig. B.11). A tighter filter (470 MHz 3 dB point) was tried, but seemed to smear close but distinct pulses into one pulse. The gain of the filter was set to give unity gain for the reference pulse (see fig. B.12).

The Path Extraction

It was decided that the best method of deciding which peaks were paths and which were caused by artifacts or noise was to use an interactive approach. This approach is similar to the "interactive heuristic computer optimization" used by Saleh [Saleh

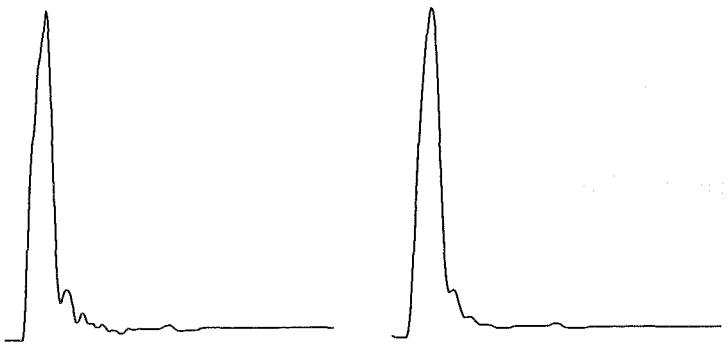

Figure B.12 Reference pulse before and after smoothing.

and Valenzuela, 1987]. The Personal Computer was chosen for this work because the interfacing involved to use the mouse for selection was simpler on the PC.

The DC level of the noise was calculated and subtracted, and the profile was displayed on the PC monitor. The zero level was also displayed so that one could see the true relative heights of the peaks. The user can then selected peaks by selecting them with the mouse cursor. To make selection simpler, the programme "snapped" to the nearest peak. The selected peaks were indicated by a colour change.

4 The Measurement Locations

The system described was used to make delay profile measurements in two different locations. The first location was in the Electrical and Electronic Engineering Department at the University of Canterbury. The room in which the measurements were made was R9, the research laboratory in which the system was developed.

The system was also used to make measurements in the Telecom District Engineers Office in central Christchurch. The room measured was an open plan office on the seventh floor of Carruca House.

4.1 Research Room R9 in the Electrical Engineering Wing

The research room R9 is located upstairs at the eastern end of the Electrical and Electronic Engineering wing. The room is approximately 18 meters by 13 metres and contains various research benches and equipment. The room has large open spaces and small areas partitioned off for privacy. These partitions are about 1.5 metres high and are wooden. Wood typically has a reflection coefficient of around 14%, and a transmission coefficient of around 50% [Samawi *et al.*, 1987]. The walls are constructed from hardboard or plasterboard on a wooden frame, which have reflection coefficients of around 14% [Samawi *et al.*, 1987]. One wall consists mainly of windows. There are various metal panels around the walls covering heating plant

and the like, which reflect close to 100% of the incident energy.

4.2 Telecom Engineers Office Carruca House 7th Floor

The District Engineers office is in Carruca House which is located in Cathedral Square, Christchurch. The room in which the measurements were made was an open plan office area on the seventh floor of the building. The area measured approximately 35 metres by 16 metres and contains a maze of partitions with employees' desks, filing cabinets and personal computers being scattered evenly across the room. This room was more cluttered than R9. The room was not one entire level. There were several offices constructed from plasterboard on a wooden frame which provided a boundary. Otherwise the building exterior walls formed the boundary. These are constructed from steel reinforced concrete.

This area seemed to contain more electrical interferers than at the university. It was decided to make 8 measurements in each location and average these to provide a single profile with less noise. The source of the noise was not determined, but it was speculated that the large number of computers may have been a contributing factor. The large bandwidth of the receiver would have resulted in noise anywhere between 500 MHz and 1.5 GHz appearing on the output.

5 The Results

5.1 Shadowing Effect

A significant shadowing effect was observed when the distance between the transmitter and receiver was large. In some cases the output was meaningless due to the extremely small signal level and the high level of noise in the Telecom building. The profiles from this building were graded by inspection with 0 for meaningless, 1 for marginal and 2 for quite good. Ten percent of the measurements were meaningless with a further 25% being marginal. This does not mean that a system would fail in 35% of the locations in this building as a real system would be using bandwidths near a thousand times less than our system, which would reduce these statistics drastically.

Further evidence of the shadow area problem was found when a ray tracing simulation was applied to a map of the 7th floor of the Telecom building. The amplitudes of the highest peaks of the resulting profiles roughly matched to measured profiles for the same locations in the room. The only major difference was that the ray tracing programme predicted deeper fades due to shadow. This was possibly due to the noise giving the measured peaks a larger apparent amplitude.

Saleh's investigations [Saleh and Valenzuela, 1987] also indicate the presence of shadowing where he states:

> "In a recent conference, Devasirvatham [Devasirvatham, 1987a] reported on rms delay spread of up to 200 ns measured in our building at 850 MHz.

This large value, however, occurred when the received signal levels were extremely low, e.g., 100–140 dB of path loss."

This received level would be too low to be useful in a system and should be considered a shadow area.

It seems that the literature has ignored shadow fades as a source of degradation. Chuang [Chuang, 1987] states that irreducible errors occur in deep fades and that diversity would be a solution. If the fade was a shadow fade, the diversity antenna would need to be outside the shadow area which would be a greater distance than needed to avoid a carrier fade due to multipath, and may therefore be unsuitable.

Winters and Yeh [Winters and Yeh, 1985] state that with diversity a stationary terminal randomly located has 0.01% probability of having a BER greater than 10^{-4}. This only considers outage due to carrier fades.

Sexton and Pahlavan [Sexton and Pahlavan, 1989] state that the performance degradation in the indoor channel is due to the occasional deep nulls in the passband of the channel caused by multipath effects.

It seems that the outage studies so far have assumed sufficient signal to noise ratio for the system to function well. The question of outage due to shadow areas should be investigated also, as a system which can provide a good signal to noise in all areas of intended coverage is unlikely.

5.2 The RMS Delay Spread

The rms delay spread (see eqn. B.1) was calculated for all of the locations in both buildings. This was a simple implementation of this equation in software. The output from this programme was compiled into a list.

5.3 The Cumulative Distribution of the RMS Delay Spread

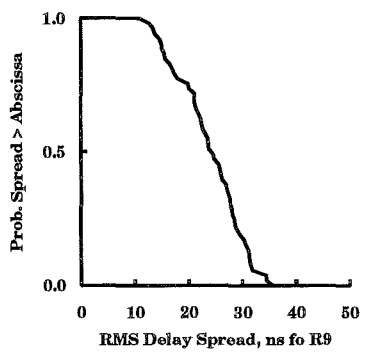

Figure B.13 Cumulative probability distribution of the rms data from R9

The cumulative distribution of the rms delay spread was plotted for R9 (see fig. B.13) and three plots were made for the Telecom building (see fig. B.14). There was one plot for all the locations and two plots with two different subsets based on

noise level in the profile (see section 5.1). The "Marginal" data subset contained both the "marginal" and "good" data points, while the "Good" data subset contained only the "good" data points.

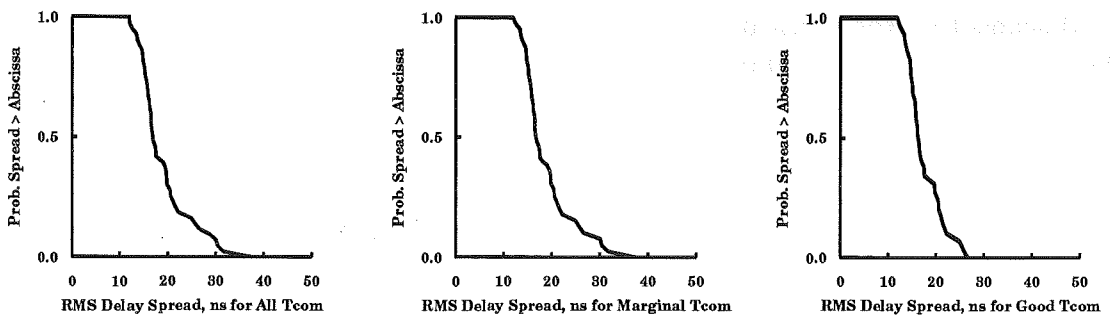

Figure B.14 Cumulative probability distributions of the rms data from Telecom

One can see that as data points are removed, the range is decreased, especially when the "marginal" points are removed. It is quite likely that the range observed for all the points is more accurate, as the large rms delay spread measurements tend to correspond to the low signal strength locations.

5.4 Average and Variance of the RMS Delay Spread

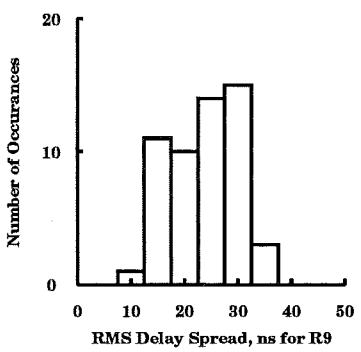

Figure B.15 Distribution histogram of the rms data from R9

Further statistical calculations were made on the sets of rms delay spread measurements. The average, variance and standard deviation was found for each of the data sets. The results were as follows:

Location, etc.	Average	Variance	Std. Deviation
R9	23.8534 ns	38.8798	6.23536
Telecom -All	19.0447 ns	32.6327	5.7125
-Marginal	19.0167 ns	32.1019	5.66585
-Good	17.5525 ns	14.6975	3.83373

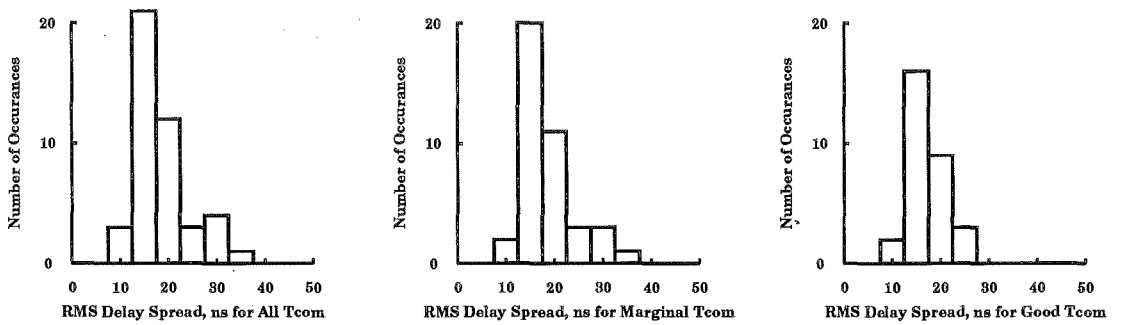

Figure B.16 Distribution histograms of the rms data from Telecom

The distribution histogram of rms delay spreads from R9 (see fig. B.15) and Telecom (see fig. B.16) were also plotted. Once again, one can see that most of the large rms delay measurements were in the marginal group due to the low signal level.

5.5 Fitting Results to Proposed Models

Out of all the proposed models, Saleh's model [Saleh and Valenzuela, 1987] is one of the more complicated. This model describes the profile in terms of clusters of rays. The arrival rate of these clusters is modeled as a Poisson process with some fixed rate Λ. Within each cluster, subsequent rays also arrive according to a Poisson process with a different fixed rate λ. Typically, there are many rays in a cluster, so $\lambda \gg \Lambda$.

The cluster arrival times are denoted by T_l, where $l = 0, 1, 2, \cdots$. The arrival time of the kth ray measured from the beginning of the lth cluster is denoted by $\tau_{kl}, k = 0, 1, 2, \cdots$. By definition, the arrival time for the first cluster, $T_0 = 0$ and the arrival time for the first ray of the lth cluster, $\tau_{0l} = 0$ also. If the gain of each ray is given by β_{kl} and the phase by θ_{kl}, the impulse response of the model is given by

$$h(t) = \sum_{l=0}^{\infty} \sum_{k=0}^{\infty} \beta_{kl} e^{j\theta_{kl}} \delta(t - T_l - \tau_{kl}) \tag{B.6}$$

The power level for each ray $\overline{\beta_{kl}^2}$ for this model is given as $\overline{\beta^2(0,0)}\, e^{-T_l/\Gamma} e^{-\tau_{kl}/\gamma}$, where $\overline{\beta^2(0,0)} = \overline{\beta_{00}^2}$ is the average power gain of the first ray of the first cluster, and Γ and γ are power decay time constants for the clusters and rays, respectively.

The method Saleh used to find the power delay time constants Γ, γ was to average all of the profiles in a room to give one profile, and then to fit the exponential decay curves to this ensemble.

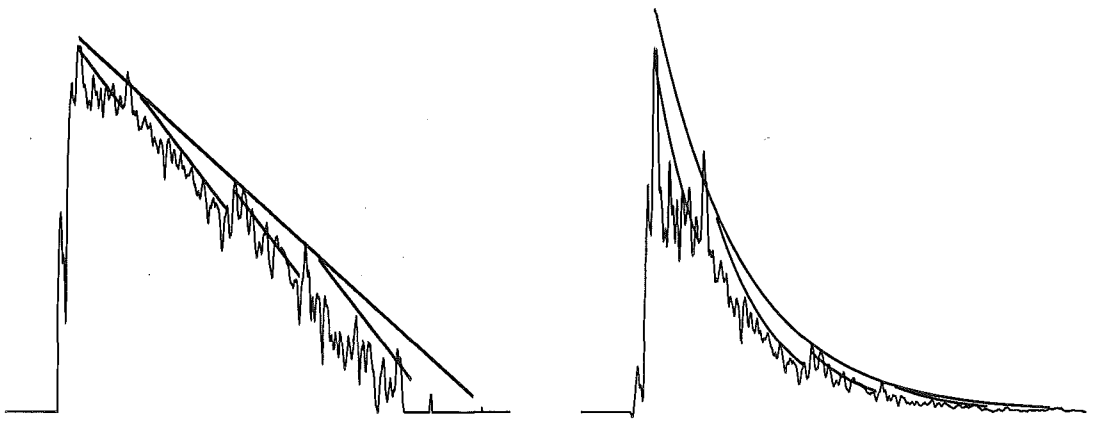

a. Log Plot of Profile Ensemble for R9 **b. Linear Plot of Profile Ensemble for R9**

Figure B.17 Logarithmic and linear scale plots for the ensemble of rays in R9

This method was used on the data from R9. The profiles were all averaged together into an ensemble. The result was then plotted and the peaks for each cluster were selected. These points were then plotted on a logarithmic scale and a least squares linear regression was performed (see fig. B.17a). The resulting straight line could be translated back to the linear plot as an exponential (see fig. B.17b). The peaks inside each cluster were chosen and a best fit for each cluster was found. Saleh's model requires the power decay constants for each cluster to be the same so the slopes were all averaged and the best fit lines altered so that the slopes were the same for each cluster (see fig. B.17a). These lines all translated back onto the linear plot as exponetials with the same power decay constants.

6 Comments and Recommendations

The following are comments on how the system performed and recommendations for improvements that could be made.

The first major problem found was the amount of noise in the Telecom Building in central Christchurch. This problem was not observed at the University site, but the system is intended for use in industrial situations so this problem should be addressed. There are several possibilities for decreasing the noise level in the current system. The first is to use more power to achieve a better signal to noise ratio. The second is to use a smaller bandwidth (longer pulses), to decrease the noise. The third is to use amplifiers with better noise figures in the receiver circuit. Amplifiers with 1.5 dB noise figures and 400 MHz bandwidth are available from Mini Circuits. This implies that a decrease in resolution (and therefore bandwidth) to 5 ns and use of the

Mini Circuits low noise amplifiers would improve the signal to noise ratio by more than 10 dB.

The other alternative would be to develop a new system. The possibilities include designing a PN code system [Devasirvatham, 1984], which has a good dynamic range but poor time resolution (25 ns equivalent pulse width), or a continuous wave system [Pahlavan and Howard, 1989b]. In the continuous wave system, the amplitude and phase are measured for a range of frequencies and the impulse response of the channel is found using the Fourier Transform of the measured data. If a bandpass filter in the receiver could track the frequency of the carrier, this system could use a very small bandwidth for any single measurement and therefore be comparatively noise free. for example, with a 1 watt transmitter as used, decreasing the bandwidth from 1 GHz to 1 MHz gives a 30 dB signal to noise ratio advantage. The major disadvantage with this system is that a large range of frequencies would need to be measured for each location to achieve a reasonable time resolution. This process would be time consuming and changes in the channel while the sets of measurements are taken could result in inaccuracies.

The second major concern is the shadow area problem. More investigation is needed in this area. A system which uses a similar bandwidth to proposed commercial systems would be best for investigating what percentages of areas would suffer greatly from shadowing.

REFERENCES

Alexander, S.E. (1982), "Radio propagation within buildings at 900 MHz," *Electronics Letters*, Vol. 18, No. 21, October, pp. 913–914.

Alexander, S.E. (1983), "Characterising buildings for propagation at 900 MHz," *Electronics Letters*, Vol. 19, No. 20, September, P. 860.

Beaulieu, N.C. (1990), "An infinite series for the computation of the complementary probability distribution function of a sum of independent random variables and its application to the sum of rayleigh random variables," *IEEE Transactions in Communications*, Vol. 38, No. 9, September, pp. 1463–1474.

Bultitude, R.J.C. (1987), "Measurement, characterization and modeling of indoor 800/900 MHz radio channels for digital communication," *IEEE Communications Magazine*, Vol. 25, No. 6, June, pp. 5–12.

Bultitude, R.J.C., Mahmoud, S.A. and Sullivan, W.A. (1989), "A comparison of indoor radio propagation characteristics at 910 MHz and 1.75 GHz," *IEEE J. Selected Areas in Communication*, Vol. 7, No. 1, January, pp. 20–30.

Chuang, J.C.I. (1987), "The effects of time delay spread on portable radio communications channels with digital modulation," *IEEE J. Selected Areas in Communication*, Vol. SAC-5, No. 5, June, pp. 879–889.

Cowl, D.J. (1990), *Indoor Radio Channel Sounding – Hardware and Results*, Technical Report, University of Canterbury, June.

Cox, D. (1989), "Portable digital radio communications — an approach to tetherless access," *IEEE Communications Magazine*, No. 7, July, pp. 30–40.

Davenport, Jr., W.B. and Root, W.L. (1958), *An Introduction to the Theory of Random Signals and Noise*, McGraw-Hill Book Company, Inc.

Devasirvatham, D.M.J. (1984), "Time delay spread measurements of wideband radio signals within a building," *Electronics Letters*, Vol. 20, No. 23, November, pp. 950–951.

Devasirvatham, D.M.J. (1986), "Time delay spread and signal level measurements of 850 MHz radio waves in building environments," *IEEE Trans on Antennas and Propagation*, Vol. AP-34, No. 11, November, pp. 1300–1305.

Devasirvatham, D.M.J. (1987a), "A comparison of time delay spread and signal level measurements within two dissimilar office buildings," *IEEE Trans on Antennas and Propagation*, Vol. AP-35, No. 3, March, pp. 319–324.

Devasirvatham, D.M.J. (1987b), "Multipath time delay spread in the digital portable radio environment," *IEEE Communications Magazine*, Vol. 25, No. 6, June, pp. 13–21.

Dixon, R.C. (1976), *Spread Spectrum Systems*, John Wiley & Sons, New York.

Eng, T. and Milstein, L.B. (1992), "On the capacity of DS-CDMA in a Nakagami multipath channel," *Proceedings Military Communications Conference*, No. , October, pp. 120–124.

Foschini, G.J. and Vannucci, G. (1988), "Using spread-spectrum in a high capacity fiber-optic local network," *Journal of Lightwave Technology*, Vol. 6, No. 3, March, pp. 370–379.

Ganesh, R. and Pahlavan, K. (1989), "On arrival of paths in fading multipath indoor radio channels," *Electronics Letters*, Vol. 25, No. 12, June, pp. 763–765.

Ganesh, R. and Pahlavan, K. (1990), "Effects of traffic and local movements on multipath characteristics of an indoor radio channel," *Electronics Letters*, Vol. 26, No. 12, June 7, pp. 810–812.

Gold, R. (1967), "Optimal binary sequences for spread-spectrum multiplexing," *IEEE Transactions on Information Theory*, Vol. IT-13, No. 1, October, pp. 619–621.

Golomb, S.W. (1967), *Shift Register Sequences*, Holden-Day San Francisco.

Golub, G.H. and Welsh, J.H. (1969), "Calculation of gauss quadrature rules," *Mathematics of Computation*, Vol. 23, No. 106, April, pp. 221–230.

Harris, F.J. (1978), "On the use of windows for harmonic analysis with the discrete fourier transform," *Proceedings of the IEEE*, Vol. 66, No. 1, January, pp. 51–83.

Hawbaker, D.A. and Rappaport, T.S. (1990), "Indoor wideband radiowave propagation measurements at 1.3 GHz and 4.0 GHz," *Electronics Letters*, Vol. 26, No. 21, October 11, pp. 1800–1802.

Haykin, S. (1983), *Communication Systems*, John Wiley and Sons Inc.

Haykin, S. (1988), *Digital Communications*, John Wiley and Sons Inc.

Holtzman, J.H. (1992a), "A simple accurate method to calculate spread spectrum multiple access probabilities," *IEEE Transactions on Communications*, Vol. 40, No. 3, March, pp. 461–464.

Holtzman, J.H. (1992b), "On calculating DS/SSMA error probabilities," *Proceedings ISSSTA '92*, November, pp. 23–26.

Howard, S.J. and Pahlavan, K. (1990), "Doppler spread measurements of indoor radio channel," *Electronics Letters*, Vol. 26, No. 2, January 18, pp. 107–109.

I, C.L., Greenstein, L.J. and Gitlin, R.D. (1993), "A microcell/macrocell cellular achitecture for low- and high-mobility wireless users," *IEEE Journal on Selected Areas in Communications*, Vol. 11, No. 6, August, pp. 885–891.

Judge, W.J. (1962), "Multiplexing using quasiorthogonal functions," *AIEEE Winter General Meeting*, January.

Jung, P., Baier, P.W. and Steil, A. (1993), "Advantages of CDMA and spread spectrum techniques over FDMA and TDMA in cellular mobile radio applications," *IEEE Transactions on Vehicular Technology*, Vol. 42, No. 3, August, pp. 357–364.

Kasami, T. (1966), "Weight distribution formula for some class of cyclic codes," *Coordinated Science Lab., Univ. Illinois, Urbana. Tech Rep. R 285*, No. .

Kavehrad, M. (1985), "Performance of nondiversity receivers for spread spectrum in indoor wireless communications," *AT & T Technical Journal*, Vol. 64, No. 6, July, pp. 1181–1201.

Kavehrad, M. and McLane, P.J. (1985), "Performance of low-complexity channel coding and diversity for spread spectrum in indoor, wireless communication," *AT & T Technical Journal*, Vol. 64, No. 8, October, pp. 1927–1965.

Kavehrad, M. and McLane, P. (1987), "Spread spectrum for indoor radio," *IEEE Communications Magazine*, Vol. 25, No. 6, June, pp. 32–40.

Kavehrad, M. and Ramamurthi, B. (1987), "Direct-sequence spread spectrum with DPSK modulation and diversity for indoor wireless communications," *IEEE Transactions on Communications*, Vol. COM-35, No. 2, February, pp. 224–236.

Laforgia, D., Luvison, A. and Zingarelli, V. (1984), "Bit error evaluation for spread-spectrum multiple access systems," *IEEE Transactions on Communications*, Vol. COM-32, No. 6, June, pp. 660–669.

Lam, A.W. and Özlütürk, F.M. (1992), "Performance bounds for DS/SSMA communications with complex signature sequences," *IEEE Transactions on Communications*, Vol. 40, No. 10, October, pp. 1607–1614.

Lam, W. and Steele, R. (1991), "Performance of direct-sequence spread-spectrum multiple-access systems in mobile radio," *IEE Proceedings*, Vol. 138, No. 1, February, pp. 1–14.

Lemieux, J.F., El-Tanany, M.S. and Hafez, H.M. (1991), "Experimental evaluation of space/frequency/polarization diversity in the indoor wireless channel," *IEEE Transactions on Vehicular Technology*, Vol. 40, No. 3, August, pp. 569–574.

Meyers, M.H. (1982), "Computing the distribution of a random variable via gauss quadrature rules," *The Bell System Technical Journal*, Vol. 61, No. 9, November, pp. 2245–2261.

Morrow, Jr., R.K. and Lehnert, J.S. (1989), "Bit-to-bit error dependence in slotted DS/SSMA packet systems with random signature sequences," *IEEE Transactions on Communications*, Vol. 37, No. 10, October, pp. 1052–1061.

Nail, J. (1953), "Designing discone antennas," *Electronics*, No. 8, August, pp. 167–169.

Oberhettinger, F. (1973), *Fourier Transforms of Distributions and Their Inverses*, Academic Press New York.

Pahlavan, K. and Howard, S.J. (1989a), "Frequency domain measurements of indoor radio channels," *Electronics Letters*, Vol. 25, No. 24, November 23, pp. 1645–1647.

Pahlavan, K. and Howard (1989b), "Frequency domain measurements of indoor radio channels," *Electronics Letters*, Vol. 25, No. 24, November, pp. 1645–1647.

Pahlavan, K., Ganesh, R. and Hotaling, T. (1989), "Multipath propagation measurements on manufacturing floors at 900 MHz," *Electronics Letters*, Vol. 25, No. 3, February, pp. 225–227.

Papoulis, A. (1984), *Probability, Random Variables, and Stochastic Processes*, McGraw-Hill Book Company, second ed.

Peterson, W.W. and E. J. Weldon, J. (1972), *Error-Correcting Codes*, The M.I.T. Press.

Pickholtz, R.L., Schilling, D.L. and Milstein, L.B. (1982), "Theory of spread spectrum communications — a tutorial," *IEEE Transactions on Communications*, Vol. COM-30, No. 5, May, pp. 855–884.

Proakis, J.G. (1983), *Digital Communications*, McGraw-Hill Book Company, Inc.

Pursley, M.B. (1977), "Performance evaluation for phase-coded spread-spectrum multiple-access communication — part I: System analysis," *IEEE Transactions on Communications*, Vol. COM-25, No. 8, August, pp. 795–799.

Pursley, M.B. and Sarwate, D.V. (1977), "Performance evaluation for phase-coded spread-spectrum multiple access communication — part II: Code sequence analysis," *IEEE Transactions on Communications*, Vol. COM-25, No. 8, August, pp. 800–803.

Quereshi, S.U.H. (1985), "Adaptive equalisation," *Proceedings of the IEEE*, Vol. 73, No. 9, September, pp. 1349–1387.

Rappaport, T.S. and McGillem, C.D. (1989), "UHF fading in factories," *IEEE J. Selected Areas in Communication*, Vol. 7, No. 1, January, pp. 40–48.

Ryser, H.J. (1963), *Combinatorial Mathematics*, The Mathematical Association of America.

Saleh, A.A.M. and Valenzuela, R.A. (1987), "A statistical model for indoor multipath propagation," *IEEE J. Selected Areas in Communication*, Vol. SAC-5, No. 2, February, pp. 128–137.

Samawi, N., Tran, V.N., Horan, P., Childs, R.E. and Ng, C.K. (1987), "Transmission and reflection of radio signals from 1 to 40 GHz," *IREECON*, pp. 184–187.

Sarwate, D.V. and Pursley, M.B. (1980), "Crosscorrelation properties of pseudorandom and related sequences," *Proceedings of the IEEE*, Vol. 68, No. 5, May, pp. 593–618.

Sexton, T.A. and Pahlavan, K. (1989), "Channel modeling and adaptive equalization of indoor radio channels," *IEEE J. Selected Areas in Communication*, Vol. 7, No. 1, January, pp. 114–121.

Springer, M.D. (1979), *The Algebra of Random Variables*, John Wiley & Sons, New York.

Stuber, G. and Kchao, C. (1992), "Analysis of a multiple-cell direct sequence CDMA cellular mobile radio system," *IEEE Journal on Selected Areas in Communication*, Vol. 10, No. 4, June, pp. 669–679.

Turin, G.L. (1980), "Introduction to spread-spectrum antimultipath techniques and their application to urban digital radio," *Proceedings of the IEEE*, Vol. 68, No. 3, March, pp. 328–353.

Turin, G.L. (1984), "The effects of multipath and fading on the performance of direct sequence CDMA systems," *IEEE Journal on Selected Areas in Communications*, Vol. SAC-2, No. 4, July, pp. 597–603.

Ungerboeck, G. (1987), "Trellis-coded modulation with redundant signal sets part II: State of the art," *IEEE Communications Magazine*, Vol. 25, No. 2, February, pp. 12–21.

Viterbi, A.M. and Viterbi, A.J. (1993), "Erlang capacity of a power-controlled CDMA system," *IEEE Journal on Selected Areas in Communication*, Vol. 11, No. 6, August, pp. 892–900.

Viterbi, A.J., Padovani, R. and de Weck, J.P. (1992), "Spread spectrum CDMA system design and comparative testing on two continents," *Proceedings ISSSTA '92*, November, P. 1.

Wang, M.M.J. and Milstein, L.B. (1992), "Predetection diversity for CDMA indoor radio communications," *Virginia Tech. Symposium on Wireless Communications*, No. , June, pp. 13.1–13.10.

Welch, L.R. (1974), "Lower bounds on the maximum cross correlation of signals," *IEEE Trans. Information Theory*, Vol. IT-20, No. 3, May, pp. 397–399.

Winters, J.H. and Yeh, Y.S. (1985), "On the performance of wideband digital radio transmission within buildings using diversity," *GLOBECOM '85*, Vol. 2, No. 5, December, pp. 991–996.

Wozencraft, J.M. and Jacobs, I.M. (1965), *Principals of Communication Engineering*, John Wiley & Sons, New York.

Xiang, H. (1985), "Binary code-division multiple-access systems operating in multipath fading, noisy channels," *IEEE Transactions on Communications*, Vol. COM-33, No. 8, August, pp. 775–784.

Yoon, Y., Kohno, R. and Imai, H. (1993), "A spread-spectrum multiaccess system with cochannel interference cancellation for multipath fading channels," *IEEE Journal on Selected Areas in Communication*, Vol. 11, No. 7, September, pp. 1067–1075.

Zaghloul, H., Morrison, G. and Fattouche, M. (1991a), "Frequency response and path loss measurements of indoor channel.," *Electronics Letters*, Vol. 27, No. 12, June 6, pp. 1021–1022.

Zaghloul, H., Fattouche, M., Morrison, G. and Tholl, D. (1991b), "Comparison of indoor propagation channel characteristics at different frequencies," *Electronics Letters*, Vol. 27, No. 22, October 24, pp. 2077–2079.

Ziemer, R.E. and Peterson, R.L. (1985), *Digital Communications and Spread Spectrum Systems*, Macmillan Publishing Company New York.